PHOTODISSOCIATION AND PREDISSOCIATION PROCESSES IN DIATOMIC MOLECULES: A TIME-DEPENDENT QUANTUM MECHANICAL STUDY

A Thesis Submitted
in Partial Fulfilment of the Requirements
for the Degree of

DOCTOR OF PHILOSOPHY

by

C. KALYANARAMAN

to the
DEPARTMENT OF CHEMISTRY
INDIAN INSTITUTE OF TECHNOLOGY KANPUR

OCTOBER, 1994

To
My Parents

STATEMENT

I hereby declare that the matter embodied in this thesis is the result of investigations carried out by me in the Department of Chemistry, Indian Institute of Technology, Kanpur, India under the supervision of Professor N. Sathyamurthy.

In keeping with the general practice of reporting scientific observations, due acknowledgement has been made wherever the work described is based on the findings of other investigators.

C. Kalyanaraman

Kanpur C. KALYANARAMAN

DEPARTMENT OF CHEMISTRY
INDIAN INSTITUTE OF TECHNOLOGY KANPUR INDIA
CERTIFICATE I

This is to certify that Mr. C. Kalyanaraman has satisfactorily completed all the courses required for the Ph. D. degree programme. These courses include:

CHM 605 Principles of Organic Chemistry

CHM 621 Chemical Binding

CHM 624 Modern Physical Methods in Chemistry

CHM 625 Principles of Physical Chemistry

CHM 632 Enzyme Reaction Mechanism and Enzyme Kinetics

CHM 645 Principles of Inorganic Chemistry

CHM 800 General Seminar

CHM 801 Special Seminar

CHM 900 Ph. D. Thesis

Mr. C. Kalyanaraman was admitted to the candidacy of the Ph. D. degree in November 1990, after he successfully completed the written and oral qualifying examinations.

P. K. Ghosh

(P. K. Ghosh)
Head,
Department of Chemistry
IIT Kanpur

S. Sarkar

(S. Sarkar)
Convenor,
Departmental Post Graduate Committee
Department of Chemistry
IIT Kanpur

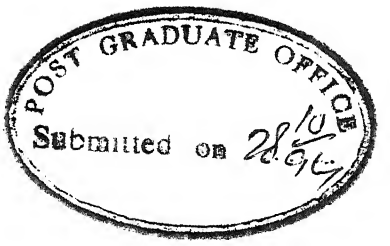

CERTIFICATE II

Certified that the work contained in this thesis entitled: "Photodissociation and Predissociation Processes in Diatomic Molecules: A Time-Dependent Quantum Mechanical Study", has been carried out by Mr. C. Kalyanaraman under my supervision and that the same has not been submitted elsewhere for a degree.

N. Sathyamurthy

(N. Sathyamurthy)
Thesis Supervisor
Professor of Chemistry
IIT Kanpur

Kanpur

ACKNOWLEDGEMENT

I have great pleasure in expressing my sincere gratitude to my thesis supervisor Professor N. Sathyamurthy for his excellent guidance and constant encouragement throughout the course of this study. His understanding nature, love and patience are highly appreciated. Through my association with him I have benefited both academically as well as personally.

I express my heartiest thanks to my labmates Dr. N. Balakrishnan, Dr. Sanjay Kumar, Mr. Susanta Mahapatra, Mr. Nilmadhab Chakrabarti and Mr. Asif Rahaman. On various occasions, through formal group meets and informal discussions, they helped me in understanding the theoretical and computational aspects of reaction dynamics. They extended me their helping hands during various needy hours. I am grateful to them for ever.

I extend my heartfelt thanks to my post-graduate teacher Dr. I. Noor Batcha for inspiring to pursue research in theoretical chemistry. Also his interest in my research work and his affection are highly appreciated. I am also thankful to Dr.(Ms). S. Thareja for her interest and encouragement.

My special thanks are to Mrs. Sathyamurthy, Dr. N. Jayaraman, Dr. V. Balasubramanian and Mrs. Balasubramanian for their kind love and encouragement.

I take this opportunity to express my sincere thanks to Professor V. Aquilanti, for helping me to participate in the Seventh European Workshop on Spectroscopy and Dynamics, where part of the thesis work was presented.

My heartiest thanks extend to my friends Kasi, Raghu, Kumar, Narayanan, Shaji,

Tamil, Pradhan, Dr. N. -S. Loc, Immi, Rangarajan, Sam, Gopathy, Prabhu, Dr. Satthiah, Ms. Sridevi and Ms. Moni Oberoi for making my stay a memorable one.

My special thanks go to Professor (Ms.) Leelavathi Krishnan for introducing me to the leterature on personality development.

Several non-teaching staff of chemistry department, library and computer centre helped me at various stages, I extend my thanks to them as well.

I am highly indebted to my parents for sending me all the way to Kanpur to pursue my higher education. I could feel their love and longingness whenever I meet them during vacation. My special thanks go to my brother Ramesh for his encouragement and cooperation. Finally, my heartiest thanks extend to my friend Kavitha for her love and understanding.

C. Kalyanaraman.

(C. Kalyanaraman)

Abstract

In recent years, time-dependent quantum mechanical approach has been used extensively to investigate various elementary chemical processes such as photodissociation, predissociation, reactive scattering, molecule-surface scattering etc., In the present study we have investigated (i) photo-predissociation of NaI using femtosecond laser pulse, (ii) channel control in chemical reactions using HI photodissociation as a case study and (iii) photodissociation and predissociation processes in OH radical.

In chapter 1 of the thesis, the necessary background material related to the TDQM approach to photodissociation and predissociation processes have been reviewed. We have also presented a short literature review emphasising mainly on the recent studies.

In chapter 2, theoretical and computational methodologies related to the TDQM approach to photodissociation and predissociation processes have been presented. This chapter has been divided into three sections. In section 1, we have described the existing computational methodologies for implementing the TDQM approach. Section 2 of this chapter is devoted mainly for the interaction of light with molecules. We have presented a semiclassical and a quantum mechanical description of the photoabsorption process. We have also described, how the photodissociation cross section is computed in the time-domain. Also we have presented a critical analysis of the nature of the wavefunction prepared by a laser pulse on the excited electronic state. In section 3, we have described the computational methodologies for investigating multieletronic state problems. Also the golden rule treatment for computing the predissociation linewidth is included in this chapter.

In chapter 3, we have presented the results of the TDQM study of the photo- predissociation of NaI using ultrashort laser pulse. We have investigated the nature of the wave packet prepared by a femtosecond laser pulse, whose excitation frequency is chosen *near*, *very near* and *far from* resonance excitation frequency. Since the excitation frequencies are different, the WPs prepared on the excited electronic state also have different characteristics. The norm of the WP on the excited electronic state during the pulse preparation step has been analysed. After the pulse preparation step is over, the WP is time-evolved for about 3 ps on the covalent excited electronic state which is coupled to the ground electronic state. Due to the diabatic coupling between the ionic ground state

and the covalent excited state, the time-evolving WP bifurcates near the crossing point and a small fraction of it (as determined by the Landau-Zener curve crossing probability) leaks through the crossing to form neutral products Na and I and the remaining part of the WP oscillates between the ionic and the covalent turning point. Whenever the WP reaches near the crossing point a small fraction of it leaks through crossing. We have estimated the oscillation periods corresponding to photoexcitation wavelengths 300, 321 and 344 nm and our results are in good agreement with the experimental results of Zewail and coworkers. However, when the excitation wavelengths are *far from* resonance, i.e., λ_{ex} = 360 and 390 nm, the WP spreads immediately (in less than 0.5 ps) and shows several interference patterns. Therefore, the oscillation period estimated by us for λ_{ex} = 360 and 390 nm are not in agreement with experimental results. In order to simulate them, a two photon calculation is required as the experimental results are strongly dependent on the probe wavelength. We have observed that the transient effect and the energy of the WP are highly responsible for the unusual characteristics of the WP evolution.

In chapter 4 of the thesis, we have presented a detailed analysis of the photodissociation of HI in its first absorption band. HI photodissociation takes place around 250nm resulting in H + I and H + I* formation. In this energy range, the following potential energy curves participate in the photodissociation: $^3\Pi_1$, $^1\Pi_1$, $^3\Sigma_1$ and $^3\Pi_0$. Among these, the former two correlate with the H + I channel and the later two correlate with the H + I* channel. Except for the $^3\Pi_0$ state, all other states are non-adiabatically coupled to each other. We have computed the photodissociation cross section(σ) corresponding to the photoexcitation from the ground vibrational level of the ground electronic state to all of the above mentioned excited states. We have made use of the PE curves, non-adiabatic coupling potentials and the coordinate dependent transition dipole moments reported earlier by Levy and Shapiro. Our computed σ and Γ values are in excellent agreement with the experimental and the time-independent quantum mechanical results. We have also computed the anisotropy parameter(β) for the H + I* channel and our β values as a function of excitation energy are in accord with the experimental and the time-independent quantal results. In addition, we show that the Γ value changes significantly with vibrational excitation of the parent molecule and point out vibrational excitation prior to photodissociation as a means of channel control. The results are interpreted in terms of the influence of the non-adiabatic

coupling on the time-evolution of the wavefunction.

In chapter 5, results obtained for the photodissociation and predissociation processes in OH radical using the TDQM method have been described. Since OH radical is one of the important constituents in the astrophysical environment, understanding various dissociation pathways in OH becomes particularly essential. Photodissociation in OH takes place due to electronic transition from the ground electronic state ($X^2\Pi$) to the excited electronic states, $1^2\Sigma^-$, $1^2\Delta$, $B^2\Sigma^+$ and $2^2\Pi$. The PE curves and the coordinate dependent transition dipole moments are taken from the *ab initio* results of Dalgarno and coworkers. Our computed photodissociation cross sections are in good agreement with the time-independent quantal results and a factor of two less than the experimental results. Predissociation in OH takes place from its first absorption band ($X^2\Pi$–$A^2\Sigma^+$) due to spin-orbit coupling between the bound state $A^2\Sigma^+$ and the repulsive states $^4\Sigma^-$, $1^2\Sigma^-$ and $^4\Pi$. Using the recent *ab initio* results of PE curves and the spin-orbit matrix elements reported by Yarknoy we have obtained predissociation linewidths corresponding to predissociation from v'=1–7 of the $A^2\Sigma^+$ state. The results are analysed in terms of the crossings between the PE curves.

A summary of our findings are given in chapter 6.

CONTENTS

LIST OF ABBREVIATIONS

CW	-	Continuous wave
DVR	-	Discrete variable representation
FFT	-	Fast Fourier transform
FTS	-	Femtosecond transition-state dpectroscopy
FWHM	-	Full width at half-maximum
GWP	-	Gaussian wave packet
IVR	-	Intramolecular vibrational relaxation
KRMC	-	Kinetic referenced modified Cayley
LIF	-	Laser-induced-fluorescence
NIP	-	Negative imaginary potential
PE	-	Potential-energy
PES	-	Potential-energy surface
REMPI	-	Resonance enhanced multiphoton inonisation
RWA	-	Rotating wave approximation
SIL	-	Short iterative Lanczos
SOD	-	Second-order differencing
SPO	-	Split operator
TDSE	-	Time-dependent Schrödinger equation
TDQM	-	Time-dependent quantum mechanical
TIQM	-	Time-independent quantum mechanical
WP	-	Wave packet

Chapter 1

Introduction

Photon-induced processes have drawn considerable attention in recent years[1–5]. One of the most important photon-induced processes which offers a wide variety of applications is *photodissociation*[6]. In chemical dynamics, for instance, photofragments produced by photodissociation are used in investigating bimolecular exchange reactions in molecular beam experiments[7–10]. Photodissociation processes have technological applications as well[11, 12]. In addition, a careful study of photodissociation provides an opportunity to verify the existing dynamical theories. Besides these applications, photodissociation is one of the fundamental processes that occur in earth's atmosphere and astrophysical environment[13–15]. Therefore, understanding the dynamics of photofragmentation becomes particularly important.

Photodissociation processes usually involve electronic transition (due to photoabsorption) from the ground electronic state to an excited repulsive electronic state. As a result, the molecule fragments into its constituents[16]. For a diatomic molecule AB, this process can be represented as

$$AB(v,j) \xrightarrow{\hbar\omega} [AB]^{*,\ddagger} \longrightarrow A + B$$

where v and j refer to the vibrational-rotational state of the parent molecule. ω is the

frequency of the photolysing radiation. Unlike a full collision process (e.g., a bimolecular reaction), the short lived intermediate (or the transition state, $[AB]^{*,\ddagger}$) is produced via photoabsorption. Thus we are mainly interested in the second half of a full collision event. Therefore, photodissociation process is often referred to as a *half-collision* process[17]. For such a half-collision process, one can experimentally measure scalar quantities such as photodissociation cross section and energy distributions of the photofragments and the vector quantities such as angular distribution of the products, anisotropy parameter and angular momentum correlations[18–25].

Sophisticated experimental techniques developed in recent years enable us to obtain these quantum state resolved quantities precisely. For instance, one can prepare the reagent in specific vibrational-rotational quantum state by techniques like stimulated emission pumping or infra-red laser excitation prior to photodissociation[22-25]. Similarly photofragment velocities can be measured by time-of-flight mass spectrometry and the internal state distributions of the products can be obtained by laser-induced-fluorescence (LIF) technique or resonance enhanced multiphoton ionisation (REMPI) technique[21–25]. The photofragment imaging technique developed recently by Chandler and coworkers[26, 27] enable an accurate determination of photofragment angular distribution. Zewail and coworkers[29–32] have demonstrated that ultrashort(femtosecond) laser pulses could be used to *map out* the molecular motion on the excited electronic state in *real time*. Thus the experimental methods have reached the *ultimate* time resolution[32].

Theoretical developments have kept pace with experiments. Within the framework of quantum mechanics, one can obtain the quantum state resolved cross section either by time-independent quantum mechanical approach (TIQM)[35–42] or by time-dependent (TDQM)[43–65]. In the former approach, the photodissociation cross section is computed

from Franck-Condon factors. Therefore, one has to know the initial and the final scattering state eigenfunctions in order to compute the cross section. However, evaluation of the scattering state eigenfunction is computationally more demanding especially when there are more than one product channel open. Such problems are circumvented in the TDQM approach[66]. The time-domain formulation of spectroscopy was pioneered by Heller and coworkers[43,67–74]. The computational simplicity of this approach and the physical insight offered it are primarily responsible for the success of the TDQM method[75, 76].

Heller and coworkers[75–77] employed the Gaussian wave packet (GWP) method (a semiclassical treatment) for following the time-evolution of the system. The GWP method assumes that the potential-energy-surface (PES), upon which the dynamics occurs, is locally quadratic and that the process of interest takes place in short time such that the Gaussian wave packet remains Gaussian during the time-evolution[75–81]. Since direct photodissociation and resonance Raman scattering processes occur usually in less than 100 fs, Heller and coworkers could successfully implement the GWP method for a variety of systems[43,67–74]. Until 1983 there was not much progress in using the TDQM approach as there were not efficient numerical algorithms and computer memory and speed were limited. However, the situation has changed now. Computers with large memory and high speed have become common. The fast Fourier transform(FFT) method[82–86] is being used extensively to obtain the spatial derivatives of the wavefunction and it is found to be accurate and much faster than the methods employed earlier[83, 85]. Several time-evolution methods have been developed in the last decade or so. The numerically exact WP propagation method (often referred as the *grid method*) offers several advantages over TIQM approach[87–90]. In addition to providing the computational simplicity and the physical insight, a single wave packet propagation is sufficient to obtain photodissoci-

ation cross section over entire photoexcitation energies. Therefore, the numerically exact WP propagation method has been used rather widely in recent years for studying several elementary chemical processes[87, 88]. For an extensive review of them and their relative merits, the reader is referred to several reviews that have appeared[87, 88, 91–97]. Several reviews[87, 88, 93] and monographs[95–97] on the applications of the TDQM approach have emerged in recent years.

One of the major difficulties with the photoabsorption and related processes is that there could be more than one electronic state participating in the dynamics[98–113]. Therefore, one has to go beyond the Born-Oppenheimer approximation and use either adiabatic or diabatic representation to investigate the dynamics[98, 115, 116]. In principle, one can extend the existing time-evolution methods for investigating the dynamics which takes place on multiple electronic states[117–120]. However, Coalson and Kinsey[78, 121, 122] introduced the WP perturbation theory approach and Alvarellos and Metiu[123, 124] introduced a computational algorithm by making use of both adiabatic and diabatic representations to study especially the coupled electronic state problems. Thus, using the quantum mechanical approach, quantum state resolved cross sections (partial photodissociation cross sections[36, 43, 54, 65, 90, 125]), branching ratio between the different products when there is more than one product channel[79, 126] and angular distribution of the products can be determined accurately[20, 35, 127–130]. Apart from these developments, theoretical and computational studies have emerged recently to investigate the nature and the dynamics of the WP prepared by an ultrashort laser pulse[131–137]. Several theoretical studies have also been carried out to simulate the experimental studies of Zewail and coworkers[132,138–147].

In addition to computing cross sections and understanding the dynamics, an investi-

gation of photodissociation also provides clue to means to *control* the product formation ratio[148, 154, 155]. Recently, various *channel control* methods which are mainly based on photoexcitation, have been developed to influence the product formation ratio[149–166].

Over the years, photodissociation in several diatomic and polyatomic molecules have been studied using the TDQM approach. A review of literature covering up to 1992 have appeared elsewhere[3]. Therefore, we only cite the most recent studies in table 1.1.

Another important photon-induced process which deserves attention is the *predissociation* [16, 116]. In predissociation process the photoabsorption takes place from a bound(ground) electronic state to a bound excited electronic state (bound $\rightarrow$ bound transition). Before the excited molecule emits the light and returns back to the ground electronic state, it dissociates because of coupling between the bound excited electronic state and a repulsive excited electronic state. Depending upon the perturbation present in the system, predissociation is classified as electronic, vibrational, rotational, spin-orbit and spin-spin types[116]. Except for rotational predissociation, other types of predissociation involve participation from more than one electronic state. Since predissociation lifetimes are of the order of 10^{-6}–10^{-12} seconds, there are only limited number of TDQM studies available in the literature[167–170]. However, vibrational predissociation in van der Waals complexes have been studied extensively in recent years as they provide mechanistic insight into the intramolecular vibrational redistribution process[171, 172]. Some of the recent studies on predissociation are also listed in table 1.1.

In the present investigation, we have undertaken a TDQM study of photodissociation and predissociation processes in some diatomic molecules. Since diatomic molecules are relatively simpler systems, a detailed insight into the dynamics of fragmentation can be obtained. As we have mentioned earlier, nonadiabatic coupling among potential-energy

curves are inevitable in the excited state dynamics. Therefore, we have paid special attention to this phenomenon. We have investigated the nature and the dynamics of the WP prepared by an ultrashort laser pulse by taking NaI predissociation as a case study. We have analysed in detail the photodissociation of HI in its first absorption band. We have also investigated the effect of vibrational excitation of HI prior to photodissociation on the product formation ratio (i.e., I^*/I branching ratio). Also we have studied photodissociation and predissociation processes in OH radical. The thesis has been divided into six chapters. In chapter 2, theoretical and computational methodologies for implementing the TDQM method to study photodissociation and predissociation processes are described. In chapter 3, NaI predissociation using femtosecond laser pulse is presented. In chapter 4, we present the results of our studies on HI photodissociation. In chapter 5, OH radical photodissociation and predissociation processes are described. Summary and conclusions are given in chapter 6.

Table 1.1: Summary of recent TDQM studies on photodissociation/predissociation processes

Sl. No.	Year	System	Time-evolution	Laplacian	Reference
1	1993	CH_3I	SOD	FFT	[173]
2	1993	CH_3ONO	Chebyschev	FFT	[174]
3	1993	HBr/LiF(001)	Chebyschev	FFT	[175]
4	1993	HCO	Chebyschev	FFT	[176]
5	1993	Na_2	SOP	FFT	[177]
6	1993	IBr	Lanczos	FFT	[119]
7	1993	HOCl	Chebyschev	FFT	[178]
8	1993	CH_2	Lanczos	FFT	[179]
9	1993	HF	SOP	FFT	[180]
10	1993	HI	SOD	FFT	[120]
11	1993	H_2^+	SOP	FFT	[181]
12	1994	HBr/LiF(001)	Chebyschev	FFT/DVR	[182]
13	1994	Cl_2	SOP	FFT	[183]
14	1994	Ar...HCl	Chebyschev	FFT/DVR	[184]
15	1994	OH	SOD	FFT	[170]
16	1994	O_3	Lanczos	FFT	[185]

Chapter 2

Methodology

This chapter has been divided into three major sections. In the first section we address the question, how the dynamical evolution of a system in the absence of any applied field can be followed quantum mechanically. The second section is devoted to a discussion of the interaction of radiation with matter and the resulting processes. In the third section, we describe how the dynamical evolution of the system is followed on nonadiabatically coupled electronic states.

2.1 Time-dependent quantum mechanical approach

The dynamical evolution of any quantum system can be followed by solving the time-dependent Schödinger equation (TDSE)

$$i\hbar\frac{\partial\Psi(t)}{\partial t} = \hat{H}(t)\Psi(t) \tag{2.1}$$

where $\hat{H}(t)$ is the Hamiltonian operator of the system. Since this is a first order differential equation, its solution will be of the form

$$\Psi(t) = \hat{U}(t,t_0)\Psi(t_0) \tag{2.2}$$

where $\hat{U}(t, t_0)$ is the time-evolution operator. It is a linear operator and it satisfies the initial condition

$$\hat{U}(t_0, t_0) = \hat{1} \tag{2.3}$$

For a Hamiltonian which is explicitly time-independent, the formal solution of eq. (2.1) is given as

$$\Psi(t) = e^{-i\hat{H}(t-t_0)/\hbar}\Psi(t_0) \tag{2.4}$$

By comparing eq. (2.4) with eq. (2.2), the time-evolution operator is identified as

$$\hat{U}(t, t_0) = e^{-i\hat{H}(t-t_0)/\hbar} \tag{2.5}$$

Hamiltonians with explicit time-dependence will be discussed in the later part of this section.

In what is termed the *grid* method, solving eq. (2.1) involves the following steps[85, 88, 87, 186]: (i) representation of the initial wavefunction on a finite grid, (ii) propagation of the wavefunction till the process of interest is over and (iii) analysing the final wavefunction for dynamical observables.

For a photodissociation process, the initial wavefunction is taken as the wavefunction corresponding to the state "prepared"(see below). The grid points should be close enough to contain all the oscillations of the wavefunction during its evolution. The grid spacing also determines the maximum energy that can be represented on the grid and it should be chosen according the energy spectrum of the Hamiltonian. The grid size (and spacing) chosen in the coordinate space is inversely related to the size in the momentum space. Therefore, if the initial wavefunction is narrow in the coordinate space, it will be spread out in the momentum space. These considerations are particularly important as the Hamiltonian operator consists of kinetic and potential energy parts and the former is local in

the momentum space while the later is local in the coordinate space. Thus one takes appropriate grid spacing and optimal width for the initial wavefunction wherever possible. Once the initial wavefunction is chosen, the next step is its propagation in time. As we can anticipate from eq. (2.4) the time-propagation will require repeated operations of $\hat{H}$ on Ψ.

2.2 Evaluation of $\hat{H}\Psi$

The evaluation of $\hat{H}\Psi$ consists of the evaluation of the kinetic energy part, $\hat{T}\Psi$, and the potential energy part, $\hat{V}\Psi$. As we mentioned earlier in the text, the latter is local in the coordinate space and its evaluation amounts to a mere multiplication of Ψ at each grid point by $\hat{V}$. However, the kinetic energy operator is nonlocal in the coordinate space and its evaluation is more complicated. A similar problem would arise with $\hat{V}$in the momentum space. Therefore, it would be better to solve the $\hat{T}\Psi$ and $\hat{V}\Psi$ parts of the Hamiltonian in the representation in which each is local. The coordinate and momentum space wavefunctions are related through the Fourier transformation as

$$\Psi(r) = \frac{1}{\sqrt{2\pi}} \int_{-\infty}^{\infty} e^{ikr}\, \Phi(k) dk \tag{2.6}$$

$$\Phi(k) = \frac{1}{\sqrt{2\pi}} \int_{-\infty}^{\infty} e^{-ikr}\, \Psi(r) dr \tag{2.7}$$

$$\Psi'(r) = \frac{1}{\sqrt{2\pi}} \int_{-\infty}^{\infty} e^{ikr}\, (ik)\, \Phi(k) dk \tag{2.8}$$

$$\Psi''(r) = \frac{1}{\sqrt{2\pi}} \int_{-\infty}^{\infty} e^{ikr}\, (ik)^2\, \Phi(k) dk \tag{2.9}$$

Therefore, the evaluation of kinetic energy operator can be carried out by the following steps:[85, 90]

1. the wavefunction $\Psi(r)$ is (forward) Fourier transformed into momentum space

2. the momentum space wavefunction $\Phi(k)$ is multiplied by $\frac{k^2\hbar^2}{2m}$ at each momentum grid point and

3. the momentum space wavefunction is brought back to the coordinate space by an inverse Fourier transformation.

The availability of fast Fourier transform (FFT) algorithms[187] enables us to accurately evaluate $\hat{T}\Psi(r)$. This method requires the wavefunction to satisfy periodic boundary conditions and for band-limited functions it is exact. In addition, the numerical grid should have optimal number of equally spaced sampling points as decided by the phase-space volume[87]. An attractive feature of the FFT method is its computational scaling property with respect to the number of grid points N: computer time increases as $\sim$ NlogN. Usually N is taken as a power of 2 as most available FFT routines require this. It is worthwhile to mention that the Fourier method can be parallelised easily and hence the computer time scaling can be reduced as $\sim$ (logN).

In the discrete representation, the operators corresponding to the original Hamiltonian are mapped onto a discrete Hilbert space. The mapping has to be carried out in such a way that the operators in the discrete Hilbert space obey all the quantum mechanical commutation relations obeyed by the corresponding physical observables in the original Hilbert space. Only then one can say that a one-to-one mapping of the operators to the discrete space is achieved. Kosloff and Kosloff have shown[85] that this is indeed the case with the Fourier discretisation for a band-limited function with a finite support - that is, of finite extent in configuration as well as momentum space. This once again reveals the versatility of the Fourier transform method over the other methods. If the wavefunction is not band-limited then one has to employ a semiclassical approximation for kinetic energy operator as has been done in the finite difference scheme.

2.3 Time-evolution

Having represented the wavefunction and the Hamiltonian on a numerical grid, the next step in the TDQM approach is to propagate the wavefunction in time. This has to be carried out by dividing the total evolution operator into short segments in such a way that the Hamiltonian does not change significantly. For instance,

$$\hat{U}(t,t_0) = \prod_{n=0}^{N-1} \hat{U}((n+1)\Delta t, n\Delta t) \tag{2.10}$$

where $\Delta t = t/N$. The spatial discretisation also has a direct influence on the time-propagation as the kinetic energy spectrum is different for different choices of Δr (see below). The most commonly used short- and long- time propagators are discussed briefly below.

2.3.1 The second-order differencing scheme(SOD)

In the second-order differencing(SOD) scheme[85, 88] which is also referred to as the explicit method[188], the temporal evolution of the wavefunction is carried out as follows:

$$\Psi^{n+1} = \Psi^{n-1} - \frac{2i\Delta t}{\hbar}\hat{H}\Psi^n + O(\Delta^3) \tag{2.11}$$

where Ψ^{n+1}, Ψ^{n-1} and Ψ^n are the wavefunctions at $(n+1)$, $(n-1)$ and n^{th} steps respectively. Therefore, once we know the wavefunction at $(n-1)$ and n^{th} steps, we can use the above relation to evaluate the wavefunction at the $(n+1)^{th}$ step. Eq.(2.11) can be easily obtained by the following route:

$$\Psi^{n+1} - \Psi^{n-1} = (\hat{U} - \hat{U}^{\dagger})\Psi^n \tag{2.12}$$

where U and $U^{\dagger}$ are the time-evolution operators. By expanding them using the Taylor series and truncating after the second-order term we get

$$\Psi^{n+1} = \Psi^{n-1} - \frac{2i\Delta t}{\hbar}\hat{H}\Psi^{n} + O(\Delta^3) \tag{2.13}$$

In order to use the SOD scheme, we need to know the wavefunction at $(n-1)^{th}$ and n^{th} steps[85, 88]. This scheme conserves both norm and energy. However, it requires a small time increment (Δt) for numerical stability as otherwise contributions from higher order terms in Δt will accumulate and make the scheme unstable. The stability criteria for step-size (Δt) can be obtained by considering the maximum energy (E_{max}) on the grid that has been introduced by the spatial discretisation. E_{max} is obtained by

$$\begin{aligned} E_{max} &= T_{max} + V_{max} \\ T_{max} &= \frac{p_{max}^2}{2m} = \frac{k_{max}^2\hbar^2}{2m} \end{aligned} \tag{2.14}$$

In the Fourier method

$$k_{max} = \frac{\pi}{\Delta r} \tag{2.15}$$

Substituting eq.(2.15) in (2.14) results in

$$E_{max} = \frac{\hbar^2\pi^2}{2m(\Delta r)^2} + V_{max} \tag{2.16}$$

From time-energy uncertainty relation we can estimate the critical value of the time step

$$\Delta t_{crit} \simeq \frac{\hbar}{E_{max}} \tag{2.17}$$

Therefore, we have to choose Δt which is smaller than Δt_{crit}. Any time step larger than this will make the scheme unstable. For all practical calculations Kosloff and Kosloff[85] recommended that

$$\Delta t = \frac{\Delta t_{crit}}{5} \tag{2.18}$$

be used. This method is easy to implement and it also conserves the norm of Ψ and energy. It can also be applied to situations where the Hamiltonian is explicitly time-dependent. Another important point to be stressed is that the Hamiltonian must be strictly Hermitian. Therefore, it cannot be used in conjunction with absorbing boundary conditions(see below). In such situations one can use first order propagation scheme[91].

2.3.2 The split operator method(SOP)

Feit and Fleck[82] introduced this scheme to solve the paraxial wave equation in optical fibres. Subsequently they extended this scheme to solve the Schrödinger equation as well[83, 84]. According to this scheme, the time-evolution operator is approximated as,

$$exp(-i\Delta t\hat{H}/\hbar) = exp(-i\Delta t\hat{T}/2\hbar)exp(-i\Delta t\hat{V}/\hbar)exp(-i\Delta t\hat{T}/2\hbar) + O(\Delta t^3) \quad (2.19)$$

Therefore, a single step propagation in time consists of the following steps: (i) the coordinate space wavefunction is Fourier transformed into momentum space and then multiplied at each grid point by half kinetic energy propagator, $exp(\frac{-i\Delta t}{2\hbar}\frac{\hat{p}^2}{2m})$, and then the wavefunction is inverse Fourier transformed into coordinate space, (ii) potential energy part is then evaluated by multiplying Ψ at each grid point by $exp(\frac{-i\Delta t\hat{V}}{\hbar})$ and (iii) step (i) is again carried out to complete a full step time-evolution.

As a result of the noncommutability of the kinetic and potential energy operators, the error accumulates in third order of Δt. This propagation scheme is unitary and conserves only the norm. The critical time-step needed for time-evolution can be determined by

$$\Delta t_{crit} < \frac{\pi}{3\Delta V}$$

where $\Delta V = V_{max} - V_{min}$. V_{max} and V_{min} are the maximum and minimum potential energy represented on the grid respectively. In comparison with the SOD scheme, we can choose

slightly larger time step in the SOP scheme. Also this method(SOP) is stable when an absorbing boundary is included.

Since the Fourier transformation is carried out four times for each step propagation, this scheme is computationally more time consuming, especially for larger dimensions. However, in practice, except for the first and the last step, the half kinetic energy operator is merged so that the action of the kinetic energy operator is evaluated in full time step.

2.3.3 The Chebyschev method

The propagation schemes considered thus far are applicable only in situations where the dynamics takes place in short time scale. However, the Chebyschev propagation scheme is a global one, meaning thereby that the time step can be taken larger[91, 186, 189]. Therefore, the Chebyschev method is, in principle, useful for investigating long time dynamical events such as reactive scattering involving complex formation, multiphoton absorption/dissociation, vibrational predissociation etc. According to this method, the time-evolution operator is approximated in terms of a Chebyschev polynomial expansion. Since the Chebyschev polynomial is bound in the interval (-1,1), the Hamiltonian has to be renormalised by shifting its eigenvalues to this range. This can be obtained from a rough estimate of the eigenvalues of the Hamiltonian. For instance, the maximum energy represented on the grid in the FFT method is

$$E_{max} = \frac{\pi^2\hbar^2}{2\mu(\Delta r)^2} + V_{max} \tag{2.20}$$

and the minimum energy is

$$E_{min} = V_{min} \tag{2.21}$$

Thus, the average energy is

$$\overline{E} = \frac{E_{max} + E_{min}}{2} \tag{2.22}$$

and the range is

$$\Delta E = \frac{E_{max} - E_{min}}{2} \tag{2.23}$$

The renormalisation of the Hamiltonian operator is then obtained by

$$\hat{H}_{norm} = \frac{\hat{H} - \hat{I}\,\overline{E}}{\Delta E} \tag{2.24}$$

where $\hat{I}$ is the identity operator. Now the time-evolution operator can be rewritten as

$$exp\left(\frac{-i\hat{H}t}{\hbar}\right) = exp\left(\frac{-it\overline{E}}{\hbar}\right) exp\left(\frac{-i\Delta E t\hat{H}_{norm}}{\hbar}\right) \tag{2.25}$$

Expanding the second exponential term in the above equation in terms of complex Chebyschev polynomials leads to

$$exp\left(\frac{-i\hat{H}t}{\hbar}\right) = exp\left(\frac{-it\overline{E}}{\hbar}\right) \sum_{n=0}^{\infty} C_n J_n\left(\frac{\Delta E t}{\hbar}\right) T_n\left(-i\hat{H}_{norm}\right) \tag{2.26}$$

where $C_n = 1$ for $n = 0$ and $C_n = 2$ for $n \geq 1$. The J_n's are Bessel functions of the first kind, of order n. $T_n(-i\hat{H}_{norm})$ are complex polynomials satisfying the recurrence relation

$$\phi_{n+1} = -2i\hat{H}_{norm}\phi_n + \phi_{n+1} \tag{2.27}$$

where $\phi_n = T_n(-i\hat{H}_{norm})\Psi(0)$ with the condition $\phi_1 = \Psi(0)$ and $\phi_2 = -i\hat{H}_{norm}\Psi(0)$. The Bessel function $J_n(\alpha)$, where $\alpha = \frac{\Delta E t}{\hbar}$, decays exponentially for $n > \alpha$. Especially for larger α, $J_n(\alpha)$ decays rather rapidly. Therefore, one has to include a few extra terms above $n = \alpha$ for convergence.

For all practical purposes the minimum number of expansion terms should be about 40, as otherwise additional terms above $n = \alpha$ needed for convergence becomes dominant and

the method become inefficient[87, 186]. In the Chebyschev scheme, there is no restriction on the size of the time step. One can even complete the entire time-propagation in a single step. However, a major disadvantage with this global propagation scheme is that the intermediate results are not available. For example, processes such as photodissociation and resonance Raman scattering etc., mainly relay on the short time dynamics of the wavefunction on the excited electronic state. In order to apply the Chebyschev method to such short time dynamical processes we have to consider the time dependence of the expansion coefficients in eq.(2.26) as they are time-dependent.

Using the time evolution operator obtained in eq.(2.26) , we can write the time evolving wavefunction as

$$\Psi(t) \;=\; exp\left(\frac{-i\overline{E}t}{\hbar}\right)\sum_{n=0}^{\infty} C_n J_n\left(\frac{\Delta E t}{\hbar}\right)\Phi_n(-i\hat{H}_{norm})\Psi(0) \tag{2.28}$$

For processes such as photoabsorption, the cross section is computed by Fourier transforming the autocorrelation function (see below) as

$$\sigma(\omega) \propto \int_{-\infty}^{\infty} e^{i\omega t}\,\langle\,\Psi(0)\,|\,\mu\,|\,\Psi(t)\,\rangle\,dt \tag{2.29}$$

Substituting for $\Psi(t)$ from eq.(2.28) and carrying out the Fourier transformation leads to

$$\sigma(\omega) \propto \sum_{n=0}^{\infty} b_n\left(\frac{\hbar(\omega-\omega_0)}{\Delta E}\right)\langle\,\Psi(0)\,|\,\mu\,|\,\phi_n\,\rangle \tag{2.30}$$

where $\omega_0 \;=\; (\overline{E}+E_{shift})/\hbar$. E_{shift} is the energy difference between the ground and the excited electronic state and $\phi_n = \Phi_n(-i\hat{H}_{norm})\Psi(0)$. b_n's are the Fourier transform of the Bessel functions (J_n).

For n = even,

$$b_n\left(\frac{\hbar(\omega-\omega_0)}{\Delta E}\right) \;=\; 4\left(1-\left(\frac{\hbar(\omega-\omega_0)}{\Delta E}\right)^2\right)^{-1/2} cos\left(n\;sin^{-1}\left(\frac{\hbar(\omega-\omega_0)}{\Delta E}\right)\right)$$

for n = odd,

$$b_n\left(\frac{\hbar(\omega-\omega_0)}{\Delta E}\right) = 4\left(1-\left(\frac{\hbar(\omega-\omega_0)}{\Delta E}\right)^2\right)^{-1/2} sin\left(n\ sin^{-1}\left(\frac{\hbar(\omega-\omega_0)}{\Delta E}\right)\right)$$

and $b_0 = 2\left(1-\left(\frac{\hbar(\omega-\omega_0)}{\Delta E}\right)\right)^{-1/2}$. Simulations carried out for the impulsive absorption spectrum of CsI yielded converged results[51]. Similar study has also been carried out for resonance Raman scattering as well[87]. This method is particularly efficient for calculating the absorption spectra of more complicated system.

A major inadequacy of this approach is that it cannot be used for explicitly time-dependent Hamiltonians, as the evolution operator then cannot be expanded in Taylor series.

2.3.4 The short iterative Lanczos(SIL) scheme

This method consists of two steps: (i) the Hamiltonian operator is reduced to a tridiagonal matrix form and (ii) the numerical solution of the TDSE is obtained by diagonalising the tridiagonal matrix[91, 190–192]. The tridiagonal matrix is much smaller compared to the actual Hamiltonian matrix and it spans only a reduced subspace of the original Hamiltonian. The tridiagonal matrix is constructed via the following steps:

$$\hat{H}\phi_0 = \alpha_0\phi_0 + \beta_0\phi_1 \tag{2.31}$$

and

$$\hat{H}\phi_j = \beta_{j-1}\phi_{j-1} + \alpha_j\phi_j + \beta_j\phi_{j+1} \quad , j = 1, N_{L-1} \tag{2.32}$$

where N_L is the number of Lanczos recursions and $\phi(0) = \Psi(0)$. The ϕ_j's are constructed such that they are orthonormal and the coefficients α_j and β_j are obtained by the usual

Hilbert space inner products:

$$\alpha_j = (\phi_j, \hat{H}\phi_j) \tag{2.33}$$

$$\beta_j = (\phi_{j-1}, \hat{H}\phi_j) \tag{2.34}$$

The reduced Hamiltonian operator has the following tridiagonal matrix form:

$$\hat{H}_{N_L} = \begin{pmatrix} \alpha_0 & \beta_0 & 0 & \cdots & \cdots & 0 \\ \beta_0 & \alpha_1 & \beta_1 & 0 & \cdots & 0 \\ 0 & \beta_1 & \alpha_2 & \beta_2 & \cdots & 0 \\ \vdots & \vdots & \vdots & \ddots & \vdots & \vdots \\ 0 & 0 & 0 & \cdots & \alpha_{N_L-2} & \beta_{N_L-2} \\ 0 & 0 & 0 & \cdots & \beta_{N_L-2} & \alpha_{N_L-1} \end{pmatrix} \tag{2.35}$$

which is $N_L \times N_L$ compared to $N \times N$ (where N is the total number of grid points) of the original Hamiltonian.

In terms of $\hat{H}_{N_L}$ we can write the evolution operator as

$$\hat{U}(\Delta t) = e^{-i\Delta t \hat{H}_{N_L}/\hbar} \tag{2.36}$$

For Δt of the order of tenth of a fs, 5–10 iterations are sufficient to construct the tridiagonal matrix. Diagonalisation of the evolution operator can be efficiently carried out so that the evolution operator becomes

$$\hat{U}(\Delta t) = Z^{\dagger} e^{-i\Delta t D_{N_L}/\hbar} Z \tag{2.37}$$

where Z is a unitary matrix that diagonalises $\hat{H}_{N_L}$ and $Z^{\dagger}$ is the Hermitian transpose of Z. D_{N_L} is the diagonal matrix of eigenvalues. Thus the time-evolving wavefunction is written as

$$\Psi(t + \Delta t) = \sum_{n=0}^{N_L-1} Z^{\dagger} e^{-i\Delta t D_{N_L}/\hbar} Z \phi_n \tag{2.38}$$

The number of recursions depends on the time step as well as the initial choice for ϕ_0 - a good initial guess for ϕ_0 leads to very fast convergence scheme. SIL scheme is unconditionally stable and it preserves norm and energy. Unlike Chebyschev method where the error is distributed uniformly, in this method the error is larger for larger eigenvalues. If the number of recursions increases then there can be rapid loss of orthogonality of the recursion vectors. Therefore, it is always desirable to keep the recursion number small. Also the error starts building up, if the recursion vectors span outside the tridiagonal space. The error analysis carried out by Park and Light[94, 193] predicts that the Lanczos method can be used efficiently provided that a good initial guess is used to initiate the recursion and small enough time steps are employed so that the convergence becomes fast and storage requirement becomes small.

2.3.5 The integral equation approach

Kouri and coworkers[194–197] have pioneered the integral equation approach for solving the TDSE. An attractive feature of this method is that it is applicable for both time-dependent and time-independent Hamiltonians. In the following, we summarise briefly the methodology and the computational algorithm of the integral equation approach.

Let us consider a situation where the potential energy part is explicitly time-dependent as it happens in the interaction of radiation with atoms and molecules (see below). Then the TDSE will have the form

$$i\hbar\frac{\partial\Psi(R,t)}{\partial t} = \left\{\hat{T}(R) + \hat{V}(R,t)\right\}\Psi(R,t) \tag{2.39}$$

where $\hat{T}(R)$ is the kinetic energy operator. For mathematical simplicity let us rewrite eq.(2.39) as

$$i\hbar\frac{\partial\Psi(R,t)}{\partial t} - \hat{T}(R)\Psi(R,t) = \hat{V}(R,t)\Psi(R,t) \tag{2.40}$$

By left-multiplying both the sides by $-\frac{i}{\hbar}e^{i\hat{T}(R)t/\hbar}$ we get

$$e^{i\hat{T}(R)t/\hbar}\left\{\frac{\partial\Psi(R,t)}{\partial t}+\frac{i}{\hbar}\hat{T}(R)\Psi(R,t)\right\} = -\frac{i}{\hbar}e^{i\hat{T}(R)t/\hbar}\hat{V}(R,t)\Psi(R,t) \tag{2.41}$$

However, we know that

$$\begin{aligned}\frac{\partial}{\partial t}\left(e^{i\hat{T}(R)t/\hbar}\Psi(R,t)\right) &= e^{i\hat{T}(R)t/\hbar}\left(\frac{i\hat{T}(R)}{\hbar}\right)\Psi(R,t)+e^{i\hat{T}(R)t/\hbar}\frac{\partial\Psi(R,t)}{\partial t}\\ &= e^{i\hat{T}(R)t/\hbar}\left\{\frac{\partial\Psi(R,t)}{\partial t}+\frac{i}{\hbar}\hat{T}(R)\Psi(R,t)\right\}\end{aligned} \tag{2.42}$$

Substituting eq.(2.42) in eq.(2.41) results in

$$\frac{\partial}{\partial t}\left(e^{i\hat{T}(R)t/\hbar}\Psi(R,t)\right) = -\frac{i}{\hbar}e^{i\hat{T}(R)t/\hbar}\hat{V}(R,t)\Psi(R,t) \tag{2.43}$$

Upon integrating this equation between the limits t and t'' leads to

$$\begin{aligned}e^{i\hat{T}(R)t''/\hbar}\Psi(R,t'') &= e^{i\hat{T}(R)t/\hbar}\Psi(R,t)\\ &\quad -\frac{i}{\hbar}\int_t^{t''}dt'e^{i\hat{T}(R)t'/\hbar}\hat{V}(R,t')\Psi(R,t')\end{aligned} \tag{2.44}$$

Now, operating on both sides by $e^{-i\hat{T}(R)t''/\hbar}$ yields

$$\begin{aligned}\Psi(R,t'') &= e^{-i\hat{T}(R)(t''-t)/\hbar}\Psi(R,t)\\ &\quad -\frac{i}{\hbar}\int_t^{t''}dt'e^{-i\hat{T}(R)(t''-t)/\hbar}\hat{V}(R,t')\Psi(R,t')\end{aligned} \tag{2.45}$$

This equation is the central equation for the time evolution in the integral equation approach. In order to make this equation computationally feasible, we make use of the trapezoidal rule for the integral that is appearing in eq.(2.45). Thus,

$$\begin{aligned}\Psi(R,t'') &= e^{-i\hat{T}(R)(t''-t)/\hbar}\Psi(R,t)\\ &\quad -\frac{i}{\hbar}\left(\frac{(t''-t)}{2}\left\{e^{-i\hat{T}(R)(t''-t)/\hbar}\hat{V}(R,t)\Psi(R,t)\right\}\right)\end{aligned} \tag{2.46}$$

By substituting $t'' = t + \tau$, we obtain

$$\Psi(R, t+\tau) = e^{-i\hat{T}(R)\tau/\hbar}\Psi(R,t) - \frac{i\tau}{2\hbar}\left(e^{-i\hat{T}(R)\tau/\hbar}\hat{V}(R,t)\Psi(R,t) + \hat{V}(R,t+\tau)\Psi(R,t+\tau)\right) \quad (2.47)$$

On rearranging eq.(2.47) we get

$$\left(1+\frac{i\tau}{2\hbar}\hat{V}(R,t+\tau)\right)\Psi(R,t+\tau) = e^{-i\hat{T}(R)\tau/\hbar}\left(1-\frac{i\tau}{2\hbar}\hat{V}(R,t)\right)\Psi(R,t)$$

or

$$\Psi(R,t+\tau) = \left(1+\frac{i\tau}{2\hbar}\hat{V}(R,t+\tau)\right)^{-1} e^{-i\hat{T}(R)\tau/\hbar}\left(1-\frac{i\tau}{2\hbar}\hat{V}(R,t)\right)\Psi(R,t) \quad (2.48)$$

Thus the kinetic energy operator is flanked by the time-dependent potential energy operators. This approach is also referred to as kinetic referenced modified Cayley (KRMC) approach. It is important to note that the time-ordering property has been retained in the eq.(2.48). Since the terms $\left(1+\frac{i\tau}{2\hbar}\hat{V}(R,t+\tau)\right)$ and $\left(1-\frac{i\tau}{2\hbar}\hat{V}(R,t)\right)$ are the first two terms of the Taylor series expansion of $exp(i\tau\hat{V}(R,t+\tau)/2\hbar)$ and $exp(-i\tau\hat{V}(R,t)/2\hbar)$ respectively, we can replace them by their appropriate exponentials. Hence, eq.(2.48) becomes

$$\Psi(R,t+\tau) = exp(\frac{-i\tau}{2\hbar}\hat{V}(R,t+\tau))exp(\frac{-i\tau}{\hbar}\hat{T}(R))exp(\frac{-i\tau}{2\hbar}\hat{V}(R,t+\tau))\Psi(R,t) \quad (2.49)$$

This equation is similar to that discussed in the split-operator method except for the time-dependent potential energy part. The time-evolution can be accomplished by evaluating the kinetic and potential energy operators in the representations in which they are local.

In a recent study, Truong et al. [92] have compared the efficiency and accuracy of the second and third order split-operator method (see below), the integral equation approach (KRMC) and the Chebyschev polynomial expansion method. Their study shows that the KRMC method is highly recommendable for short time dynamics as (i) this approach

requires only 2 FFT calls for each time step propagation, (ii) the trapezoidal rule that is employed in approximating the integral is a linear function of time; hence, one can choose larger time step as well, (iii) the Hamiltonian may be either time-dependent or time-independent and (iv) the norm and energy are conserved. However, for long time dynamics the Chebyschev method is preferable in comparison with the KRMC method. But if the potential under consideration is time-dependent, then one has to use the integral equation approach.

2.3.6 The exponential split operator method

Bandrauk and coworkers[181, 198, 199] have developed the exponential split operator method, as an extension of the split operator method discussed earlier(section 2.3.2). It is superior to its predecessor in that it is applicable for both time-dependent and time-independent Hamiltonians.

For time-dependent Hamiltonians, the time-evolution operator will have the form

$$\hat{U}(t+\Delta t,t) = \hat{T}exp\left(\frac{-i}{\hbar}\int_t^{t+\Delta t}\hat{H}(t)dt\right) \tag{2.50}$$

where $\hat{T}$ is the time-ordering operator. By expanding eq.(2.50) one obtains

$$\hat{U}(t+\Delta t,t) = exp\left(\frac{-i}{\hbar}\int_t^{t+\Delta t}\hat{H}(t)dt\right) + D_3(t)(i\Delta t/\hbar)^3 + D_4(t)(i\Delta t/\hbar)^4 + .. \tag{2.51}$$

where $D_3(t)$ and $D_4(t)$ are higher order terms in commutators of $\hat{H}(t)$. The unitarity property of the time-evolution operator allows us to omit the even order error terms in eq.(2.51), as they are real quantities and vanish. Therefore, $\hat{U}(t+\Delta t,t)$ becomes

$$\hat{U}(t+\Delta t,t) = exp\left(\frac{-i}{\hbar}\int_t^{t+\Delta t}\hat{H}(t)dt\right) + D_3(t)(i\Delta t/\hbar)^3 + D_5(t)(i\Delta t/\hbar)^5 + .. \tag{2.52}$$

In order to develop the new propagation scheme, let us split the time interval $(t+\Delta t)$ into $(t+s\Delta t,t)$, $(t+(1-s)\Delta t,t+s\Delta t)$ and $(t+\Delta t,t+(1-s)\Delta t)$ subintervals. $\hat{U}(t+\Delta t,t)$

will then become

$$\hat{U}(t+\Delta t,t) = \hat{U}(t+s\Delta t,t)\hat{U}(t+(1-s)\Delta t,t+s\Delta t)\hat{U}(t+\Delta t,t+(1-s)\Delta t) \quad (2.53)$$

The time evolution operator for each of the subintervals can be obtained by making use of eq.(2.52) as

$$\begin{aligned}\hat{U}(t+s\Delta t,t) &= exp\left(\frac{-i}{\hbar}\int_t^{t+s\Delta t}\hat{H}(t)dt\right)+D_3(t)\times(s\Delta t)^3+O(\Delta t)^5 \\ &= S_3(t+s\Delta t,t)+[C_3(t)+D_3(t)]\times(s\Delta t)^3+O(\Delta t)^5 \qquad (2.54)\end{aligned}$$

where $S_3(t+s\Delta t,t) = exp(-is\Delta tA/2\hbar)exp(-iB/\hbar)exp(-is\Delta tA/2\hbar)$ with $A=\hat{T}(R)$ and $B=\int_t^{t+s\Delta t}V(R,t)dt$.

Similarly,

$$\begin{aligned}\hat{U}(t+(1-s)\Delta t,t+s\Delta t) &= S_3(t+(1-s)\Delta t,t+\Delta t) \\ &\quad +[C_3(t)+D_3(t)]\times[(1-2s)s\Delta t]^3+O(\Delta t)^5 \qquad (2.55)\end{aligned}$$

where

$$\begin{aligned}S_3(t+(1-s)\Delta t,t+s\Delta t) &= exp(-i(1-2s)\Delta tA/2\hbar)exp(-iB/\hbar) \\ &\quad exp(-i(1-2s)\Delta tA/2\hbar)\end{aligned}$$

with $A=\hat{T}(R)$ and $B=\int_{t+s\Delta t}^{t+(1-s)\Delta t}V(R,t)dt$ and

$$\begin{aligned}\hat{U}(t+\Delta t,t+(1-s)\Delta t) &= S_3(t+\Delta t,t+(1-s)\Delta t) \\ &\quad +[C_3(t)+D_3(t)]\times(s\Delta t)^3+O(\Delta t)^5 \qquad (2.56)\end{aligned}$$

where

$$S_3(t+\Delta t,t+(1-s)\Delta t) = exp(-is\Delta tA/2\hbar)exp(-iB/\hbar)exp(-is\Delta tA/2\hbar)$$

with $A = \hat{T}(R)$ and $B = \int_{t+(1-s)\Delta t}^{t+\Delta t} V(R,t)dt$. Therefore, combining eq.(2.54), (2.55) and (2.56) we obtain

$$\hat{U}(\Delta t) = S_3(s\Delta t)S_3((1-2s)\Delta t)S_3(s\Delta t) + [2s^3 + (1-2s)^3] \times [C_3(t) + D_3(t)]\Delta t^3 + O(\Delta t)^5 \quad (2.57)$$

where $C_3(t)$ and $D_3(t)$ are higher order commutators. When s satisfies the equation $2s^3 + (1-2s)^3 = 0$, the leading error in Δt^3 vanishes even for a time-dependent potential. Thus the eq.(2.55) can be used to accomplish the time propagation. An important point to note is that the time-dependent potential which is appearing in equations (2.54–2.56) can be solved by using the middle point formula[199]:

$$\int_t^{t+\Delta t} f(t)dt = \Delta t f(t + \Delta t/2) + O(\Delta t^3) \quad (2.58)$$

More recently, Bandrauk and Shen[181] have applied this method to investigate the photodissociation of H_2^+ molecule by an intense laser pulse. The kinetic energy operator has been evaluated using the FFT method. Since the higher order split operator is unitary, the norm of the wavefunction is conserved for all the time steps. An added advantage of the higher order splitting scheme is that the phase of the wavefunction is also reproduced. Therefore, this is an ideal scheme for evaluating the eigenvalues. Also this method can be applied to studying nonadiabatic processes.

In addition to these methods, recently, Fujimura and coworkers[200] have introduced a *sliced propagator method* for solving the TDSE with explicitly time-dependent potentials. According to this propagation scheme, the time evolution operator is sliced into several small segments in such a way that the time evolving wave packet becomes

$$\begin{aligned} \phi(t+\epsilon) &= \hat{U}(\epsilon)\phi(t) \\ &= exp(-i\hat{H}(t)\epsilon/\hbar)\phi(t) \end{aligned} \quad (2.59)$$

where ϵ is an infinitesimally small time step. The sliced-propagator, $\hat{U}(\epsilon)$, is expanded in Taylor series and the terms up to third-order are retained. Therefore,

$$\hat{U}(\epsilon) = 1 + \left(\frac{-i\hat{H}(t)\epsilon}{\hbar}\right) + \frac{1}{2!}\left(\frac{-i\hat{H}(t)\epsilon}{\hbar}\right)^2 + \frac{1}{3!}\left(\frac{-i\hat{H}(t)\epsilon}{\hbar}\right)^3 \tag{2.60}$$

This method was employed to investigate the above-threshold dissociation of H_2^+ molecular ions. It was used in conjunction with FFT method for spatial evolution and the norm was found to be conserved for substantially small time steps.

2.3.7 Long time dynamics

In the earlier sections we have discussed various short time and long time propagation methods. However, if the process of interest is one of the following kind: (i) reactions involving intermediate complex formation (ii) nonadiabatic coupling between electronic states occurring at large internuclear distances (iii) unimolecular dissociation processes such as vibrational predissociation and (iv) systems having heavier masses, then one is expected to time evolve the wavefunction long enough to complete the process. One of the major difficulties with the long time dynamical processes is that a portion of the wavefunction (fast moving component) reaches the grid edge (asymptotic limit) while other portions of it are residing in the interaction region[201, 202]. Those components which are reaching the grid edge will show spurious oscillations and lead to error in the calculation. One way of circumventing this problem is to use larger spatial grid. However, this is not advisable as this makes the process computer intensive. Several authors have proposed various numerical methods (described below) to study the long time dynamical processes without extending the grid size.

For instance, Neuhauser and Baer[203] have successfully demonstrated in collinear H + H_2 reaction that a negative imaginary potential(NIP) can be used to absorb the product

channel wave packets whenever they are reaching near the grid edge. They have also shown that the inclusion of a NIP does not alter the reaction probability results. Subsequently, Neuhauser et al.[204–206] have explicitly derived the functional form of the NIP and the selection criterion for it. The widely used absorbing boundary has the form:

$$V_{abs} = \begin{cases} -iV_{i0}\frac{R-R_{abs}}{\Delta R_{abs}} & R_{abs} < R \leq R_{abs} + \Delta R_{abs} \\ 0 & R \leq R_{abs} \end{cases} \tag{2.61}$$

where V_{i0} is the height of the absorbing potential and ΔR is its width. R_I is the internuclear distance at which the absorbing potential starts building up. Invariably R_I is selected far away from the interaction region.

The height and width of the absorbing potential are selected based on the energy(E) of the time-evolving wave packet. It has been shown by Neuhauser et al.[204, 205] that the height of the absorbing potential must satisfy the following condition:

$$\frac{E^{1/2}}{\sqrt{8\mu}\Delta R} \leq V_{i0} \leq \sqrt{8\mu}\Delta R E^{3/2} \tag{2.62}$$

where μ is the reduced mass of the system. Similarly the width of the absorbing potential must be such that

$$\frac{E_{max}^{1/4}}{\sqrt{8\mu}E_{min}^{3/4}} \leq \Delta R \tag{2.63}$$

where $E_{max} = \frac{\pi^2\hbar^2}{2\mu(\Delta R)^2} + V_{max}$ and $E_{min} = V_{min}$.

Since the product channel wave packet is absorbed near the grid boundary, one has to use alternative methods to compute the final state distribution. Recently, Child has carried out a detailed analysis of the properties of the complex absorbing potential[207]. Several reactive scattering[94, 208, 209] and photodissociation[125, 170] calculations have been performed using the absorbing potentials and they have shown that the absorbing potentials are highly useful when the dynamics requires long time propagation. More

recently, Vibok and Balint-Kurti have discussed various functional forms of the absorbing potentials and their applications[210, 211].

One of the major drawbacks in using the absorbing potential is that the information contained in the wavefunction is lost once it is absorbed. In order to circumvent this problem Heather and Metiu had proposed the wavefunction splitting algorithm[212, 213]. According to this algorithm, the time evolving wavefunction is split into an interaction part, $\Psi_I(R,t)$, and an asymptotic part, $\Psi_A(R,t)$, before it reaches the grid boundary. The splitting is carried out efficiently using a splitting function ($f(R)$) as follows:

$$\Psi_{I,1}(R_m,t_1) = f(R_m)\Psi(R_m,t_1), m = 1,2,\ldots N \tag{2.64}$$

and

$$\Psi_{A,1}(R_m,t_1) = (1-f(R_m))\Psi(R_m,t_1), m = 1,2,\ldots N \tag{2.65}$$

where the subscript 1 refers to the splitting performed at time t_1. The function $f(R)$ is chosen such that it remains 1 throughout the interaction region and decays smoothly to zero near the asymptotic region. For instance,

$$f(R) = \frac{1}{1+exp(-\alpha(R-\overline{R}))} \tag{2.66}$$

The parameters α and $\overline{R}$ are chosen depending upon the size of the asymptotic region. It is worthwhile to add that the time evolving wavefunction is not altered by this splitting procedure as we have only multiplied $\Psi(R,t)$ by $1 = f(R) + 1 - f(R)$. Since the time evolution operator is linear, both $\Psi_I(R,t)$ and $\Psi_A(R,t)$ can be propagated independently. As we know that $\Psi_A(R,t)$ is in the force-free region, i.e., V(R) = 0, its temporal evolution is obtained by multiplying it with the free particle propagator at each momentum grid point as

$$\Psi_A(t_1+n\Delta t,p_j) = exp\left(-\frac{i\ n\Delta t p_j^2}{2\mu\hbar}\right)\Psi_A(t_1,p_j)\ \ j = 1,2,\ldots N \tag{2.67}$$

where p_j's are the momentum values discretised as $p_j = (j - N/2 - 1)\Delta p, j = 1, 2, \ldots N$ with $\Delta p = \frac{2\pi\hbar}{L}$, where L is the length of the grid in coordinate space.

The time evolution of the interaction region wavefunction is carried out by applying any one of the time propagation methods discussed earlier. Further wavefunction splitting is carried out when a part of the time evolving wavefunction reaches near the grid boundary as

$$\Psi_{I,2}(R_m, t_2) = f(R_m)\Psi_{I,1}(R_m, t_2), m = 1, 2, \ldots N \tag{2.68}$$

and

$$\Psi_{A,2}(R_m, t_2) = (1 - f(R_m))\Psi_{I,1}(R_m, t_2), m = 1, 2, \ldots N \tag{2.69}$$

where t_2 is the time at which the 2^{nd} splitting is performed. Again the asymptotic and interaction region wavefunctions are propagated in the same way as discussed above and the splitting is carried out whenever the interaction region wavefunction reaches the edge of the grid. The splitting frequency depends upon the size of the asymptotic region. If the asymptotic region is small, then greater number of splittings are required. This procedure is continued till all the wavefunction residing in the interaction region reaches the asymptotic region. In the end, after M splittings, we can reassemble the wavefunction in the momentum space in the following manner:

$$\Psi(t_f, p_j) = \sum_{\alpha=1}^{M} exp\left(\frac{-i[t_f - t_\alpha]p_j^2}{2\mu\hbar}\right)\Psi_{A,\alpha}(t_\alpha, p_j), \quad j = 1, 2, \ldots N. \tag{2.70}$$

where the asymptotic pieces $\Psi_{A,\alpha}$ which have been separated at times $t_\alpha, \alpha = 1, 2, \ldots M$, are propagated from t_α to t_f by the application of a free particle propagator in the momentum space, and are added coherently. This method is easy to implement and it does not require much numerical effort.

Metiu and coworkers have extended this method to determine the final state distribution in the case of polyatomic photofragmentation[212–214]. For further applications please see reference [94].

Thus far we have concentrated mainly on the elimination of the wavefunction reflection from the grid edge. The spreading of the wavefunction all over the grid is an inherent property of the Schrödinger picture wavefunction as it contains both kinematical and dynamical information. However, if the TDQM calculations are performed in the interaction picture formalism, the wavefunction spreading can be avoided to a large extent. Since the kinematic information is removed in the interaction picture wavefunction (see below), it does not spread or translate in the coordinate space. As a result, one can chose smaller spatial grid and larger time step in the interaction picture formalism. Recently, Zhang and coworkers have utilised this method to study the vibrational predissociation[215–218] and molecule surface scattering processes[219]. The interaction picture wavefunction is obtained from the Schrödinger picture wavefunction through unitary transformation as

$$\Psi_I(t) = exp\left(i\hat{H}_0 t/\hbar\right)\Psi_S(t) \tag{2.71}$$

$$= exp\left(i\hat{H}_0 t/\hbar\right) exp\left(-i\hat{H}t/\hbar\right)\Psi_S(0) \tag{2.72}$$

where $\hat{H} = \hat{H}_0 + \hat{V}$ and $\hat{H}_0$ and $\hat{V}$ are the free part of the Hamiltonian and the interaction potential respectively. From eq.(2.71) it is clear that $\Psi_I(t)$ is obtained by back propagating $\Psi_S(t)$ with the free Hamiltonian $\hat{H}_0$. Interestingly, both the Schrödinger picture and the interaction picture coincide at time $t = 0$. The Hamiltonian in the interaction picture is obtained by

$$\hat{H}_I = exp\left(i\hat{H}_0 t/\hbar\right)\hat{V} exp\left(-i\hat{H}_0 t/\hbar\right) \tag{2.73}$$

It is important to note that $\hat{H}_I$ is explicitly time-dependent, even when $\hat{V}$ is time-

independent. If we differentiate eq.(2.71) with respect to t and multiply by $i\hbar$, we obtain a Schrödinger type equation

$$i\hbar\frac{\partial\Psi_I(t)}{\partial t} = \hat{H}_I\Psi_I(t) \tag{2.74}$$

This equation can also be written as

$$i\hbar\frac{\partial\Psi_I(t)}{\partial t} = exp\left(i\hat{H}_0t/\hbar\right)\hat{V}\Psi_S t \tag{2.75}$$

Since the interaction picture equations (2.74) and (2.75) are similar to the TDSE eq.(2.1), the time propagation methods discussed earlier can be easily implemented. However, care must be taken, since the interaction picture Hamiltonian is explicitly time-dependent.

Zhang and coworkers[219, 220] and Tannor and coworkers[221–223] have extended this method to obtain product vib-rotational state distributions in vibrational predissociation and photodissociation processes. More recently, Williams et al.[222, 223] have developed a modified version of the above method known as nested-interaction representation and successfully applied it for studying three dimensional (3D) (J=0) photodissociation dynamics of triatomic molecules.

Apart from these numerical methods, more recently, Guo[59] has introduced a novel method while investigating the 3D (J=0) photodissociation of CH_3I. According to this method, the translational coordinate(R) is shifted during the time evolution depending upon the location of the center of the wave packet, $\langle R\rangle$. Since the wave packet remains compact in most of the direct photodissociation processes, the center of the wave packet can be estimated periodically. Whenever the center of the wave packet is larger than the center of the R grid, the grid will be shifted by an amount ΔR so as to accommodate the change. By shifting the grid in this way, the momentum space picture is not affected as the total number of grid points are not changed. The norm has been monitored carefully and the grid edge reflections are successfully avoided by this technique.

2.4 Interaction of radiation with matter

Interaction of radiation with matter is one of the fundamental problems in physics. It has been studied extensively by both semiclassical and quantum mechanical approaches. In the former, the atom or the molecule (matter) is treated quantum mechanically and the electromagnetic radiation is treated classically. Such a treatment gives accurate results for processes like photoabsorption and emission. But it is not adequate to describe purely quantum mechanical phenomena such as spontaneous emission or quantum beats etc. In the following sections we will show how the semiclassical and the quantum mechanical treatments yield the same formula for the single photon absorption process. Such a treatment is essential to see the correspondence between classical and quantum approaches and to obtain an insight into the dynamics.

2.4.1 Semiclassical treatment

As we stated above, the system (i.e., atom or molecule) is described quantum mechanically and the radiation is described classically. To start with, let us consider the relativistically invariant form of the Hamiltonian for the motion of a charged particle in an electromagnetic field[224, 225]:

$$\hat{H} = \frac{1}{2m}\{\ -i\hbar\nabla - \frac{e}{c}\mathbf{A}\ \}^2 + e\phi \tag{2.76}$$

where m is the mass of the particle with charge e and c is the velocity of light. $\mathbf{A}$ and ϕ are the vector and the scalar potentials associated with the field.

The Hamiltonian in eq.(2.76) can be rewritten as,

$$\hat{H} = -\frac{\hbar^2}{2m}\nabla^2 + \frac{i\hbar e}{2mc}\{\nabla.A + A.\nabla\} + \frac{e^2}{2mc^2}\mathbf{A}^2 + e\phi \tag{2.77}$$

From the commutator relation of [A, -$i\hbar\nabla$] we can show that,

$$i\hbar\nabla.(\mathbf{A}\psi) = i\hbar(\nabla.\mathbf{A})\psi + \mathbf{A}.(i\hbar\nabla\psi) \tag{2.78}$$

However, in Coulomb gauge we have $\nabla.\mathbf{A} = 0$ and $\phi = 0$. Therefore,

$$i\hbar\nabla.\mathbf{A} = i\hbar\mathbf{A}.\nabla \tag{2.79}$$

Substituting this result in eq.(2.77) gives,

$$\hat{H} = -\frac{\hbar^2}{2m}\nabla^2 + \frac{i\hbar e}{mc}\mathbf{A}.\nabla + \frac{e^2}{2mc^2}A^2 \tag{2.80}$$

The dynamics of any system in the presence of the electromagnetic field can be obtained by solving the time-dependent Schrödinger equation (TDSE):

$$i\hbar\frac{\partial|\,\Psi(t)\,\rangle}{\partial t} = \{\frac{-\hbar^2}{2m}\nabla^2 + \frac{i\hbar e}{mc}\mathbf{A}.\nabla + \frac{e^2}{2mc^2}A^2 + V(r)\}\,|\,\Psi(t)\,\rangle \tag{2.81}$$

where $|\,\Psi(t)\,\rangle$ represents the state of the system at any time t. Here $V(r)$ is the system potential.

The vector potential **A** describes the time-dependence of the radiation field and can be defined as[224],

$$\mathbf{A}(\mathbf{r},t) = \mathbf{A_0}e^{(i\mathbf{k}.\mathbf{r}-i\omega t)} + \mathbf{A_0^\star}e^{(-i\mathbf{k}.\mathbf{r}+i\omega t)} \tag{2.82}$$

where A_0 is related to both intensity and polarisation of the radiation. The electric and magnetic fields of the radiation are related to **A** as follows:

$$\begin{aligned}\boldsymbol{\epsilon}(\mathbf{r},t) &= i\omega\{\mathbf{A_0}e^{(i\mathbf{k}.\mathbf{r}-i\omega t)} - \mathbf{A_0^\star}e^{(-i\mathbf{k}.\mathbf{r}+i\omega t)}\}\\ \mathbf{B}(\mathbf{r},t) &= (i/\mu_0)\{\mathbf{A_0}e^{(i\mathbf{k}.\mathbf{r}-i\omega t)} - \mathbf{A_0^\star}e^{(-i\mathbf{k}.\mathbf{r}+i\omega t)}\}\end{aligned} \tag{2.83}$$

B(**r**,t) is always oriented perpendicular to $\boldsymbol{\epsilon}$(**r**,t).

For a weak electromagnetic field we can neglect the A^2 term and therefore eq.(2.81) becomes

$$i\hbar\frac{\partial|\,\Psi(t)\,\rangle}{\partial t} = \{\frac{-\hbar^2}{2m}\nabla^2 + V(r) + \frac{i\hbar e}{mc}\boldsymbol{A}.\boldsymbol{\nabla}\}\,|\,\Psi(t)\,\rangle \tag{2.84}$$

The general solution of eq.(2.84) can be written as,

$$|\,\Psi(r,t)\,\rangle = \sum_k c_k(t)\,|\,\psi_k(r)\,\rangle\, e^{-iE_kt/\hbar} \tag{2.85}$$

where summation is over all the discrete and continuous sets of $|\,\psi_k\,\rangle$ and E_k refers to the k^{th} energy eigenvalue of the field free Hamiltonian $\hat{H}_0$ for the system.

For an electronic transition from a discrete level $|\,\psi_i\,\rangle$ to a final state $|\,\psi_f\,\rangle$, the wave-function for the system is written as a linear combination of the initial and final states:

$$|\,\Psi(r,t)\,\rangle = c_i(t)e^{-iE_it/\hbar}\,|\,\psi_i(r)\,\rangle + c_f(t)e^{-iE_ft/\hbar}\,|\,\psi_f(r)\,\rangle \tag{2.86}$$

Substitution of the above expression for $|\,\Psi(r,t)\,\rangle$ in eq.(2.84) and further simplification yields,

$$\begin{aligned} &i\hbar\frac{\partial c_i(t)}{\partial t}e^{-iE_it/\hbar}\,|\,\psi_i(r)\,\rangle + i\hbar\frac{\partial c_f(t)}{\partial t}e^{-iE_ft/\hbar}\,|\,\psi_f(r)\,\rangle \\ &\qquad = \hat{H}(t)c_i(t)e^{-iE_it/\hbar}\,|\,\psi_i(r)\,\rangle + \hat{H}(t)c_f(t)e^{-iE_ft/\hbar}\,|\,\psi_f(r)\,\rangle \end{aligned} \tag{2.87}$$

Now, left-multiplying with $\langle\,\psi_f(r)\,|$ on both sides of eq.(2.87) and integrating over r, we obtain

$$\begin{aligned} &i\hbar\frac{\partial c_i(t)}{\partial t}e^{-iE_it/\hbar}\langle\psi_f|\psi_i\rangle + i\hbar\frac{\partial c_f(t)}{\partial t}e^{-iE_ft/\hbar}\langle\psi_f|\psi_f\rangle \\ &= \langle\,\psi_f\,|\,\hat{H}(t)\,|\,\psi_i\,\rangle\, c_i(t)e^{-iE_it/\hbar} + \langle\,\psi_f\,|\,\hat{H}(t)\,|\,\psi_f\,\rangle\, c_f(t)e^{-iE_ft/\hbar} \end{aligned} \tag{2.88}$$

The first term in the left hand side of the above equation vanishes, because $|\,\psi_i\,\rangle$ and $|\,\psi_f\,\rangle$ are orthonormal.

For a system in the state $|\psi_i\rangle$ before the field is turned "on", $c_i(t=-\infty)=1$ and $c_f(t=-\infty)=0$. In addition, for a weak field $c_i(t)\sim 1$ and $c_f(t)<<1$. Under these conditions, eq.(2.88) becomes[3],

$$\frac{dc_f(t)}{dt} = -\frac{i}{\hbar}\langle\psi_f|\hat{H}(t)|\psi_i\rangle e^{i(E_f-E_i)t/\hbar} \tag{2.89}$$

Substituting for $\hat{H}$(t) we obtain,

$$\begin{aligned}
\frac{dc_f(t)}{dt} &= -\frac{i}{\hbar}\langle\psi_f|\frac{i\hbar e}{mc}\mathbf{A}.\boldsymbol{\nabla}|\psi_i\rangle e^{i(E_f-E_i)t/\hbar} \\
&= -\frac{i}{\hbar}\langle\psi_f|\frac{i\hbar e}{mc}\{\mathbf{A_0}e^{(i\mathbf{k}.\mathbf{r}-i\omega t)}+\mathbf{A_0}^*e^{(-i\mathbf{k}.\mathbf{r}+i\omega t)}\}.\boldsymbol{\nabla}|\psi_i\rangle e^{i(E_f-E_i)t/\hbar} \\
&= \frac{e}{mc}\langle\psi_f|\{\mathbf{A_0}e^{(i\mathbf{k}.\mathbf{r}-i\omega t)}+\mathbf{A_0}^*e^{(-i\mathbf{k}.\mathbf{r}+i\omega t)}\}.\boldsymbol{\nabla}|\psi_i\rangle e^{i(E_f-E_i)t/\hbar} \\
&= \frac{e}{mc}\langle\psi_f|\mathbf{A_0}e^{i\mathbf{k}.\mathbf{r}}.\boldsymbol{\nabla}|\psi_i\rangle e^{i(E_f-(E_i+\hbar\omega))t/\hbar} \\
&\quad +\frac{e}{mc}\langle\psi_f|\mathbf{A_0}^*e^{-i\mathbf{k}.\mathbf{r}}.\boldsymbol{\nabla}|\psi_i\rangle e^{i(E_f+\hbar\omega-E_i))t/\hbar} \\
&= \alpha_{fi}e^{-i(\hbar\omega-(E_f-E_i))t/\hbar}+\alpha_{fi}^*e^{i(\hbar\omega+E_f-E_i)t/\hbar}
\end{aligned} \tag{2.90}$$

where

$$\begin{aligned}
\alpha_{fi} &= \frac{e}{mc}\langle\psi_f|\mathbf{A_0}e^{i\mathbf{k}.\mathbf{r}}.\boldsymbol{\nabla}|\psi_i\rangle \\
\alpha_{fi}^* &= \frac{e}{mc}\langle\psi_f|\mathbf{A_0}^*e^{-i\mathbf{k}.\mathbf{r}}.\boldsymbol{\nabla}|\psi_i\rangle
\end{aligned} \tag{2.91}$$

Therefore,

$$\begin{aligned}
c_f(t) &= \alpha_{fi}\int_0^t dte^{-i(\hbar\omega-(E_f-E_i))t/\hbar}+\alpha_{fi}^*\int_0^t dte^{i(\hbar\omega+(E_f-E_i))t/\hbar} \\
&= \alpha_{fi}\left\{\frac{e^{-i(\omega-\omega_{fi})t}-1}{-i(\omega-\omega_{fi})}\right\}+\alpha_{fi}^*\left\{\frac{e^{i(\omega+\omega_{fi})t}-1}{i(\omega+\omega_{fi})}\right\}
\end{aligned} \tag{2.92}$$

where $\omega_{fi}=(E_f-E_i)/\hbar$

The first term in eq.(2.92) vanishes when $E_f=E_i+\hbar\omega$, i.e., for absorption process and the second term vanishes when $E_f=E_i-\hbar\omega$, i.e., for emission process. Therefore, the

first and the second term in eq.(2.92) represent the absorption and the emission processes respectively.

Photoabsorption

The probability for photoabsorption from state $|\psi_i\rangle$ to state $|\psi_f\rangle$ is, therefore, given by

$$\begin{aligned} P_{fi}(t) &= |c_f(t)|^2 \\ &= |\alpha_{fi}|^2 \left\{ \frac{(e^{-i(\omega-\omega_{fi})t}-1)^*(e^{-i(\omega-\omega_{fi})t}-1)}{(\omega-\omega_{fi})^2} \right\} \\ &= |\alpha_{fi}|^2 \left\{ \frac{1-e^{i(\omega-\omega_{fi})t}-e^{-i(\omega-\omega_{fi})t}+1}{(\omega-\omega_{fi})^2} \right\} \\ &= |\alpha_{fi}|^2 \left\{ \frac{2-2cos([\omega-\omega_{fi}]t)}{(\omega-\omega_{fi})^2} \right\} \\ &= 2|\alpha_{fi}|^2 \left\{ \frac{1-cos([\omega-\omega_{fi}]t)}{(\omega-\omega_{fi})^2} \right\} \end{aligned} \tag{2.93}$$

Making use of the fact[226] that the

$$\lim_{t\to\infty} \frac{1-cos[(\omega-\omega_{fi})t]}{(\omega-\omega_{fi})^2 t} = \pi t \delta(\omega-\omega_{fi}) \tag{2.94}$$

eq.(2.93) becomes,

$$P_{fi}(t) = 2\pi t |\alpha_{fi}|^2 \delta(\omega-\omega_{fi}) \tag{2.95}$$

Therefore the transtion rate

$$R_{fi} = \frac{dP_{fi}(t)}{dt} = 2\pi |\alpha_{fi}|^2 \delta(\omega-\omega_{fi}) \tag{2.96}$$

The exponential part in the expression for α_{fi} in eq.(2.91) can be expanded in Taylor series:

$$e^{i\mathbf{k}.\mathbf{r}} = 1 + i\mathbf{k}.\mathbf{r} + \frac{1}{2!}(i\mathbf{k}.\mathbf{r})^2 + \ldots \tag{2.97}$$

Optical transitions typically involve atomic wavefunctions which extend over the order of the first Bohr radius of the atom, i.e., about 1 Å. Since the wavelength (λ) associated with optical transitions are of the order of 1000 Å, k ($= 2\pi/\lambda$) will be of the order of 10^5 cm^{-1}. Thus the quantity **k.r** will be very small for r < 1 Å. Therefore, we can replace $e^{i\mathbf{k}.\mathbf{r}}$ by unity, i.e., all other terms including the first order term in eq.(2.40) are neglected. This approximation is known as, "electric-dipole approximation" or "long wavelength approximation". But this approximation becomes less accurate as the frequency of the radiation increases[224, 227]. Therefore, within the electric-dipole approximation α_{fi} becomes,

$$\alpha_{fi} = \frac{e}{mc} \langle \psi_f | \mathbf{A_0}.\nabla | \psi_i \rangle \tag{2.98}$$

Replacing ∇ by $\frac{im}{\hbar}\dot{\mathbf{r}}$, (viz., $\mathbf{p} = m\ \dot{\mathbf{r}}\ = -i\ \hbar\nabla$), the above equation becomes,

$$\begin{aligned} \alpha_{fi} &= \frac{e}{mc} \langle \psi_f | \mathbf{A_0}.\frac{im}{\hbar}\dot{\mathbf{r}} | \psi_i \rangle \\ &= \frac{ie}{\hbar c} \langle \psi_f | \mathbf{A_0}.\dot{\mathbf{r}} | \psi_i \rangle \end{aligned} \tag{2.99}$$

However, in the Heisenberg equation of motion[224] both $\dot{\mathbf{r}}$ and $\mathbf{r}$ are related through,

$$\dot{\mathbf{r}} = \frac{1}{i\hbar}[\mathrm{r}, \hat{H}_0] \tag{2.100}$$

Thus,

$$\begin{aligned} \alpha_{fi} &= \frac{ie}{\hbar c} \langle \psi_f | \mathbf{A_0}.\frac{1}{i\hbar}[\mathrm{r}, \hat{H}_0] | \psi_i \rangle \\ \alpha_{fi} &= \frac{e}{\hbar c}\omega_{fi} \langle \psi_f | \mathbf{A_0}.\mathbf{r} | \psi_i \rangle \end{aligned} \tag{2.101}$$

Substituting for α_{fi} in eq.(2.96) we obtain

$$R_{fi} = 2\pi \left(\frac{e}{\hbar c}\right)^2 \omega_{fi}^2 | \langle \psi_f | \mathbf{A_0}.\mathbf{r} | \psi_i \rangle |^2 \delta(\omega - \omega_{fi}) \tag{2.102}$$

The energy removed from the radiation field of frequency,ω, will be[228],

$$\begin{aligned} -E_{rad} &= \hbar\omega R_{fi} \\ &= \hbar\omega 2\pi \left(\frac{e}{\hbar c}\right)^2 \omega_{fi}^2 |\langle \psi_f | \mathbf{A_0}.\mathbf{r} | \psi_i \rangle|^2 \delta(\omega - \omega_{fi}) \end{aligned} \tag{2.103}$$

Now, the photoabsorption cross section, $\sigma(\omega)$, can be defined as the rate of removal of energy from the radiation field due to transition of interest divided by the intensity of the incident radiation[38],

$$\begin{aligned} \sigma(\omega) &= \frac{-E_{rad}}{I(\omega)} \\ &= \frac{\hbar\omega}{I(\omega)} 2\pi \left(\frac{e}{\hbar c}\right)^2 \omega_{fi}^2 |A_0|^2 |\langle \psi_f | \epsilon.\mathbf{r} | \psi_i \rangle|^2 \delta(\omega - \omega_{fi}) \end{aligned} \tag{2.104}$$

where $\mathbf{A_0} = A_0\epsilon$, ϵ is the polarization vector of the radiation. However, from the Poynting vector theorem[229] we know

$$|A_0|^2 = \frac{2\pi c}{\omega^2} I(\omega) \tag{2.105}$$

Substitution for $|A_0|^2$ in eq.(2.105) gives,

$$\sigma(\omega) = \frac{4\pi^2\omega}{\hbar c} |\langle \psi_f | \epsilon.(e\mathbf{r}) | \psi_i \rangle|^2 \delta(\omega - \omega_{fi}) \tag{2.106}$$

We can also replace the term, er, by the electric-dipole operator($\boldsymbol{\mu}$) and $\frac{1}{4\pi}$ by the vacuum permittivity constant(ϵ_0). Thus, the most general form of $\sigma(\omega)$ is written as,

$$\sigma(\omega) = \frac{\pi\omega}{\hbar\epsilon_0 c} |\langle \psi_f | \epsilon.\boldsymbol{\mu} | \psi_i \rangle|^2 \delta(\omega - \omega_{fi}) \tag{2.107}$$

2.4.2 Quantum mechanical treatment

The total Hamiltonian of the system in the presence of radiation is given by[227, 230]

$$\hat{H} = \hat{H}_m + \hat{H}_r + \hat{H}_i \tag{2.108}$$

where $\hat{H}_m$ is the Hamiltonian of the atom/ molecule in the absence of any external field, $\hat{H}_r$ is the Hamiltonian of the radiation field,

$$\hat{H}_r = \hbar\omega\left(\hat{a}^\dagger\hat{a} + \frac{1}{2}\right) \tag{2.109}$$

with $\hat{a}^\dagger$ and $\hat{a}$ the creation and the annihilation operator respectively. $\hat{H}_i$ is the Hamiltonian for the radiation-matter interaction and within the electric-dipole approximation $\hat{H}_i$ is given by,

$$\hat{H}_i(t) = i\left(\frac{\hbar\omega}{2\epsilon_0 V}\right)^{1/2} \boldsymbol{\mu}.\boldsymbol{\epsilon}\left(\hat{a} - \hat{a}^\dagger\right) \tag{2.110}$$

where V is the volume of the cavity in which the radiation field is considered and ϵ_0 is the vacuum permittivity constant. Photoabsorption causes transition from state $|\,\psi_i; N_i\,\rangle$ to $|\,\psi_f; N_0\,\rangle$, where $|\,\psi_i\,\rangle$ and $|\,\psi_f\,\rangle$ are the initial and the final state of the molecule and the states $|\,N_i\,\rangle$ and $|\,N_0\,\rangle$ are the photon eigenstates before and after absorption.

The time-development of the system in the presence of radiation can be obtained by solving the TDSE,

$$i\hbar\frac{\partial|\,\Psi(t)\,\rangle}{\partial t} = \{\hat{H}_0 + \hat{H}_i(t)\}\,|\,\Psi(t)\,\rangle \tag{2.111}$$

where $\hat{H}_0 = \hat{H}_m + \hat{H}_r$. Since $\hat{H}_0$ and $\hat{H}_i(t)$ do not commute with each other the usually stated solution

$$|\,\Psi(t)\,\rangle = \hat{U}(t,0)\,|\,\Psi(0)\,\rangle = e^{-i\hat{H}t/\hbar}\,|\,\Psi(0)\,\rangle \tag{2.112}$$

becomes inapplicable in the present case. However, we can use the time-ordered integral equation form of the time-evolution operator[231, 232]. Thus,

$$\begin{aligned}\hat{U}(t,0) = {} & \hat{U}_0(t,0) - \frac{i}{\hbar}\int_0^t dt'\hat{U}_0(t,t')\hat{H}(t')\hat{U}_0(t',0) \\ & -\frac{1}{\hbar^2}\int_0^t dt'\int_0^{t'} dt''\hat{U}_0(t,t')\hat{H}(t')\hat{U}_0(t',t'')\hat{H}(t'')\hat{U}_0(t'',0) + \ldots\end{aligned} \tag{2.113}$$

Alternatively,

$$\begin{aligned}\hat{U}(t,0) &= e^{-i\hat{H}_0 t/\hbar} - \frac{i}{\hbar}\int_0^t dt' e^{-i\hat{H}_0(t-t')/\hbar}\hat{H}_i(t')e^{-i\hat{H}_0 t'/\hbar} \\ &\quad -\frac{1}{\hbar^2}\int_0^t dt' \int_0^{t'} dt'' e^{-i\hat{H}_0(t-t')/\hbar}\hat{H}_i(t')e^{-i\hat{H}_0(t'-t'')/\hbar}\hat{H}_i(t'')e^{-i\hat{H}_0 t''/\hbar} + \ldots\end{aligned} \tag{2.114}$$

where the subscript i referes to the matter-field interaction Hamiltonian. For transitions between two orthonormal states $|\psi_i\rangle$ and $|\psi_f\rangle$, the zero order term in eq.(2.115) does not contribute towards the transition probability. However, the higher order perturbation terms do contribute significantly. For a weak radiation field we need to concentrate only on the first-order perturbation term. Therefore, the transition amplitude is given by,

$$\begin{aligned}W_{fi}^{(1)}(t) &= \langle \psi_f; N_0 | \hat{U}^{(1)} | \psi_i; N_i \rangle \\ &= \langle \psi_f; N_0 | -\frac{i}{\hbar}\int_0^t dt' e^{-i\hat{H}_0(t-t')/\hbar}\hat{H}_i(t')e^{-i\hat{H}_0 t'/\hbar} | \psi_i; N_i \rangle\end{aligned} \tag{2.115}$$

Substituting for $\hat{H}_i(t')$ in the above gives,

$$\begin{aligned}W_{fi}^{(1)}(t) &= \langle \psi_f; N_0 | -\frac{i}{\hbar}\int_0^t dt' e^{-i\hat{H}_0(t-t')/\hbar}\left(i\left\{\frac{\hbar\omega}{2\epsilon_0 V}\right\}^{1/2}\boldsymbol{\mu}.\boldsymbol{\epsilon}(\hat{a}-\hat{a}^\dagger)\right)e^{-i\hat{H}_0 t'/\hbar}|\psi_i; N_i\rangle \\ &= \left(\frac{\omega}{2\epsilon_0\hbar V}\right)^{1/2}\int_0^t dt' \langle \psi_f; N_0 | e^{-i\hat{H}_0(t-t')/\hbar}\boldsymbol{\mu}.\boldsymbol{\epsilon}(\hat{a}-\hat{a}^\dagger)e^{-i\hat{H}_0 t'/\hbar}|\psi_i; N_i\rangle \\ &= \left(\frac{\omega}{2\epsilon_0\hbar V}\right)^{1/2}\int_0^t dt' \langle \psi_f; N_0 | e^{-i\hat{H}_0 t/\hbar}\boldsymbol{\mu}.\boldsymbol{\epsilon}(\hat{a}-\hat{a}^\dagger)|\psi_i; N_i\rangle e^{i(E_f+E_0-[E_i+E_0+\hbar\omega])t'/\hbar} \\ &= \left(\frac{\omega}{2\epsilon_0\hbar V}\right)^{1/2}\langle \psi_f; N_0 | e^{-i\hat{H}_0 t/\hbar}\boldsymbol{\mu}.\boldsymbol{\epsilon}(\hat{a}-\hat{a}^\dagger)|\psi_i; N_i\rangle \int_0^t dt' e^{-i(\hbar\omega-[E_f-E_i])t'/\hbar}\end{aligned} \tag{2.116}$$

where E_i and E_f are the initial and the final eigenvalue corresponding to states $|\psi_i\rangle$ and $|\psi_f\rangle$ and $E_0+\hbar\omega$ and E_0 are the eigenvalues corresponding to the photon states $|N_i\rangle$ and $|N_0\rangle$. The latter is considered as a vacuum state. Further simplification of eq.(2.117) leads to,

$$W_{fi}^{(1)}(t) = i\left(\frac{\omega}{2\epsilon_0\hbar V}\right)^{1/2}\langle \psi_f; N_0 | e^{-i\hat{H}_0 t/\hbar}\boldsymbol{\mu}.\boldsymbol{\epsilon}(\hat{a}-\hat{a}^\dagger)|\psi_i; N_i\rangle \left\{\frac{e^{-i(\omega-\omega_{fi})t}-1}{(\omega-\omega_{fi})}\right\} \tag{2.117}$$

Upon integrating over radiation field variables we obtain,

$$W_{fi}^{(1)}(t) = i\left(\frac{N_i\omega}{2\epsilon_0\hbar V}\right)^{1/2}\langle\psi_f|e^{-i\hat{H}_m t/\hbar}\boldsymbol{\mu}.\boldsymbol{\epsilon}|\psi_i\rangle\left\{\frac{e^{-i(\omega-\omega_{fi})t}-1}{(\omega-\omega_{fi})}\right\} \tag{2.118}$$

The probability of transition at any time t is,

$$\begin{aligned} P_{fi}(t) &= |\, W_{fi}^{(1)}(t)\,|^2 \\ &= \left(\frac{N_i\omega}{2\epsilon_0\hbar V}\right)\left|\langle\psi_f|e^{-i\hat{H}_m t/\hbar}\boldsymbol{\mu}.\boldsymbol{\epsilon}|\psi_i\rangle\right|^2\frac{|e^{-i(\omega-\omega_{fi})t}-1|^2}{(\omega-\omega_{fi})^2} \end{aligned} \tag{2.119}$$

In the limit $t\rightarrow\infty$,

$$\lim_{t\rightarrow\infty}P_{fi}(t) = \left(\frac{N_i\omega}{2\epsilon_0\hbar V}\right)|\langle\psi_f|\boldsymbol{\mu}.\boldsymbol{\epsilon}|\psi_i\rangle|^2\,2\pi t\delta(\omega-\omega_{fi}) \tag{2.120}$$

In the limit $t\rightarrow\infty$, the last term in the right hand side of eq.(2.120) reduces to a δ-function representation as in the semiclassical description. The rate of transition will be given by,

$$\begin{aligned} R_{fi} &= \frac{dP_{fi}}{dt} \\ &= \left(\frac{N_i\pi\omega}{\epsilon_0\hbar V}\right)|\langle\psi_f|\boldsymbol{\mu}.\boldsymbol{\epsilon}|\psi_i\rangle|^2\,\delta(\omega-\omega_{fi}) \end{aligned} \tag{2.121}$$

Now we can define the photodissociation cross section, $\sigma(\omega)$, as the rate of removal of energy from the radiation field of frequency ω, divided by the intensity of the incident radiation[38],

$$\sigma(\omega) = \frac{\hbar\omega R_{fi}}{N_i\hbar\omega c/V} \tag{2.122}$$

$$= \frac{\hbar\omega(\frac{N_i\pi\omega}{\epsilon_0\hbar V})\,|\langle\psi_f|\boldsymbol{\mu}.\boldsymbol{\epsilon}|\psi_i\rangle|^2\,\delta(\omega-\omega_{fi})}{N_i\hbar\omega c/V}$$

$$= \frac{\pi\omega}{\hbar\epsilon_0 c}|\langle\psi_f|\boldsymbol{\mu}.\boldsymbol{\epsilon}|\psi_i\rangle|^2\,\delta(\omega-\omega_{fi}) \tag{2.123}$$

The transition matrix element $\mu_{fi}=\langle\psi_f|\boldsymbol{\mu}.\boldsymbol{\epsilon}|\psi_i\rangle$ plays an important role in deciding whether the given transition is allowed or not. μ_{fi} also depends on the angle between the

vectors μ and ϵ, i.e.,

$$\begin{aligned} \mu.\epsilon &= |\mu||\epsilon|cos\theta \\ |\langle \psi_f | \mu.\epsilon | \psi_i \rangle|^2 &= |\langle \psi_f | \mu\epsilon | \psi_i \rangle|^2 cos^2\theta \end{aligned} \tag{2.124}$$

If the radiation under consideration is not polarised, then ϵ will be oriented randomly. Therefore, $cos^2\theta$ can be replaced by its average, 1/3[224]. The photoabsorption cross section(for the unpolarised light) can thus be rewritten as,

$$\sigma(\omega) = \frac{\pi\omega}{3\hbar\epsilon_0 c}|\langle \psi_f | \mu\epsilon | \psi_i \rangle|^2 \delta(\omega - \omega_{fi}) \tag{2.125}$$

This expression is widely used to compute the photoabsorption cross section over all photon frequencies(ω)[3, 225]. The $\sigma(\omega)$ obtained by eq.(2.126) is the partial photoabsorption cross section for transition into state f. The total photoabsorption cross section is calculated by summing over all the final states,

$$\sigma(\omega) = \frac{\pi\omega}{3\hbar\epsilon_0 c}\sum_f |\langle \psi_f | \mu\epsilon | \psi_i \rangle|^2 \delta(\omega - \omega_{fi}) \tag{2.126}$$

Nearly two decades ago, Heller and coworkers[75] had shown that $\sigma(\omega)$ could be computed easily in the time-domain. Substituting the integral form of the δ-function,

$$\delta(\omega - \omega_{fi}) = \frac{1}{2\pi}\int_{-\infty}^{\infty} e^{i(\omega-\omega_{fi})t} dt \tag{2.127}$$

in eq.(2.127) yields:

$$\begin{aligned} \sigma(\omega) &= \frac{\pi\omega}{3\hbar\epsilon c}\sum_f |\langle \psi_f | \mu\epsilon | \psi_i \rangle|^2 \frac{1}{2\pi}\int_{-\infty}^{\infty} e^{i(\omega-\omega_{fi})t} dt \\ &= \left(\frac{2\pi\omega}{3\hbar c}\right)\sum_f \int_{-\infty}^{\infty} dt e^{iEt/\hbar} \langle \psi_i | \mu\epsilon e^{-iE_f t/\hbar} | \psi_f \rangle \langle \psi_f | \mu\epsilon | \psi_i \rangle \\ &= \left(\frac{2\pi\omega}{3\hbar c}\right)\int_{-\infty}^{\infty} dt e^{iEt/\hbar} \langle \phi_i | e^{-i\hat{H}_f t/\hbar} | \phi_i \rangle \\ &= \frac{2\pi\omega}{3\hbar c}\int_{-\infty}^{\infty} dt e^{iEt/\hbar} \langle \phi_i | \phi_i(t) \rangle \end{aligned} \tag{2.128}$$

where $E = E_i + \hbar\omega$ and $|\,\phi_i(t)\,\rangle = e^{-iH_f t/\hbar}\,|\,\phi_i\,\rangle$. $\hat{H}_f$ is the Hamiltonian corresponding to the final state f. ϵ_0 has been replaced by $1/4\pi$. $|\,\phi_i\,\rangle = \mu\epsilon|\,\psi_i\,\rangle$ is frequently referred to as the "promoted state". The final state wavefunction is normalised such that $\sum_f |\,\psi_f\,\rangle\,\langle\,\psi_f\,| = 1$. It can be seen from eq.(2.129) that the photodissociation cross section is the "full" Fourier transform of the autocorrelation function ($C(t) = \langle\phi_i|\phi_i(t)\rangle$). Therefore, from a practical point of view, $\sigma(\omega)$, can be computed readily by computing $C(t)$ and obtaining its Fourier transform.

2.4.3 Nature of the wavefunction prepared on the excited state under the influence of light

In this section we will consider an electronic transition form the ground electronic state to an excited electronic state. Within the electric-dipole approximation the transition-dipole moment is given by $\boldsymbol{\mu}.\boldsymbol{\epsilon}(t)$, where $\boldsymbol{\epsilon}(t)$ is the electric field vector defined as,

$$\boldsymbol{\epsilon}(t) \;=\; A_0'\boldsymbol{\epsilon} f(t) cos(\omega t)$$

where $A_0' = 2\,A_0$. $f(t)$ defines the shape and duration of the laser pulse. The TDSE of the radiation-coupled system is given by[233],

$$i\hbar\,\frac{\partial}{\partial t}\begin{pmatrix}\psi_g(t)\\ \psi_e(t)\end{pmatrix} = \begin{pmatrix} H_g & \boldsymbol{\mu}.\boldsymbol{\epsilon}(t)\\ \boldsymbol{\mu}.\boldsymbol{\epsilon}(t) & H_e\end{pmatrix}\begin{pmatrix}\psi_g(t)\\ \psi_e(t)\end{pmatrix} \tag{2.129}$$

where the subscripts g and e refer to the ground and the excited electronic state respectively. We can rewrite the TDSE as,

$$i\hbar\frac{\partial\Psi(t)}{\partial t} \;=\; \{H_0 + H(t)\}\Psi(t) \tag{2.130}$$

where, $\Psi(t) = \begin{pmatrix}\psi_g(t)\\ \psi_e(t)\end{pmatrix}$; $H_0 = \begin{pmatrix} H_g & 0\\ 0 & H_e\end{pmatrix}$ and $H(t) = \begin{pmatrix} 0 & \boldsymbol{\mu}.\boldsymbol{\epsilon}(t)\\ \boldsymbol{\mu}.\boldsymbol{\epsilon}(t) & 0\end{pmatrix}$.

Eq.(2.131) is similar to eq.(2.112), for which the solution has been obtained already. Since it is fair to assume that the laser pulse begins to interact with the molecule only at time $t = 0$, there is no wavefunction on the excited state at $t = 0$, i.e., $\psi_e(0) = 0$. Therefore, the time-evolving wavefunctions on the ground and the excited electronic state[131, 234] respectively are:

$$\begin{aligned} \psi_g(t) &= e^{-iE_g t/\hbar}\psi_g(0) \\ \psi_e(t) &= -\frac{i}{\hbar}\int_0^t dt' e^{-iH_e(t-t')/\hbar} H(t') e^{-iE_g t'/\hbar}\psi_g(0) \end{aligned} \tag{2.131}$$

We have assumed a weak field and hence the higher order terms have been neglected in writing the above equation. On substituting for $H(t')$ in eq.(2.132) we get,

$$\begin{aligned} \psi_e(t) &= -\frac{i}{\hbar}\int_0^t dt' e^{-iH_e(t-t')/\hbar}\boldsymbol{\mu}.\boldsymbol{\epsilon}(t') e^{-iE_g t'/\hbar}\psi_g(0) \\ &= -\frac{i}{\hbar}\int_0^t dt' e^{-i\tilde{H}_e(t-t')/\hbar}\boldsymbol{\mu}.A_0'\boldsymbol{\epsilon}\ cos(\omega t) e^{-iE_g t'/\hbar}\psi_g(0) \\ &= -\frac{i}{\hbar}A_0\int_0^t dt' e^{-iH_e(t-t'/\hbar}\boldsymbol{\mu}.\boldsymbol{\epsilon} e^{-iEt'/\hbar}\psi_g(0) \end{aligned} \tag{2.132}$$

where $E = E_g + \hbar\omega$. In order to arrive at eq.(2.133) we have made use of the rotating wave approximation (RWA)[227], $cos(\omega t) = \frac{1}{2}e^{-i\omega t'}$. This approximation is valid near resonance condition ($\hbar\omega = E_f - E_i$). From eq.(2.133) we can draw the following conclusions: the ground state wavefunction, $\psi_g(0)$, is constantly transferred to the excited state as long as the light is 'on'. While the wavefunction is being transferred, the initially arrived wavefunctions are propagated under the influence of the excited state Hamiltonian.

Since in practice excitation is caused by pulsed lasers or continuous wave (CW) lasers, we consider two limits: (i) δ-function and (ii) continuous wave (CW).

δ-function limit

Experimentally it is not possible to obtain a δ-function laser pulse. But theoretically it is important to consider this limit as it helps us understanding the Heller's approach[75],

which has been employed extensively in the present work. In the δ-function limit, when t'=0 the laser pulse suddenly promotes the ground state wavefunction to the excited state and hence eq.(2.133) will be modified as,

$$\begin{aligned}\psi_e(t) &= -\frac{iA_0}{\hbar}e^{-iH_e t/\hbar}\boldsymbol{\mu}.\boldsymbol{\epsilon}\psi_g(0) \\ &= -\frac{iA_0}{\hbar}e^{-iH_e t/\hbar}\phi_g(0) \end{aligned} \tag{2.133}$$

where $\phi_g(0) = \boldsymbol{\mu}.\boldsymbol{\epsilon}\psi_g(0)$.

CW limit

In this limit, the light is on for ever, i.e., $t \rightarrow \infty$ and $A_0 = f(t) = 1$. Therefore, we have,

$$\psi_e(t) = \lim_{t\rightarrow\infty} -\frac{i}{\hbar}\int_0^\infty dt' e^{-iH_e(t-t')/\hbar}\boldsymbol{\mu}.\boldsymbol{\epsilon}e^{-iEt'/\hbar}\psi_g(0) \tag{2.134}$$

By substituting $u = t - t'$ in eq.(2.135) we obtain,

$$\begin{aligned}\psi_e(t) &= \lim_{t\rightarrow\infty}\frac{i}{\hbar}\int_0^\infty du e^{-iH_e u/\hbar}\boldsymbol{\mu}.\boldsymbol{\epsilon}e^{-iE(t-u)/\hbar}\psi_g(0) \\ &= \lim_{t\rightarrow\infty}\frac{i}{\hbar}e^{-iEt/\hbar}\int_0^\infty du e^{iEu/\hbar}e^{-iH_e u/\hbar}\phi_g(0) \\ &= \lim_{t\rightarrow\infty}\frac{i}{\hbar}e^{-iEt/\hbar}\int_0^\infty du e^{iEu/\hbar}\phi_g^e(u) \end{aligned} \tag{2.135}$$

Here $\phi_g^e(u) = e^{-iH_e u/\hbar}\phi_g(0)$, the time-evolving wavefunction on the excited electronic state. Eq.(2.136) suggests that the ground state wavefunction is suddenly transferred to the excited electronic state as in the δ-function case, it is then propagated on the excited state and after substantial time-evolution, the stored wavefunction is *half* Fourier transformed into energy domain. This energy domain wavefunction was previously defined by Heller and coworkers as the Raman wavefunction[72, 234–236],

$$\psi_R(E) = \int_0^\infty du e^{iEu/\hbar}\phi_g^e(u) \tag{2.136}$$

Thus we can rewrite the wavefunction prepared on the excited state by a CW laser as,

$$\psi_e(t) = \lim_{t\to\infty} \frac{i}{\hbar} e^{-iEt/\hbar}\psi_R(E) \tag{2.137}$$

We can see from the above equation that the Raman wavefunction is what is prepared by the CW laser on the excited state. Now let us turn our attention to the photoabsorption cross section defined in eq.(2.129),

$$\sigma(\omega) = \frac{2\pi\omega}{3\hbar c}\int_{-\infty}^{\infty} e^{iEt/\hbar}\langle\phi_g(0)|\phi_g^e(t)\rangle dt \tag{2.138}$$

On further simplification we obtain,

$$\begin{aligned}
\sigma(\omega) &= \frac{2\pi\omega}{3\hbar c}\langle\phi_g(0)|\left\{\int_{-\infty}^{0} e^{iEt/\hbar}|\phi_g^e(t)\rangle dt + \int_0^{\infty} e^{iEt/\hbar}|\phi_g^e(t)\rangle dt\right\} \\
&= \frac{2\pi\omega}{3\hbar c}\langle\phi_g(0)|\left\{\int_0^{\infty} e^{-iEt/\hbar}|\phi_g^e(-t)\rangle dt + \int_0^{\infty} e^{iEt/\hbar}|\phi_g^e(t)\rangle dt\right\} \\
&= \frac{2\pi\omega}{3\hbar c} 2Re\left\{\langle\phi_g(0)|\int_0^{\infty} e^{iEt/\hbar}|\phi_g^e(t)\rangle dt\right\} \\
&= \frac{4\pi\omega}{3\hbar c} Re\{\langle\phi_g(0)|\psi_R(\omega)\rangle\}
\end{aligned} \tag{2.139}$$

Eq.(2.140) clearly demonstrates that the Heller's approach to determine the photoabsorption cross section falls in the CW limit and hence it is applicable to most of the experimental situations.

2.5 Dynamics involving more than one excited (electronic) state

2.5.1 Adiabatic and diabatic representations

We have discussed above the computation of $\sigma(\omega)$ for a direct photoabsorption/dissociation process. However, in several photodissociation processes one frequently encounters more than one electronic state participating in the dynamics[99, 103, 107]. In order to describe

the coupling between several electronic states, we have to go beyond the Born-Oppenheimer approximation. This can be achieved by going over to either the **adiabatic** (non-crossing) representation or the **diabatic** (crossing) representation. In the former the nuclear kinetic energy operator, $\hat{T}_N(R)$, is non-diagonal and the potential energy operator, $\hat{V}(R)$, is diagonal. In contrast, in the diabatic representation $\hat{T}_N(R)$ is diagonal and $\hat{V}(R)$ is non-diagonal. For a two state system, we can write the TDSE in the adiabatic representation as,

$$i\hbar \frac{\partial}{\partial t}\begin{pmatrix}\psi_1(t)\\ \psi_2(t)\end{pmatrix} = \left\{\frac{-\hbar^2}{2m}\begin{pmatrix}\nabla_R^2+T_{11} & T_{12}\\ T_{21} & \nabla_R^2+T_{22}\end{pmatrix}+\begin{pmatrix}V_1^a & 0\\ 0 & V_2^a\end{pmatrix}\right\}\begin{pmatrix}\psi_1(t)\\ \psi_2(t)\end{pmatrix} \quad (2.140)$$

where T_{11}, T_{12}, T_{21} and T_{22} are defined as follows:

$$\begin{aligned} T_{11} &= \langle \phi_1^a | \nabla_R^2 | \phi_1^a \rangle \\ T_{12} &= \langle \phi_1^a | \nabla_R^2 | \phi_2^a \rangle + 2\langle \phi_1^a | \nabla_R | \phi_2^a \rangle \nabla_R \\ T_{21} &= \langle \phi_2^a | \nabla_R^2 | \phi_1^a \rangle + 2\langle \phi_2^a | \nabla_R | \phi_1^a \rangle \nabla_R \end{aligned}$$

and

$$T_{22} = \langle \phi_2^a | \nabla_R^2 | \phi_2^a \rangle$$

Here $\psi_{1(2)}$ and $\phi_{1(2)}^a$ are the nuclear and the adiabatic electronic eigenfunctions for the state 1(2) respectively. $\hat{V}_1^a$ and $\hat{V}_2^a$ are the adiabatic potential-energy curves for states 1 and 2 in that order.

The perturbations arising from the off-diagonal matrix elements are referred to as non-adiabatic perturbations. It is worth emphasising that the off-diagonal matrix elements in this case are exclusively due to the nuclear kinetic energy operator.

For the same two state system we can write the TDSE in the diabatic representation as,

$$i\hbar \frac{\partial}{\partial t}\begin{pmatrix}\psi_1(t)\\ \psi_2(t)\end{pmatrix} = \left\{\begin{pmatrix}\hat{T}_1(R) & 0\\ 0 & \hat{T}_2(R)\end{pmatrix}+\begin{pmatrix}\hat{V}_{11} & \hat{V}_{12}\\ \hat{V}_{21} & \hat{V}_{22}\end{pmatrix}\right\}\begin{pmatrix}\psi_1(t)\\ \psi_2(t)\end{pmatrix} \quad (2.141)$$

where $\hat{T}_1(R)$ and $\hat{T}_2(R)$ are the kinetic energy operators for nuclear motion on surfaces 1 and 2 respectively. $V_{11(22)}$ and $V_{12(21)}$ are the matrix elements $\left\langle \phi^d_{1(2)} \middle| \hat{H}_{el} \middle| \phi^d_{1(2)} \right\rangle$ and $\left\langle \phi^d_{1(2)} \middle| \hat{H}_{el} \middle| \phi^d_{2(1)} \right\rangle$. $\phi^d_{1(2)}$ and $\psi_{1(2)}$ are the diabatic electronic and the nuclear wavefunctions. In this representation the off-diagonal matrix elements are due to the nuclear potential energy term(i.e., $\hat{H}_{el}$). Perturbations arising from these off-diagonal matrix elements are termed as electrostatic perturbations. In the adiabatic representation the potential-energy curves may approach each other closely but they will not cross (avoided crossing). But in the diabatic representation the PE curves do cross whenever degeneracies occur.

The two representations are related to each other via the following unitary transformation:

$$\begin{pmatrix} \phi^a_1 \\ \phi^a_2 \end{pmatrix} = \begin{pmatrix} cos\theta(R) & -sin\theta(R) \\ sin\theta(R) & cos\theta(R) \end{pmatrix} \begin{pmatrix} \phi^d_1 \\ \phi^d_2 \end{pmatrix} \tag{2.142}$$

where the R-dependent angle θ is obtained from

$$tan2\theta(R) = \frac{2V_{12}}{V_{11} - V_{22}} \tag{2.143}$$

The adiabatic PE curves are related to the diabatic PE curves through

$$V^a_{1,2} = \frac{(V_{11} + V_{22}) \pm \sqrt{(V_{11}-V_{22})^2+4V_{12}^2}}{2} \tag{2.144}$$

2.5.2 Time-evolution on coupled electronic states

The various methods described in section 2.3 for time-evolving the wavefunction on a single PES can be extended readily to systems involving more than one PES which are coupled with each other. For a 2-level system, for instance, at any point on the spatial grid, the SOD scheme will be as follows:

$$\begin{pmatrix} \psi_1(t_{n+1}) \\ \psi_2(t_{n+1}) \end{pmatrix} = \begin{pmatrix} \psi_1(t_{n-1}) \\ \psi_2(t_{n-1}) \end{pmatrix} - \frac{2i\Delta t}{\hbar} \begin{pmatrix} \hat{T}_1(R) + \hat{V}_{11} & \hat{V}_{12} \\ \hat{V}_{21} & \hat{T}_2(R) + \hat{V}_{22} \end{pmatrix} \begin{pmatrix} \psi_1(t_n) \\ \psi_2(t_n) \end{pmatrix} \tag{2.145}$$

where 1 and 2 refer to the two states and the rest of the variables have their usual meaning as in eq.(2.142).

Different authors have used the different schemes: SOD, Lanczos, Chebyschev, etc., depending upon the nature of the non-adiabatic dynamics. In addition, Coalson and Kinsey[78] and Alvarellos and Metiu[123] have proposed alternative strategies to study non-adiabatic interactions.

Coalson and Kinsey[78] proposed the wave packet perturbation theory for a two-state system and it can be extended to more complex systems.

They partitioned the diabatic Hamiltonian that appeared in eq.(2.142) into the unperturbed and the perturbation parts as,

$$\hat{H} = \hat{H}_0 + \hat{H}' \tag{2.146}$$

where $\hat{H}_0 = \begin{pmatrix} \hat{H}_{11} & 0 \\ 0 & \hat{H}_{22} \end{pmatrix}$ and $\hat{H}' = \begin{pmatrix} 0 & \hat{V}_{12} \\ \hat{V}_{21} & 0 \end{pmatrix}$. Here $\hat{H}_{11}$ and $\hat{H}_{22}$ are the zeroth order Hamiltonians for states 1 and 2 respectively. Letting $\Psi(t) = \begin{pmatrix} \psi_1(t) \\ \psi_2(t) \end{pmatrix}$ and substituting it in eq.(2.142) yields

$$i\hbar \frac{\partial \Psi(t)}{\partial t} = \{\hat{H}_0 + \hat{H}'\}\Psi(t) \tag{2.147}$$

By making use of the integral equation form of the time-evolution operator (cf. eq.(2.115)) we obtain,

$$\begin{aligned} \Psi(t) = {} & e^{-i\hat{H}_0 t/\hbar}\Psi(0) - \frac{i}{\hbar}\int_0^t dt' e^{-i\hat{H}_0(t-t')/\hbar}\hat{H}' e^{-i\hat{H}_0 t'/\hbar}\Psi(0) \\ & - \left(\frac{1}{\hbar^2}\right)\int_0^t dt' \int_0^t dt'' e^{-i\hat{H}_0(t-t')/\hbar}\hat{H}' \\ & e^{-i\hat{H}_0(t'-t'')/\hbar}\hat{H}' e^{-i\hat{H}_0 t''/\hbar}\Psi(0) + \ldots \end{aligned} \tag{2.148}$$

where the exponential operator is,

$$e^{-i\hat{H}_0 t/\hbar} = \begin{pmatrix} e^{-i\hat{H}_{11}t/\hbar} & 0 \\ 0 & e^{-i\hat{H}_{22}t/\hbar} \end{pmatrix} \tag{2.149}$$

By substituting the respective terms in eq.(2.149) and assuming that at t=0 there was no population in state 2 (i.e., $\psi_2(0) = 0$) we obtain:

$$\begin{aligned}\psi_1(t) &= e^{-i\hat{H}_{11}t/\hbar}\psi_1(0) \\ &\quad -\left(\frac{1}{\hbar^2}\right)\int_0^t dt' \int_0^{t'} dt'' e^{-i\hat{H}_{11}(t-t')/\hbar}\hat{V}_{12} \\ &\quad e^{-i\hat{H}_{22}(t'-t'')/\hbar}\hat{V}_{21}e^{-i\hat{H}_{11}t''/\hbar}\psi_1(0) + O(\hat{V}_{12}^4) \end{aligned} \tag{2.150}$$

and

$$\psi_2(t) = -\frac{i}{\hbar}\int_0^t dt' e^{-i\hat{H}_{22}(t-t')/\hbar}\hat{V}_{21}e^{-i\hat{H}_{11}t'/\hbar}\psi_1(0) + O(\hat{V}_{12}^3) \tag{2.151}$$

Coalson and coworkers[121, 237] have successfully carried out several numerical studies by making use of Gaussian wave packet method. These studies showed that the WP perturbation theory approach was adequate only when the coupling between the potential energy curves was weak. It failed to describe strong coupling situations. Also the GWP remained Gaussian only on harmonic or quadratic potentials. One can apply this method to anharmonic potentials, only if the dynamics takes place in short-time scales. Therefore, if the non-adiabatic transitions occur slowly, then we cannot use the GWP method. A more detailed account of the strength and weakness of the GWP method for studying the non-adiabatic transitions is given by Ramakrishna[237].

Alvarellos and Metiu[123] suggested an algorithm which is an extension of the split operator method (see section 2.3.2) to study curve crossing problems. In their scheme, the exponential operator is calculated in the representation in which it is diagonal. For a two-state system, the algorithm consists of the following two steps.

Step 1: The diabatic nuclear wavefunctions are first transformed into adiabatic wavefunctions and then multiplied by the phase factor $\begin{pmatrix} e^{-i\Delta t\hat{V}_{11}^a/\hbar} & 0 \\ 0 & e^{-i\Delta t\hat{V}_{22}^a/\hbar} \end{pmatrix}$. Then the resultant

wavefunctions are transformed back into the diabatic ones:

$$\begin{pmatrix} \chi_1(R) \\ \chi_2(R) \end{pmatrix} = T^\dagger \begin{pmatrix} e^{-i\Delta t \hat{V}^a_{11}/\hbar} & 0 \\ 0 & e^{-i\Delta t \hat{V}^a_{22}/\hbar} \end{pmatrix} T \begin{pmatrix} \psi_1(R) \\ \psi_2(R) \end{pmatrix} \tag{2.152}$$

where T and $T^\dagger$ are the transformation matrices to carry out the transformation between diabatic-to-adiabatic and adiabatic-to-diabatic representations respectively. They are defined as

$$T^\dagger = \begin{pmatrix} cos\theta(R) & sin\theta(R) \\ -sin\theta(R) & cos\theta(R) \end{pmatrix}; T = \begin{pmatrix} cos\theta(R) & sin\theta(R) \\ -sin\theta(R) & cos\theta(R) \end{pmatrix}$$

ψ's and χ's in eq.(2.153) are the diabatic nuclear wavefunctions before and after evaluating the potential energy part respectively. The R-dependent angle θ has been defined earlier.

Step 2: The wavefunctions obtained at the end of step 1 were Fourier-transformed into the momentum domain and then the kinetic energy operation was carried out by multiplying at each grid points with $\begin{pmatrix} e^{-i\Delta t\hbar k_{11}^2/2m} & 0 \\ 0 & e^{-i\Delta t\hbar k_{22}^2/2m} \end{pmatrix}$, where k_{11} and k_{22} are the wave numbers corresponding to states 1 and 2 respectively. An inverse Fourier transformation is then carried out to complete one step time-evolution,

$$\begin{pmatrix} \psi_1(R,\Delta t) \\ \psi_2(R,\Delta t) \end{pmatrix} = FT^- \begin{pmatrix} e^{-i\Delta t\hbar k_{11}^2/2m} & 0 \\ 0 & e^{-i\Delta t\hbar k_{22}^2/2m} \end{pmatrix} FT^+ \begin{pmatrix} \chi_1(R) \\ \chi_2(R) \end{pmatrix} \tag{2.153}$$

The efficiency of this method will improve if the following conditions are met:

(i) total number of grid points must be less and the grid increment (ΔR) may be large;

(ii) the dynamics must take place in short-time scales.

This method can easily be extended to more complex systems. The relevant adiabatic-to-diabatic transformation matrix elements are obtained from the diabatic potentials (Cf. equations 2.143–2.145).

The major time consuming step in this approach is the transformation between the two representations. However, a new scheme proposed recently by Broeckhove et al[238]

makes use of Lie algebraic manipulation to determine the time-evolution without switching between the adiabatic and the diabatic representations. According to this approach the diabatic potential energy matrix given in eq.(2.142) can be written in terms of Pauli matrices as,

$$V^d = \frac{1}{2}(V_{11}+V_{22})\sigma_0 + V_{12}\sigma_1 + \frac{1}{2}(V_{11}-V_{22})\sigma_3 \tag{2.154}$$

where the Pauli matrices are given by,

$$\sigma_0 = \begin{pmatrix} 1 & 0 \\ 0 & 1 \end{pmatrix}; \ \sigma_1 = \begin{pmatrix} 0 & 1 \\ 1 & 0 \end{pmatrix}; \ \sigma_2 = \begin{pmatrix} 0 & -i \\ i & 0 \end{pmatrix}; \ \sigma_3 = \begin{pmatrix} 1 & 0 \\ 0 & -1 \end{pmatrix}$$

For mathematical convenience we can use the following simplifications to write the diabatic potentials:

$$\begin{aligned} V^d &= \sum_{i=0}^{3} \nu_i \sigma_i \qquad (2.155) \\ &= \nu_0\sigma_0 + \nu_1\sigma_1 + \nu_2\sigma_2 + \nu_3\sigma_3 \end{aligned}$$

where

$$\begin{aligned} \nu_0 &= \frac{1}{2}(V_{11}+V_{22}) \\ \nu_1 &= V_{12} \\ \nu_2 &= 0 \\ \nu_3 &= \frac{1}{2}(V_{11}-V_{22}) \end{aligned}$$

and σ_{0-3} are the Pauli matrices. Once we have represented the diabatic potentials using the summation as shown in eq.(2.156), we can always use the following relation to compute the exponential operator,

$$exp(i\sum_{i=0}^{3}\nu_i\sigma_i) = exp(i\nu_0)\left(\sigma_0 cos|\nu| + i\left(\sum_{i=1}^{3}\nu_i\sigma_i\right)\frac{sin|\nu|}{|\nu|}\right), \tag{2.156}$$

$$|\nu| = \left(\sum_{i=1}^{3}\nu_i^2\right)^2 \tag{2.157}$$

This equation allows to calculate the potential as well as the kinetic energy operator in the diabatic representation and more efficiently computes the wave packet time-evolution. Using model studies Broeckhove and coworkers[238] have shown several application of this method. This scheme has one major drawback that is this method is applicable only for a two state problem. For multielectronic state cases determining the exponential operator through eq.(2.156) will be difficult.

2.6 Predissociation

If the molecule is excited to a state which is quasi-bound with respect to dissociation, then it may undergo predissociation. In diatomic molecules the following two types of predissociation have been observed. They are (i) rotational predissociation and (ii) electronic predissociation[16, 116]. For a rotating molecule the inclusion of centrifugal potential results in a centrifugal barrier to dissociation. Therefore the molecules are quasi-bound with respect to dissociation; they can undergo predissociation by tunneling through the barrier. However, in the case of electronic predissociation, a molecule which is residing in a bound state that is well below the dissociation limit can dissociate by mixing with a continuum level of another electronic state. The two electronic states involved in this predissociation may or may not cross with each other.

Due to predissociation the spectral characteristics will be altered significantly. For example, the intensity of the spectral lines will be lowered, spectral lines may be diffused or the energy of the spectral lines may be shifted. Experimentally, in a collision-free environment, it is possible to determine the predissociation lifetime (τ^{pr}) or the line-width (Γ, more precisely the full width at half-maximum (FWHM)). Most of the calculations till this date have been carried out using TIQM approach[116, 239, 240], the primary

reason being the τ^{pr} is of the order of 10^{-6}–10^{-12} s. Naturally, the TDQM approach without approximation would require propagation for a long time. However, with the developments of newer algorithms (see section 2.3) and computer architecture, it is now possible to investigate such long-time dynamics using TDQM approach[139, 167].

Recently, Villarreal et al.[168] have proposed a wave packet golden rule treatment to determine the line-width of the vibrational predissociation of Ne...ICl. According to this approach, the time-independent Fermi-Wintzel golden rule expression is transformed into time-domain as has been done for the photoabsorption process(cf. section 2.4.2). The Fermi-Wintzel golden rule expression for the predissociation rate (k^{pr}) is,

$$k^{pr} = \frac{1}{\tau^{pr}} = 2\pi \sum_f \left| \left\langle \psi_f^-(E) \right| \hat{V}_{ij} \left| \psi_i(E) \right\rangle \right|^2 \delta(E_f - E_i) \tag{2.158}$$

where $|\psi_i(E)\rangle$ and $\left|\psi_f^-(E)\right\rangle$ are the initial bound and the final continuum state of the molecule respectively. Similarly E_i and E_f are the eigenvalues corresponding to the initial and the final state of the molecule respectively. $\hat{V}_{ij}$ is the interaction potential corresponding to the coupling between the bound and the continuum PE curves. On replacing the δ function in eq.(2.159) by its integral form and simplifying it further we obtain,

$$k^{pr} = \frac{1}{\hbar} \int_{-\infty}^{\infty} e^{iE_i t/\hbar} \langle \phi_i(0) | \phi_i^f(t) \rangle dt \tag{2.159}$$

where $\phi_i(0) = \hat{H}_i \psi_i(0)$ and $\phi_i^f(t) = e^{-i\hat{H}_f t/\hbar} \phi_i(0)$. $\hat{H}_f$ is the Hamiltonian for the final state.

Similarly the predissociation line-width, $\Gamma(E)$, can be determined by

$$\Gamma(E) = \frac{1}{2\pi\hbar c} \int_{-\infty}^{\infty} e^{iE_i t/\hbar} \langle \phi_i(0) | \phi_i^f(t) \rangle dt \tag{2.160}$$

where $\Gamma(E)$ and τ^{pr} are related through

$$\Gamma(E) = \frac{1}{2\pi c \tau^{pr}} \qquad (cm^{-1}) \tag{2.161}$$

In summary, computation of $\Gamma(E)$ involves the following steps:

1. the initial state eigenfunction (ψ_i)is placed on the final continuum state after operating it with the coupling potential($\hat{V}_{ij}$).
2. the autocorrelation function,$C(t) = \langle \phi_i(0) | \phi_i^f(t) \rangle$, is computed at each time-step during the time-evolution.
3. $\Gamma(E)$ is then obtained by Fourier transforming the $C(t)$. Since we have chosen a specific initial state ψ_i, we have to extract $\Gamma(E)$ corresponding to the eigenvalue E_i.

Further details regarding the computation of $\Gamma(E)$ are given in chapter 5 for hydroxyl radical predissociation.

Chapter 3

NaI Predissociation: A Case Study Using Femtosecond Laser Pulses

3.1 Introduction

Technological developments in recent years have enabled the study of chemical reactions in real-time using femtosecond laser pulses[29, 241]. For instance, Zewail and coworkers[242] have investigated several unimolecular and bimolecular reactions using ultrashort laser pulses and they have demonstrated that the transition from reagents to products could be *monitored* while the process is occurring. Among various femtosecond transition-state spectroscopy (FTS) studies, NaI predissociation is particularly well studied[243]. The importance of NaI predissociation emerges mainly due to the nature of its potential energy (PE) curves shown in figure 3.1 [244]. The ionic ground electronic state($X^1\Sigma_0^+$) and the covalent excited electronic state (A 0^+) exhibit a diabatic crossing near 7 Å. In the adiabatic picture these two PE curves show an avoided crossing and the excited state becomes a (quasi)bound state. Therefore, if the laser pulse prepares a wave packet on the excited adiabatic state, it will undergo(damped) periodic oscillations. Depending upon the Landau-Zener curve crossing probability(P_{LZ}), whenever the wave packet representing the state of the system reaches near the crossing point, some part of it leaks into the lower

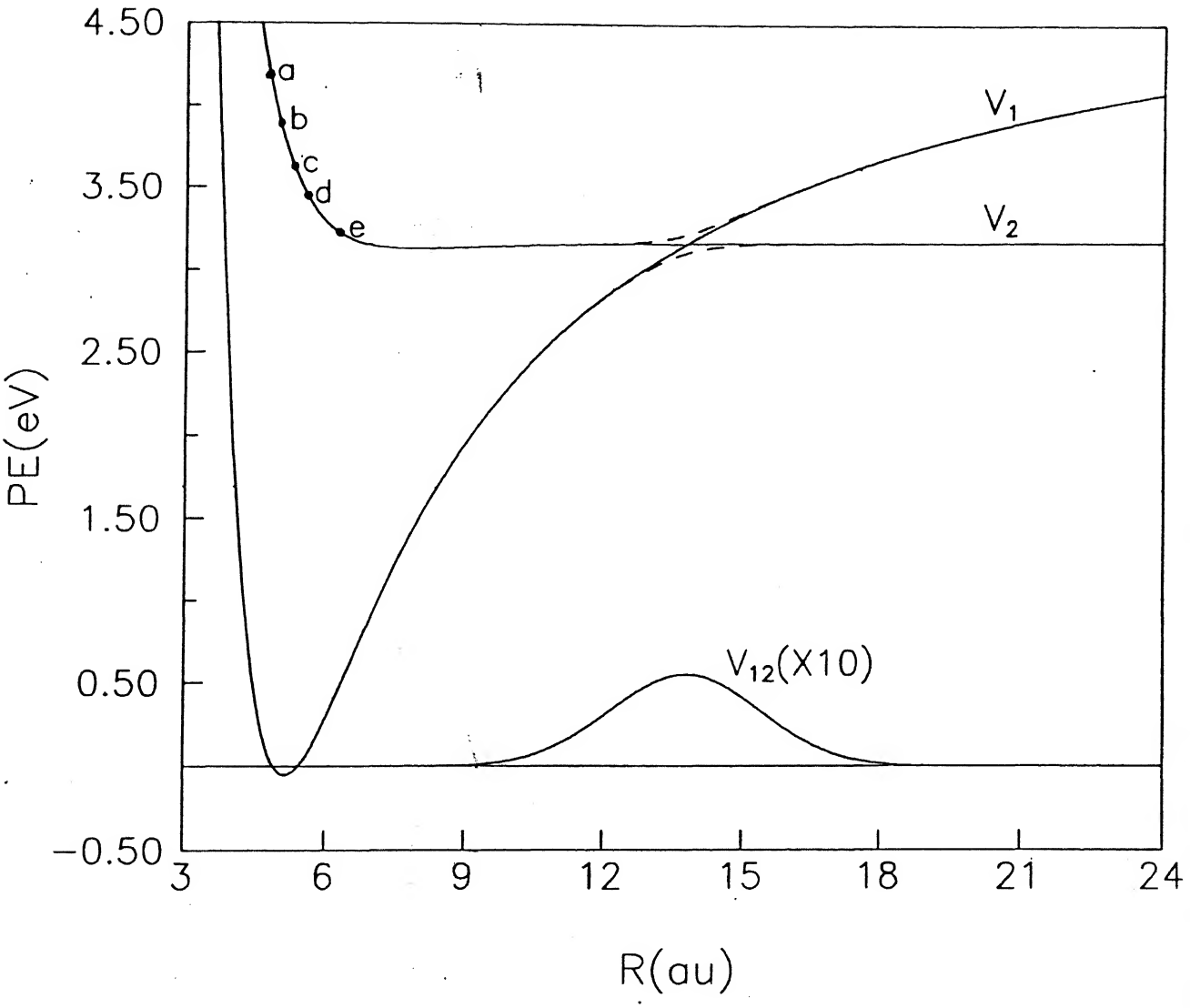

Figure 3.1. PE curves in the diabatic representation, for NaI. The points marked as (a), (b), (c), (d) and (e) correspond to photoexcitation energies for the wavelengths 300, 321, 344, 360 and 390 nm respectively. Adiabatic PE curves are shown as dashed lines.

adiabatic state and results in the neutral products Na and I. The remaining part of the wave packet will continue to oscillate in the adiabatic well with a characteristic oscillation period. Thus, the (electronic) predissociation of NaI has become an ideal candidate to investigate using the ultrashort (pump - probe) laser technique[242].

In the experimental studies, Zewail and coworkers employed a femtosecond pump laser pulse to prepare NaI on the covalent excited state and the system was later probed using another femtosecond laser pulse. When the wavelength of the latter was in resonance with the Na D-line, i.e., $\lambda = 589$ nm, *free* Na produced due to predissociation was monitored (on-resonance probing). However, when the probe wavelength was either red or blue- shifted from 589nm, the Na atoms which were *trapped* in the adiabatic well (i.e., the transition-state, $[Na...I]^{\ddagger,*}$) were probed (off-resonance probing). The laser-induced fluorescence(LIF) signal corresponding to the off-resonance probing showed an oscillatory pattern persisting up to 10 ps and the on-resonance probing signal showed a stair-case like increment[243]. The oscillation period was found to be dependent on the photoexcitation wavelength. Subsequent experiments carried out by Zewail and coworkers[245] over photoexcitation wavelengths (pump pulse) in the range 300 – 390nm enabled them to characterise the excited state PE curve and also to observe the dynamical evolution of the system in real-time. In addition, Cong et al.[246] showed that the damped oscillations of the off-resonance LIF signals were recurring every 30 ps (revival time) and were persisting for about 40 ps or so.

Subsequent to these experimental investigations several theoretical studies have been carried out using classical[247] and quantum mechanical[138, 139, 248] approaches. Choi and Light[248] and Engel and Metiu[139] have carried out time-dependent quantum mechanical calculations of NaI predissociation. The former authors assumed that the pump

wave packet(WP) prepared under various pump pulse excitation wavelengths. We have chosen the following photoexcitation wavelengths: 300, 321, 344, 360 and 390 nm. Since resonance excitation occurs at 320 nm, these wavelengths would cause *near*, *very near* and *far from resonance* excitation.

In the next section we describe the computational method employed in our study. Results obtained are discussed in section 3.3 and the conclusions are given in section 3.4.

3.2 Computational method

Our computational approach is similar to that of Metiu and coworkers[133, 139]. The wave packet prepared on the excited electronic state by a pump laser pulse is given by (see section 2.4.3)

$$\psi_2(t) = -\frac{i}{\hbar}\int_{-\infty}^{\infty} dt' e^{-i\hat{H}_2(t-t')/\hbar}\boldsymbol{\mu}.\boldsymbol{\epsilon}(t')e^{-iE_{v''=0}t'/\hbar}\psi_1(0) \tag{3.1}$$

where subscripts 1 and 2 refer to the ionic ground state and the covalent excited state respectively. $\psi_1(0)$ is the ground electronic state eigenfunction. We have taken a harmonic oscillator wavefunction corresponding to $v'' = 0$. $E_{v''=0}$ represents the zero-point-energy of the NaI molecule. We have not considered the vibrational excitation of the molecule in its ground electronic state as our interest is mainly in studying the time-evolving characteristics of the wave packet prepared by the laser pulse. $\boldsymbol{\mu}$ is the electric dipole vector of the molecule. $\boldsymbol{\epsilon}(t')$ is the electric field vector of the electromagnetic field represented by

$$\boldsymbol{\epsilon}(t') = \boldsymbol{\epsilon}_0 f(t') e^{-i\omega_l t'} \tag{3.2}$$

where $\boldsymbol{\epsilon}_0$ relates to the intensity of the field and $f(t')$ defines the shape of the pulse. ω_l is the frequency of the laser pulse. We have used the Gaussian pulse

$$f(t') = e^{-b_f(t'-t_0)^2} \tag{3.3}$$

where b_f is related to the width of the pulse and t_0 is the center of the pulse. We have used the same pulse parameters as used earlier by Engel and Metiu[139]. They are: b_f = 1.1 $\times$ 10^{-3} fs^{-2} and t_0 = 80 fs. The operator $e^{-i\hat{H}_2(t-t')/\hbar}$ is the time-evolution operator corresponding to the covalent excited state.

As we have discussed earlier, the ionic ground state and the covalent excited state are nonadiabatically coupled to each other. We use the diabatic representation[238] to describe the time evolution on the coupled electronic states as it is computationally convenient. Since Choi and Light[248] have pointed out that the diabatic coupling between the electronic states are not important during the pulse preparation, we ignored them during the pulse preparation step. The Gaussian pulse considered in the present calculation dies off in about 160 fs. Therefore, we have performed the pulse preparation calculation up to 160 fs. After the completion of the pump pulse preparation, we have carried out the time-evolution of the WP on the coupled electronic state, where we have explicitly included the nonadiabatic coupling. We have employed the second-order differencing (SOD) scheme[85, 88] for time evolution. Since NaI is a heavy mass system, i.e., its reduced mass, μ_{NaI} = 19.5 amu, we had to choose a small grid spacing (ΔR). Our numerical grid consisted of$R$ = 3.0 (0.03) 33.69 au (1024 grid points). We have carried out time-evolution for 3 ps using time steps of 0.53875 fs. In order to avoid WP reflection from the grid edge we have used a damping function as was suggested by Guo[250].

3.3 Results and discussion

As has been mentioned in the Introduction, we have considered a single photon absorption from the ground electronic (ionic) state to the covalent excited electronic state. Functional

forms of the relevant PE curves and nonadiabatic coupling potentials used are[251]:

$$V_1(R) = \left\{A_1 + \left(\frac{B_1}{R}\right)^8\right\} e^{-R/\rho_1} - \frac{C_1}{R^6} + E_1^0 - \left(\frac{e^2}{4\pi\epsilon_0}\right)\left\{\frac{D_1}{R} + \frac{\alpha_{Na}+\alpha_I}{2R^4} + \frac{2\alpha_{Na}\alpha_I}{R^7}\right\} \quad (3.4)$$

$$V_2(R) = \left\{A_2 + \left(\frac{B_2}{R+R_0}\right)^{12}\right\} e^{-(R+R_0)/(\rho_2)} - \frac{C_1}{(R+R_0)^6} + E_2^0 \quad (3.5)$$

$$V_{12}(R) = h_x e^{-\beta_{12}(R-Rx)^2} \quad (3.6)$$

Relevant parameters have been taken from the work of Wang et al.[251] and they are reproduced in table 3.1. The PE curves and the coupling potentials are illustrated in figure 3.1. Since we have no information about the transition dipole moment, we have taken it to be unity. In figure 3.1 we have indicated the points a–e referring to the photoexcitation wavelengths: 300, 321, 344, 360 and 390 nm respectively. It is clear from this figure that the latter two wavelengths correspond to off-resonance excitation.

The norm of the wave packet during the pulse preparation is given in figure 3.2 as a function of time for different pump pulse wavelengths. Since the laser pulse is essentially *off* in about 160 fs, we have plotted the norm only up to this time. The variation of the norm for different photoexcitation wavelengths show the characteristic behaviour of *near*, *very near* and *off -resonance* photoexcitation. This trend was predicted earlier by Williams and Imre[131] for a model system and it can be understood in terms of the *transients* prepared by the laser pulse. In order to explain this transient formation, let us rewrite the integral given in eq.(3.1) as a summation:

$$\psi_2(t) = \sum_{n=0}^{N}\left(\frac{-i\Delta t}{\hbar}\right) e^{-i\hat{H}_2(N-n)\Delta t/\hbar}\epsilon_0 f(n\Delta t) e^{-i(E_{v''=0}+\hbar\omega_l)n\Delta t/\hbar}\phi(0) \quad (3.7)$$

where $\phi(0) = \mu\psi_1(0)$ and the following substitutions are made for time: $\Delta t = dt'$, $t = N\Delta t$

Table 3.1: Parameters for the PE curves[251].

A_1	2758.0 eV
B_1	3.2919 $eV^{1/8}$ au
C_1	579.270 eV au^6
D_1	1.072
ρ_1	0.6809 au
α_{Na}	9.2789 au^3
α_I	36.7515 au^3
E_1^0	5.312 eV
A_2	3150.0 eV
B_2	5.1212 $eV^{1/12}$ au
C_2	45540.13 eV au^6
ρ_2	0.80824 au
E_2^0	3.18 eV
R_0	1.1527 au
h_x	0.055 eV
β_{12}	0.1920 au^{-2}
Rx	13.782 au

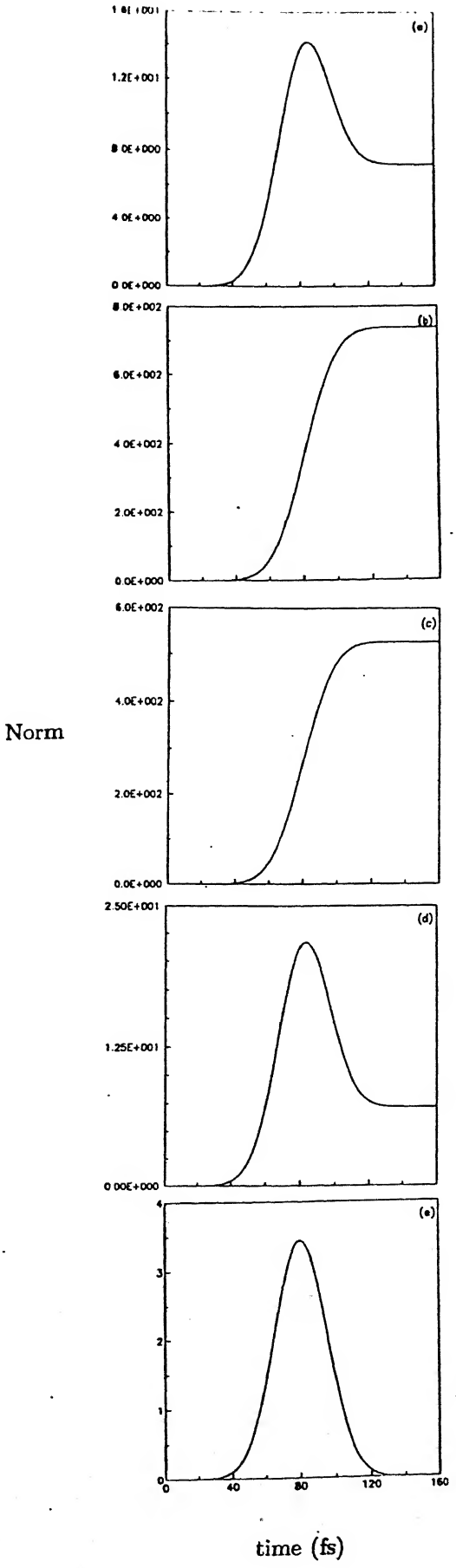

Figure 3.2. Norm of the wave packet as a function of time during the pump pulse

and $t' = n\Delta t$.

Eq.(3.7) can be rewritten as

$$\psi_2(t) = \sum_{n=0}^{N} \psi_2(n\Delta t) \tag{3.8}$$

where

$$\psi_2(n\Delta t) = \left(\frac{-i\Delta t}{\hbar}\right) e^{-i\hat{H}_2(N-n)\Delta t/\hbar} \epsilon f(n\Delta t) e^{-i(E_{v^*=0}+\hbar\omega_l)n\Delta t/\hbar} \phi(0) \tag{3.9}$$

Alternatively we can write eq.(3.8) as

$$\psi_2(t) = \psi_2(0) + \psi_2(\Delta t) + \psi_2(2\Delta t) + \ldots + \psi_2(N\Delta t) \tag{3.10}$$

Thus it is clear from eq.(3.10) that the pump pulse prepared WP, $\psi_2(t)$, contains information of all $\psi_2(n\Delta t)$. Since we do not know at what instant the pump pulse photon is absorbed by the molecule, we add all the transient WPs produced on the excited electronic state[133]. Under *resonance* or *near resonance* photoexcitation, i.e., when λ_{ex} = 321 nm and 344 nm, the WPs which are arriving on the excited electronic state add up *constructively* and lead to a steady increase in population. This maximum population remains stable for all the time even when the pulse is *off*. However, in the *off-resonance* cases shown in figures 3.2a, 3.2c and 3.2d, the norm increases when the pump pulse reaches its maximum amplitude and then decays with time. This is because the WPs which are arriving after the pulse maximum is reached ($t > t_0$), interfere with the components which arrived earlier. They are invariably out of phase with each other, and therefore they interfere destructively and the norm decreases[66, 131]. Nevertheless, it is interesting to note that some part of the WP *survives* from this interference and continues to remain on the excited electronic state. Therefore, even when the pulse is *off* there is a small amount of norm stabilised on the excited electronic state. However, the norm showed in 3.2e for

390 nm photoexcitation, rises to a maximum at $t = t_0$ and falls down subsequently. This phenomenon is purely due to *destructive* interference. It is also important to notice the magnitude of the norm for all photoexcitation wavelengths. Also the interferences between WP components are particularly important as it will affect the population significantly. This point will be clarified further (see below).

After the pulse excitation step is over, we have plotted the probability density of the WP as a function of internuclear distance for different photoexcitation wavelengths in figure 3.3. The magnitude of the probability density varies drastically with the excitation wavelength considered in this study. Another interesting feature of figure 3.3 is that the width of the probability density profile decreases as the excitation energy is decreased. This is because the number of superposition states contained in the WP prepared on the excited electronic state decreases when the photoexcitation energy is decreased. Plots of $|\psi_2(R)|^2$ for 360 and 390 nm, excitation in figure 3.3d and 3.3e respectively require some additional comments. They show that the probability density amplitude is particularly low. In addition, for the excitation wavelength 390 nm, there is an additional peak near R = 11.5 au. This unusual characteristic of the WP prepared by the laser pulse is purely due to the *transient* effect. As we have mentioned earlier, the *early* arriving components of the WP start leaving the Franck-Condon region while other components are still arriving. Thus there are *constructive* and *destructive* interferences. Any amount of WP that has *escaped* from the Franck-Condon region starts moving towards larger internuclear separation. This happens especially when the photoexcitation wavelength is away from resonance[131]. As a result of this *transient* effect we see a decrease in the probability density amplitude as well as unusual preparation of the WP. When these WPs are time-evolved on the coupled electronic states (i.e., diabatically coupled excited and ground

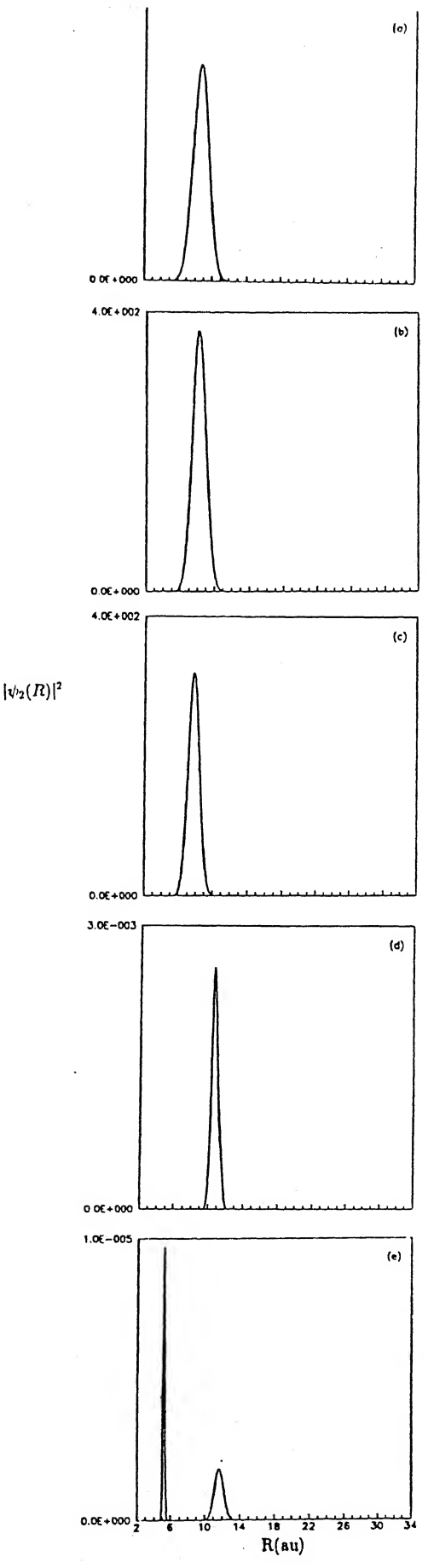

Figure 3.3. Probability density of the wave packet after the pulse excitation. (a), (b),

electronic states) they exhibit some interesting features which are described below.

Engel and Metiu had already pointed out that the coherently prepared wave packet ($\psi_2(t)$) remains *intact* even after long time[139]. Since the oscillating WP gets *refocussed* at the ionic and the covalent turning points, the WP remains Gaussian for a substantially long time. We have also observed this characteristic in our studies. However, we have observed some noticeable differences when we move away from resonance excitation. In figures 3.4a and 3.4b, we have illustrated the probability density of the time-evolving WP as a function of R corresponding to the photoexcitation wavelengths 300 nm and 390 nm respectively. The upper and lower panels of figures 3.4a and 3.4b are the probability density profiles of the WP on the covalent and the ionic state respectively. As we have mentioned earlier, the pump pulse prepares the WP in about 0.16 ps. Therefore, at t = 0.16ps there is only the pump pulse prepared WP on the covalent electronic state. As the time progress, the WP spreads and a part of it is transferred to the ionic state at around 0.26 ps. During the crossing, a small amount of WP is leaking and travelling towards larger R on the covalent excited state. Since its magnitude is relatively small, it is not visible in these plots. At a larger time, i.e., around 0.56 ps, the WP on the ionic state reaches the turning point. The WP becomes narrow at this time and then starts moving towards lower R. It reaches the crossing point around 1.16 ps. a part of the WP has already been transferred to the covalent state. After the WP reaches the covalent state, it moves towards lower R and collides with the repulsive wall and produces severe oscillations at 1.26 ps. Thus the *intact* WP fractures into several small fragments. However, these fragments add up again and continues to oscillate between ionic and covalent turning points. Since the pump pulse prepares a *coherent* WP on the excited electronic state, it acts like a classical particle for a long time.

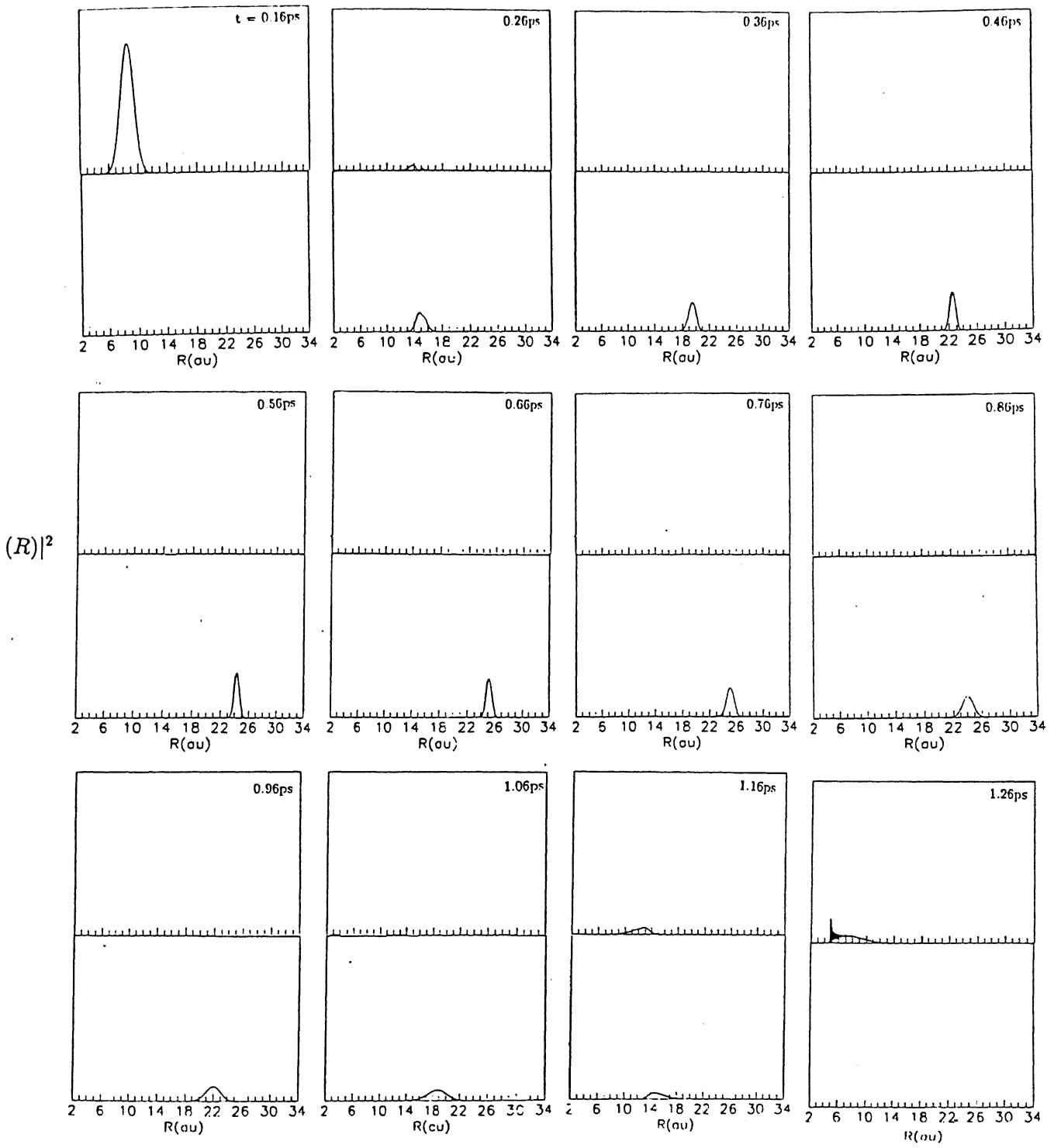

Figure 3.4a. Probability density of the time-evolving WP on both covalent and ionic states after the pulse preparation (photoexcitation wavelength corresponds to 300 nm). Upper and lower panels correspond to the WP on covalent and ionic states respectively.

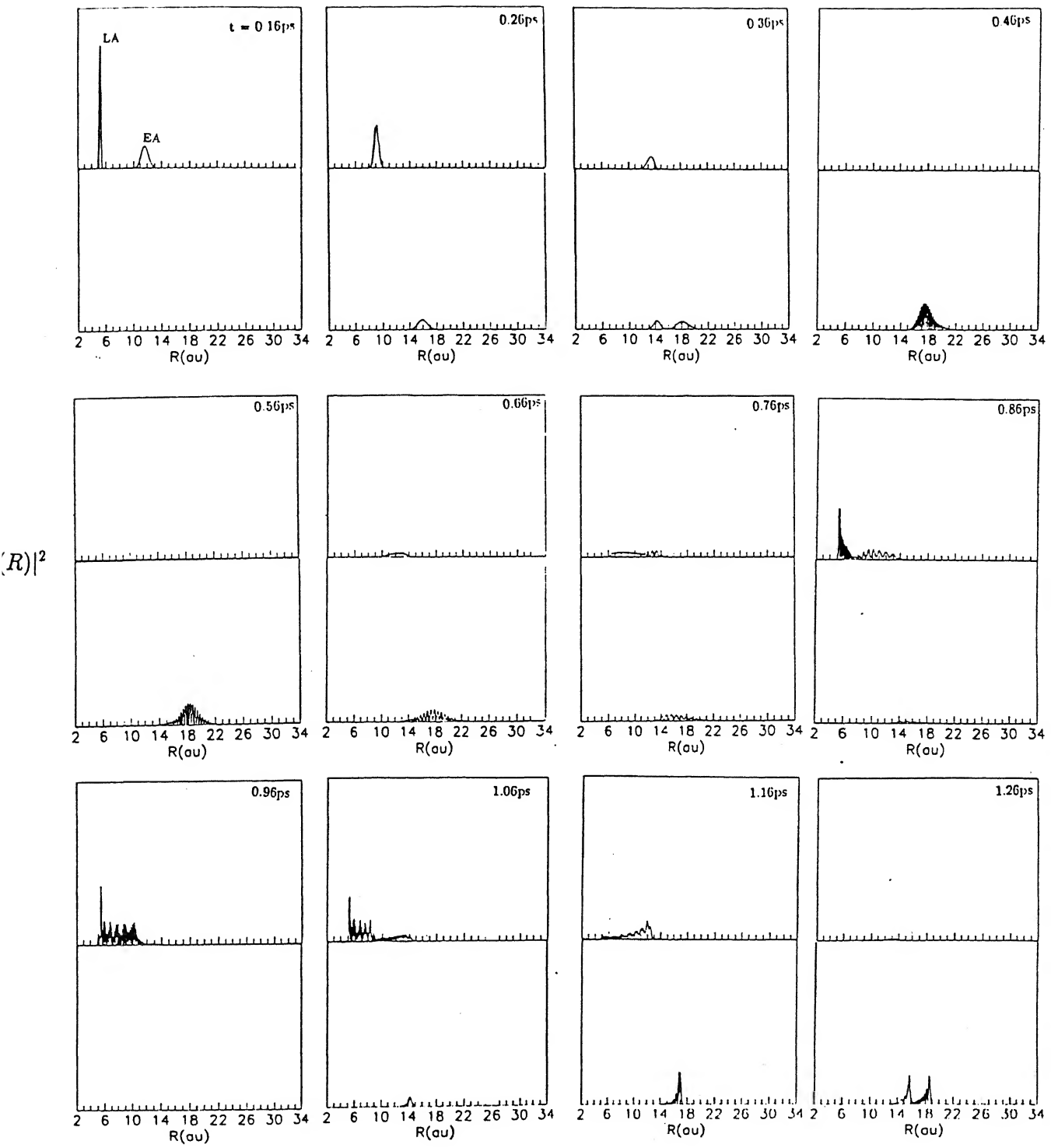

Figure 3.4b. Probability density of the time-evolving WP on both covalent and ionic states after the pulse preparation (photoexcitation wavelength corresponds to 390 nm). Upper and lower panels correspond to the WP on covalent and ionic states respectively.

This is, however, not valid when the photoexcitation wavelength is completely away from resonance (particularly when detuning is done towards lower energy). For instance, the figures given in figures 3.4b for 390 nm show several interference patterns. In order to understand them let us focus our attention on the WP prepared by the pump pulse as shown in the first panel of figures 3.4b. It has two peaks and its origin has been explained earlier. The *early* arrived component of the WP (marked as EA) has already reached near the crossing point while the *late* arrived one (marked as LA) is in the Franck-Condon region. At 0.26 ps, the *early* arrived one is transferred to the ionic state, whereas the *late* arrived component is still remaining on the covalent state. Within the next 100 fs, i.e., 0.36 ps, some part of the *late* arrived WP is transferred to the ionic state and it moves towards the ionic turning point. However, the *early* arrived WP component had already reached the ionic turning point and started moving towards the covalent state. Around 0.46 ps, these two *oppositely* travelling WPs collide with each other and produce the interference. Due to this interference, the probability density amplitude decreases and the total WP fractures into several small WPs and time-evolves further on the ionic and covalent states. However, when they reach the repulsive wall of the covalent excited state, they do not add up constructively, instead they will further split into multiple WPs as shown in figure 3.4b for times 0.86–1.06 ps. For 360 nm pulse excitation also we have observed the WP spreading in about 0.5 ps. Therefore, based on our studies we can draw the following conclusion, when the photoexcitation energy is much lower than the resonance excitation energy, the WP prepared by the laser pulse spreads in a short while unlike the one prepared near the *resonance* excitation energy. Both the *transient* effect and the pump pulse energy are responsible for the observed behaviour of the WP.

We have carried out the time-evolution of the WP up to 3 ps. We have determined the

population of the Na which is *trapped* in the adiabatic well using the formula,

$$P_{bound}(t) = \int_{R_{min}}^{Rx} |\psi_2(R,t)|^2 dR \tag{3.11}$$

where R_{min} and Rx are the minimum R value represented on the grid and the covalent-ionic crossing point respectively. $P_{bound}(t)$ values obtained in this calculation are plotted as a function of time in figure 3.5a–e. For 300, 321 and 344 nm excitation(figures 3.5a, 3.5b and 3.5c), $P_{bound}(t)$ obtained in the present calculation shows oscillation periods which are in good agreement with the previous results[29, 139]. However, the bound Na populations shown in figures 3.5a–c, differ from the experimental results. The experimental peaks are broader and the oscillation periods are slightly larger than ours. However, a better agreement can be obtained if we include the Boltzmann average of the populations. Since the WP prepared by low energy excitation spreads immediately during the time-evolution, we notice a difference in the $P_{bound}(t)$ behaviour as a function of time for 360 and 390 nm. These plots shown in figures 3.5d and 3.5e are not in accord with experimental results of Zewail and coworkers[243]. In order to simulate their results one has to perform a two-photon calculation.

3.4 Conclusion

We have carried out TDQM calculations within the first-order perturbation theory and computed the pump pulse prepared WP on the excited electronic state corresponding to the photoexcitation wavelengths: 300, 321, 344, 360 and 390 nm. These photoexcitation wavelengths are *near*, *very near* and *far away* from resonance excitation wavelength(i.e., 320 nm). Therefore the WP prepared by laser pulses of different wavelength exhibits different characteristics. Norm of the WP prepared during the pulse preparation, time-evolution characteristics of the WP and bound Na population have been computed. Our

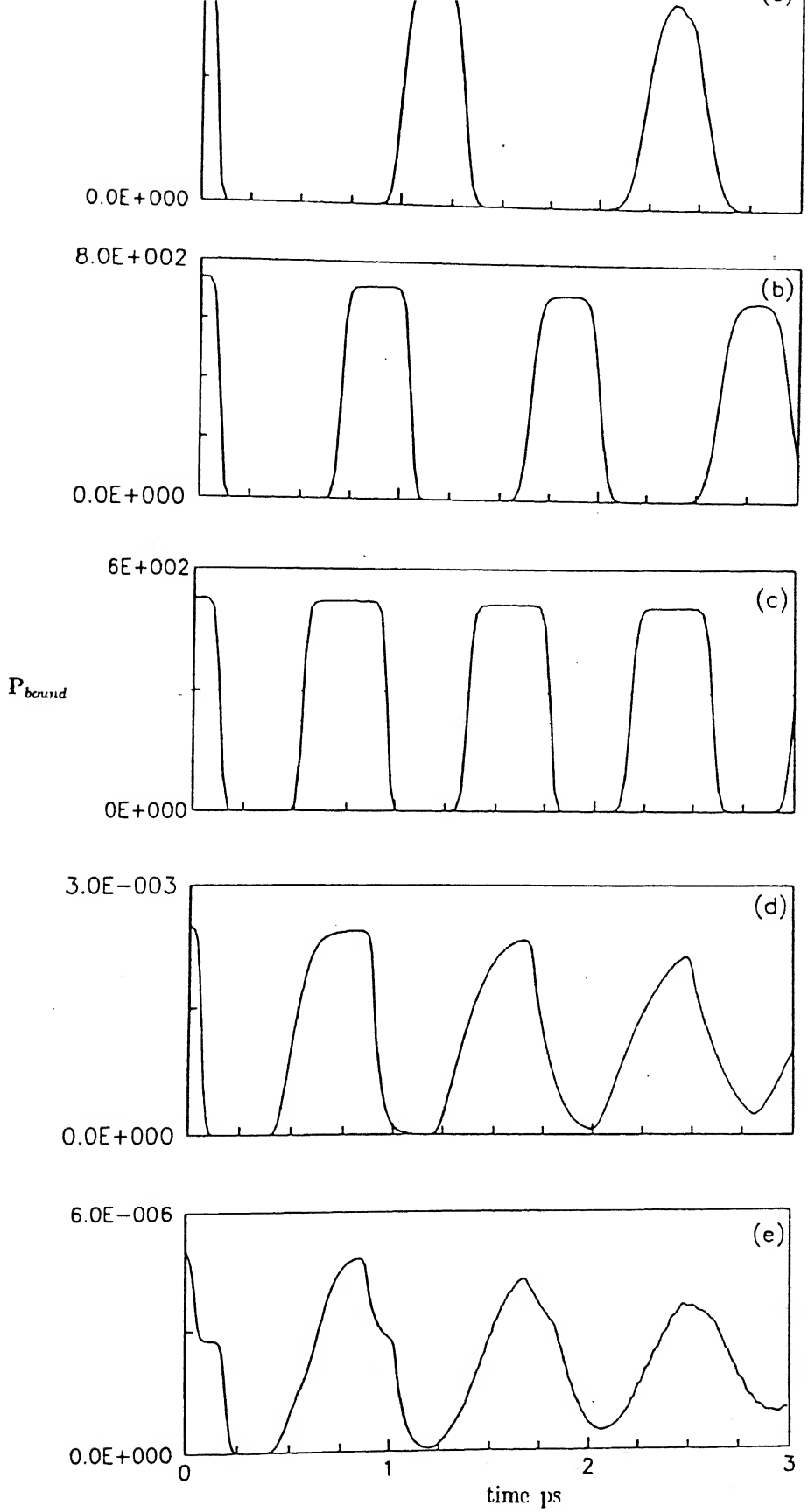

Figure 3.5. Bound Na population (P_{bound}) as a function of time. (a), (b), (c), (d) and (e) correspond to photoexcitation wavelengths 300, 321, 344, 360 and 390 nm respectively.

results are interpreted in terms of the *transient* effect. In general, the oscillation period obtained from the bound Na population for 300, 321 and 344 nm agree well with earlier results.

Chapter 4

Channel Control in a Chemical Reaction. Vibrational Enhancement of I^*/I Branching Ratio in HI Photodissociation

4.1 Introduction

Several strategies have been proposed over the years to control the outcome of a collision event, to effect one channel preferentially over the other. Considering one of the simplest collisions, that between an atom(A) and a diatom(BC) as an example, several outcomes are possible depending upon energy and other factors:

$$A + BC \rightarrow A + BC \quad \text{(NR)}$$
$$\rightarrow AB + C \quad \text{(R1)}$$
$$\rightarrow AC + B \quad \text{(R2)}$$
$$\rightarrow A + B + C \quad \text{(CID)}$$
$$\rightarrow \ldots$$

The simplest means of channel control known to chemists for a long time has been to increase the relative translational energy (E_{trans}) of reactants by supplying heat. For $E_{trans} < E_{th}$ where E_{th} is the threshold energy for the exchange reaction, the only channel available is NR. For $E_{trans} > E_{th}$ the exchange channel R1 opens up. Similar constraints

hold for R2 and CID channels. Depending upon the system, charge transfer and other channels open up at different E_{trans}. In the last 2–3 decades it has been realised that for many reactions the reagent vibrational excitation enhances the reaction cross section more selectively than E_{trans}[252]. The reagent rotation plays a subtler role[253]. For many reactions, rotational excitation of a reactant molecule leads initially to a decrease in the reaction cross section. Invariably this trend is followed by rotational enhancement, becoming comparable to vibrational enhancement.

While such strategies rely upon initial state preparation of reactants, substantial effort has gone into examining the possibility of controlling the collisional outcome by intervening at the transition state[254]. We must add that the success via this route has been rather limited so far.

In the case of unimolecular reactions, one is always concerned about the possibility of energy randomisation. Attempts have been made to understand the factors responsible for intramolecular vibrational relaxation (IVR) and to look for means of attaining mode selectivity[255].

Several schemes have been proposed in the last few years to achieve channel control. Rice and coworkers[117, 256] proposed a pump and dump scheme which envisages electronically exciting a molecule (using a pump laser), letting the system time-evolve on the excited state and stimulating de-excitation (dump) onto the lower channel. Using a model system they showed (numerically) that channel control could be achieved by adjusting the time delay between pump nd dump pulses. Gadzuk[257] pointed out how the same could be accomplished in an adsorbate molecule by altering the workfuncion of a metal surface by depositing alkali metal atoms, without using laser pulses. Brumer and Shapiro[156] pointed out how it might be possible to utilise the coherence property of a laser for the same pur-

pose. Several workers (for example, see ref.[155, 258, 259]) have examined the possibility of using differently shaped pulses to attain the same goal. More recently, Rabitz[260] and coworkers have examined the possibility of inverse quantum mechanical control. That is, depending upon the choice of products, work out (inversely) the requirement of the shape of the field and then put it to practice.

Attempts have also been made to obtain one set of products preferentially over another by combining initial state preparation with photodissociation. For example, using model calculations, Imre and coworkers[50, 52] pointed out the predominance of one isotopic channel over the other in the photodissociation of HOD, arising from initial vibrational excitation. Crim and coworkers[261] have demonstrated experimentally vibrationally mediated photodissociation in HOD leading to a higher OD/OH branching ratio. Shapiro[99] had pointed out the importance of including non-adiabatic coupling while investigating the photodissociation of CH_3I. Schatz and coworkers[53, 56, 262] showed that, vibrational excitation of the molecule in its ground electronic state could influence the branching ratio, Γ, for I^* and I formation, in the photodissociation of CH_3I. Kash and Butler[263] demonstrated that vibrational excitation prior to photodissociation serves as a probe of the nature of non-adiabatic coupling.

Photodissociation of hydrogen iodide (HI) in the near UV region has been studied extensively by theory[265–268] and experiment[269–273]. It is of interest in both dynamical and spectroscopic studies. In dynamical studies, for instance, the translationally *hot* hydrogen atoms produced in the HI photodissociation are used as a source for the H atom to study H atom exchange reactions[273, 274] and translational $\rightarrow$ vibrational energy transfer processes[275, 276].

As early as 1930, Mulliken[264, 265] predicted that the photodissociation of HI involved

photoabsorption from the ground electronic state ($X\ ^1\Sigma_0$) to excited electronic states: $^3\Pi_1$, $^1\Pi_1$ and $^3\Pi_0$. Among the excited states, photoexcitation to $^3\Pi_1$ and $^1\Pi_1$ states led to $H(^2S) + I(^2P_{3/2})$ and to $^3\Pi_0$ state led to $H(^2S) + I^*(^2P_{1/2})$. He also clarified that the electronic transitions $^1\Sigma_0 \rightarrow {}^3\Pi_1$, $^1\Pi_1$ as perpendicular transitions and $^1\Sigma_0 \rightarrow {}^3\Pi_0$ as a parallel transition. Therefore, according to this interpretation H + I^* products are essentially produced from the parallel transition. Subsequently various experimental and theoretical studies have been carried out to understand the photodissociation mechanism and to obtain the nature of the potential energy curves for the system.

For example, Ogilvie employed a δ - function approximation to the spectral profile and constructed a single repulsive excited electronic state[266]. Clear et al.[270] applied photofragmentation spectroscopy and estimated that 36 $\pm$ 5 % of I were produced in the photodissociation of HI at the excitation wavelength, λ_{ex} = 266.2 nm. Also the measured kinetic energy distribution and the product angular distribution were found to be in agreement with Mulliken's interpretation. Schmiedl et al.[271] implemented laser Doppler spectroscopic technique and obtained similar results. The I^*/I branching ratio (Γ) obtained by them at λ_{ex} = 266 nm was $\sim$ 1.5. The photofragmentation mechanism proposed in the former studies was in accord with the earlier predictions of Mulliken. However, the photofragmentation spectroscopic studies carried out by Van Veen et al.[272] at λ_{ex} = 193 nm, 222 nm and 248 nm, suggested a slightly different mechanism. Accordingly, the observed photodissociation of HI was ascribed to the following electronic transitions: $^1\Sigma_0 \rightarrow {}^3\Pi_1$, $^1\Sigma_0 \rightarrow {}^1\Pi_1$, $^1\Sigma_0 \rightarrow {}^3\Pi_0$ and $^1\Sigma_0 \rightarrow {}^3\Sigma_1$. The former two transitions were of perpendicular type and led to H + I formation and the later two transitions were of perpendicular and parallel types respectively and they both led to H + I^* formation. All these excited states, except $^3\Pi_0$, were nonadiabatically coupled to each other. Since the

coupling potentials were weak, the photodissociation cross sections and the I*/I branching ratio calculated by Van Veen et al. without including nonadiabatic couplings were found to be in good agreement with experimental results. Mulliken also considered the $^1\Sigma_0 \rightarrow {}^3\Sigma_1$ transition in his studies[264]. However, he assumed that the $^3\Sigma_1$ state was lying higher in energy than the other states. Recently, Wittig and coworkers[100] have carried out high resolution spectroscopy studies on the photofragmentation of HI and HBr and the results obtained by them are in good agreement with the photofragmentation spectroscopy measurements of Van Veen et al. Therefore, it can be concluded the location of the $^3\Sigma_1$ state and its nonadiabatic coupling with other electronic states are playing vital rule in deciding the outcome of the photodissociation.

By making use of the experimental values such as the photodissociation cross sections and I*/I branching ratios at different excitation energies, Levy and Shapiro[267] constructed semiempirical potential energy curves and nonadiabatic couplings for the different states of HI. Subsequently they employed the TIQM approach and obtained the photodissociation cross sections, the I*/I branching ratio and the anisotropy parameter(β) over the energy range 30,000–50,000 cm^{-1}. The results obtained by them were in good agreement with the earlier studies. An important conclusion from their study was that the inclusion of nonadiabatic coupling was highly essential to estimate Γ accurately. Once Γ as a function of the excitation energy is known, one can select λ_{ex} and produce H atoms with specific translational energy for use in dynamical experiments. In addition, understanding the mechanism of branching might help us to look for some means to control Γ.

Since the previous study carried out by Levy and Shapiro[267] was restricted only for the ground vibrational state ($v'' = 0$) of HI in its ground electronic state, we decided to investigate the HI photodissociation in detail, including the effect of vibrational excitation

of HI on the nonadiabatic coupling using the TDQM approach. Since the method of computing the photodissociation cross section has been discussed explicitly in chapter 2 (section 2.4.2.), we only state the salient features and present the results and discussion in the next section.

4.2 Results and discussion

As mentioned in the Introduction HI photodissociation involves photoexcitation from the ground electronic state ($^1\Sigma_0$) to the excited states $^3\Pi_1$, $^1\Pi_1$, $^3\Sigma_1$ and $^3\Pi_0$. The potential energy curves are shown in figure 4.1. Except for the $^3\Pi_0$ state all the other states are nonadiabatically coupled to each other. As we have discussed in the methodology chapter(see section 2.5), the multielectronic state dynamics can be easily solved in the diabatic representation. Therefore, we have carried out our calculations in this representation.

The functional form of the diabatic potential energy curves for the excited states and the nonadiabatic coupling potentials are taken from Levy and Shapiro's work. They are,

$$\langle \xi | V(R) | \xi \rangle = A(\xi) exp\left(-B(\xi)(R - R_e)\right) + c(\xi) \tag{4.1}$$

and

$$\langle \xi' | V(R) | \xi \rangle = \frac{V(\xi' | \xi)}{[1 + exp(R - 7)]} \tag{4.2}$$

where $\xi, \xi' = {}^3\Pi_1, {}^1\Pi_1, {}^3\Sigma_1$ and $^3\Pi_0$. The parameters used to fit the potential energy curves are given in table 4.1.

The ground electronic state of HI is represented by a Morse curve and the ground vibrational state (v"=0) wavefunction is transposed on the excited state potential energy curves given by Levy and Shapiro[267] and time-evolved using the corresponding excited state Hamiltonian. We have made use of the transition dipole moments reported by the

Table 4.1: HI potential energy parameters

Ground electronic state parameters:

$D_{eq} = 0.117\ 450\ 259$, $\beta_g = 0.926\ 910\ 853$, $R_g = 3.040\ 872\ 9$

Excited electronic state parameters:

ξ	$^3\Pi_1$	$^1\Pi_1$	$^3\Sigma_1$	$^3\Pi_0$
$A(\xi)$	0.055 09	0.1087	0.04174	0.04664
$B(\xi)$	1.043	1.101	1.588	1.843
$C(\xi)$	0.0	0.0	0.034 650 9	0.034 650 9
$\mu(\xi)$	0.007 830 4	0.019 287	0.009 983	0.011 451

Nonadiabatic coupling potentials:

ξ'/ξ	$^3\Pi_1$	$^1\Pi_1$	$^3\Sigma_1$	$^3\Pi_0$
$^3\Pi_1$	...	0.001 959	0.001 909	0.0
$^1\Pi_1$	0.001 959	...	0.001 620	0.0
$^3\Pi_0$	0.0	0.0	0.0	...

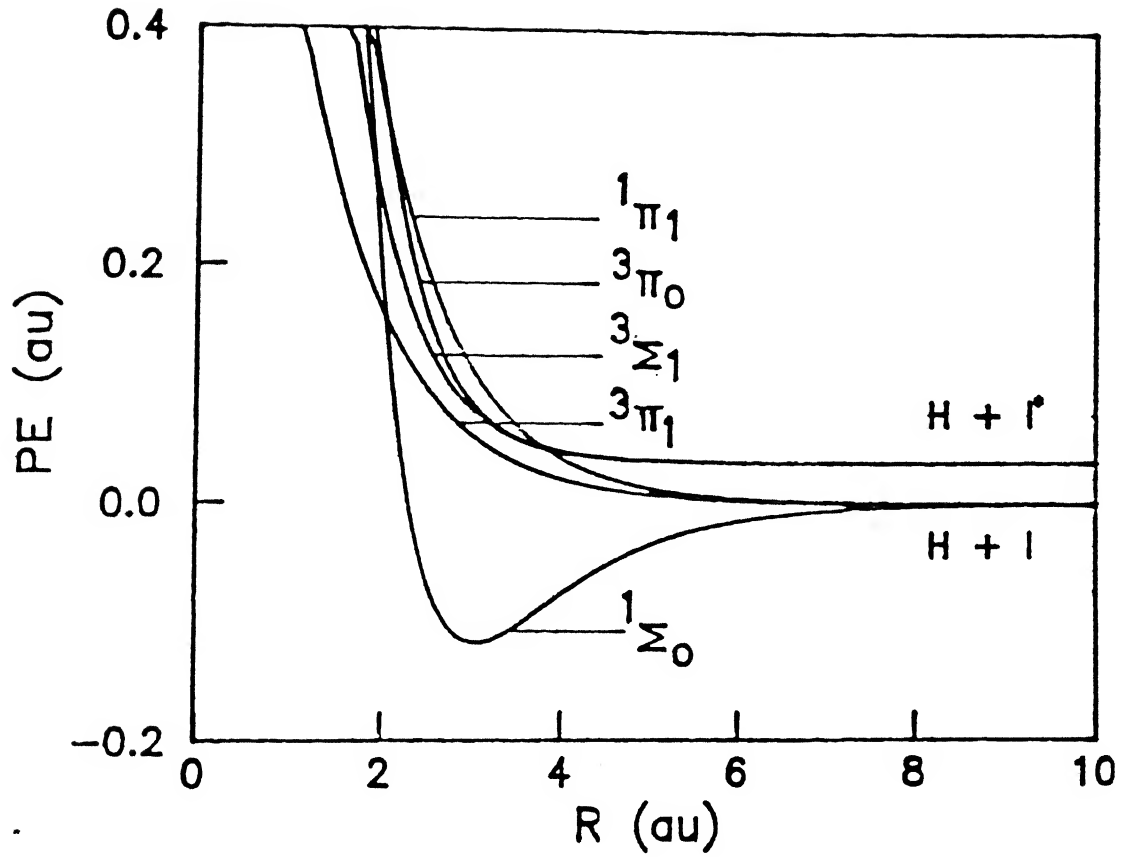

Figure 4.1. Potential-energy curves for the ground and the first four excited states of HI [267]

same authors. The nonadiabatic effects are fully taken into account by solving the multi-electronic state time-dependent Schrödinger equation:

$$i\hbar \frac{\partial}{\partial t} \begin{pmatrix} \Psi_1 \\ \Psi_2 \\ \Psi_3 \\ \Psi_4 \end{pmatrix} = \begin{pmatrix} H_{11} & V_{12} & V_{13} & 0 \\ V_{21} & H_{22} & V_{23} & 0 \\ V_{31} & V_{32} & H_{33} & 0 \\ 0 & 0 & 0 & H_{44} \end{pmatrix} \begin{pmatrix} \Psi_1 \\ \Psi_2 \\ \Psi_3 \\ \Psi_4 \end{pmatrix} \tag{4.3}$$

where the subscripts 1,2,3 and 4 represent $^3\Pi_1$,$^1\Pi_1$,$^3\Sigma_1$ and $^3\Pi_0$ states respectively. The second derivative of the wavefunction with respect to R, the internuclear distance of HI, was obtained by the FFT method[85] and the time-evolution was accomplished by the second order finite difference(SOD) method[88]. The spatial grid consisted of $R = 0.1(0.1)25.6$ au and the time-evolution involved a total of 27,384 steps with each time step(Δt) = 0.00218fs.

The time-evolution was followed graphically for 11,000 steps by which time the population in each state, reflected in the value of $\langle\Psi|\Psi\rangle$, levelled off as shown in figure 4.2. This ensured that the effect of diabatic crossings on the wavefunction was fully taken into account as has been done by others[126]. For the wavefunction at the 11,000th time step, the autocorrelation function $\langle\Psi(T)|\Psi(T+t)\rangle$ was evaluated for the remaining 16,384 (=2^{14}) steps. Here T refers to 11,000Δt. In order to compute the partial photodissociation cross section, the choice of T is irrelevant. But for computing the Γ, T must be greater than τ, the time taken by the wavefunction to traverse the diabatic crossings[126]. The partial photodissociation cross section for each electronic channel was obtained by Fourier transforming the respective autocorrelation function and the results are shown labelled 1,2,3 and 4 in figure 4.3a. All these results are in excellent agreement with those obtained by the time-independent route by Levy and Shapiro[267]. The value of Γ was obtained by taking the ratio of the sum of the partial photodissociation cross sections[79] for I^* and

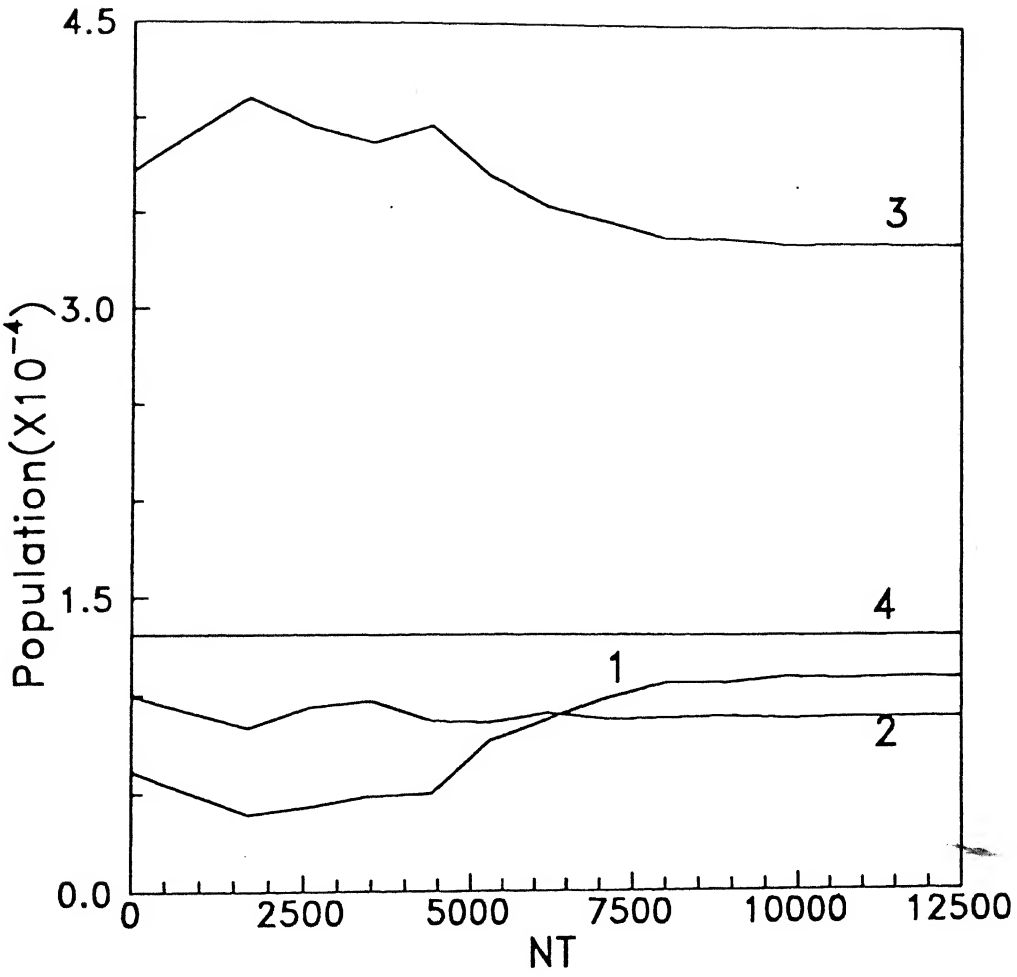

Figure 4.2. Norm on the four excited states as a function of number of time steps (NT). Each time step $\Delta t = 0.00218$fs.

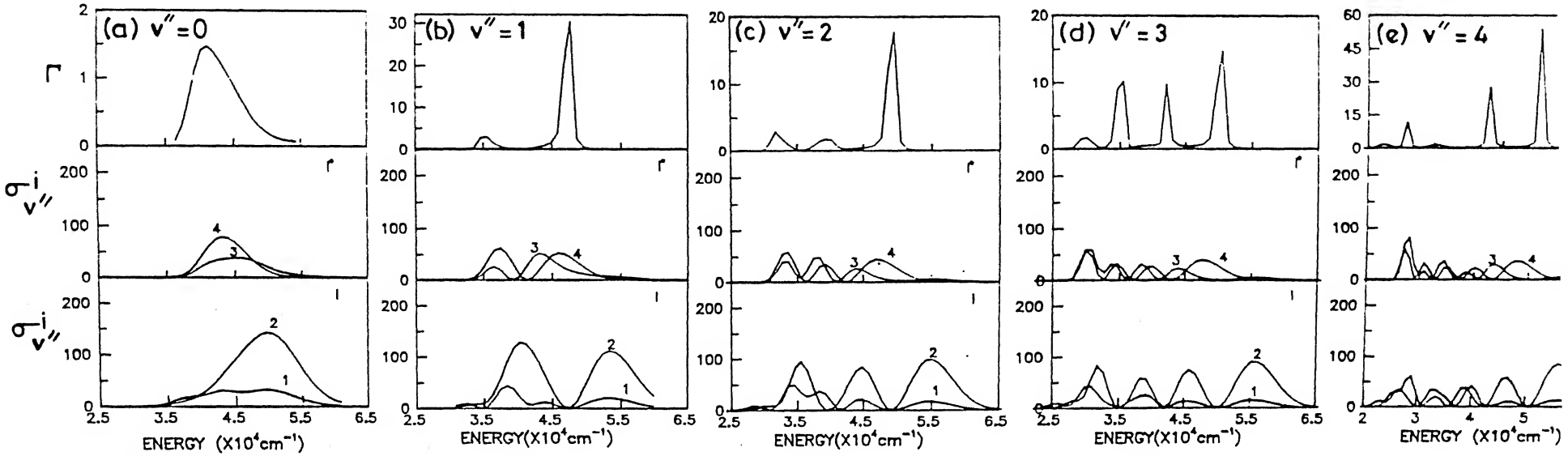

Figure 4.3. Partial photodissociation cross sections ($\sigma^i_{v''}$)(in arbitrary units) for HI in different electronic states. The superscript i= 1,2,3 and 4 refers to $^3\Pi_1$,$^1\Pi_1$,$^3\Sigma_1$ and $^3\Pi_0$ states respectively and the subscript v" indicates the vibrational state of HI. Results of branching ratio $\Gamma = \sigma(H+I')/\sigma(H+I)$ for different v" are included in the top panels.

I channels and the results included in figure 4.3a are also in accord with the previously reported values. It is worthwhile to mention that due to the presence of nonadiabatic couplings the intensity of the $^3\Pi_1$ and $^3\Sigma_1$ are affected appreciably (intensity borrowing) though $^1\Pi_1$ is not affected much.

The anisotropy parameter (β) is an important experimental quantity which characterises the nature of the electronic transitions[18, 128, 272, 277]. In the center of mass frame β parameter is related to the angular distribution of the products through

$$I(\theta) = \left(\frac{\sigma_0}{4\pi}\right)[1 + \beta P_2(cos\theta)] \tag{4.4}$$

where θ is the angle between the detection direction and the direction of the polarisation vector of the incident light (ϵ), σ_0 is the total cross section, 4π is a normalisation factor and P_2 is the second order Legendre polynomial. In the case of a purely parallel transition β = 1 and the net electronic angular momentum change during the electronic transition will be $\Delta\Omega = 0$. On the other hand for a purely perpendicular transition β = -0.5 and the net electronic angular momentum change will be $\Delta\Omega = \pm 1$. Therefore, in HI photodissociation $^1\Sigma_0 \rightarrow ^3\Pi_0$ transition is of purely parallel type whereas $^1\Sigma_0 \rightarrow ^3\Pi_1, ^1\Pi_1$ and $^3\Sigma_1$ transitions are of purely perpendicular type. For a parallel type transition the intensity is proportional to $\cos^2\theta$. But for a perpendicular type transition it is proportional to $\sin^2\theta$. If a particular product channel originates from parallel and perpendicular transitions as it happens in the H + I* channel, then we can write the β parameter as

$$\beta = A - 0.5\,B \tag{4.5}$$

where A and B are the percentages of parallel and perpendicular transitions respectively. Similarly, if β parameter is known A and B can be obtained from it by

$$A = \frac{(2\beta+1)}{3}, \quad B = \frac{(2-2\beta)}{3}$$

By making use of eq.(4.5), we computed the β parameter over the energy range 34,000 - 52,000 cm^{-1}. The results are shown in figure 4.4 along with the experimental values obtained by Van Veen et al.[272]. Our results are in good agreement with the experimental values[272] and the time-independent quantal results[267]. In the low energy region I^* formation is predominantly due to parallel transition whereas in the high energy region it is due to perpendicular transition.

We have repeated the above calculations for different initial vibrational states of HI and the results are included in figure 4.3b–4.3e for v"=1–4. In general, one finds that there is an order of magnitude increase in Γ with increase in v". Further, for each v" there are v"+1 peaks in the Γ versus energy plot. For v"=1, the peak at the higher energy is particularly strong. For v"=2 and 3, this peak becomes less intense but the peaks at the lower energy become stronger. For v"=4, the higher energy peak is the strongest with two additional peaks being strong and two weak. Much of the structure in plots of $\Gamma(E)$ can be understood from the structures in plots of $\sigma^i_{v''}$, i=1,2,3,4. For convenience, we have grouped the results for i=1 and 2 corresponding to the H + I channel in one part of the figure and for i=3 and 4 corresponding to H + I^* in another. The major features in the $\sigma^i_{v''}$ curves can be understood in terms of the "reflection principle" which predicts v"+1 peaks. The additional structures in the $\sigma^i_{v''}$ curves can be traced to the nonadiabatic coupling between the different electronic states.

In order to further elucidate the mechanism underlying the vibrational enhancement of Γ we have plotted in figure 4.5, the steady state population, as determined from the $\langle\Psi|\Psi\rangle$ value for distances beyond the diabatic crossings, on the four excited states as a function of v". It is clear from this figure that the population on the $^3\Sigma_1$ state increases gradually with increase in vibrational excitation. However, on the $^3\Pi_1$ and $^1\Pi_1$ states the population

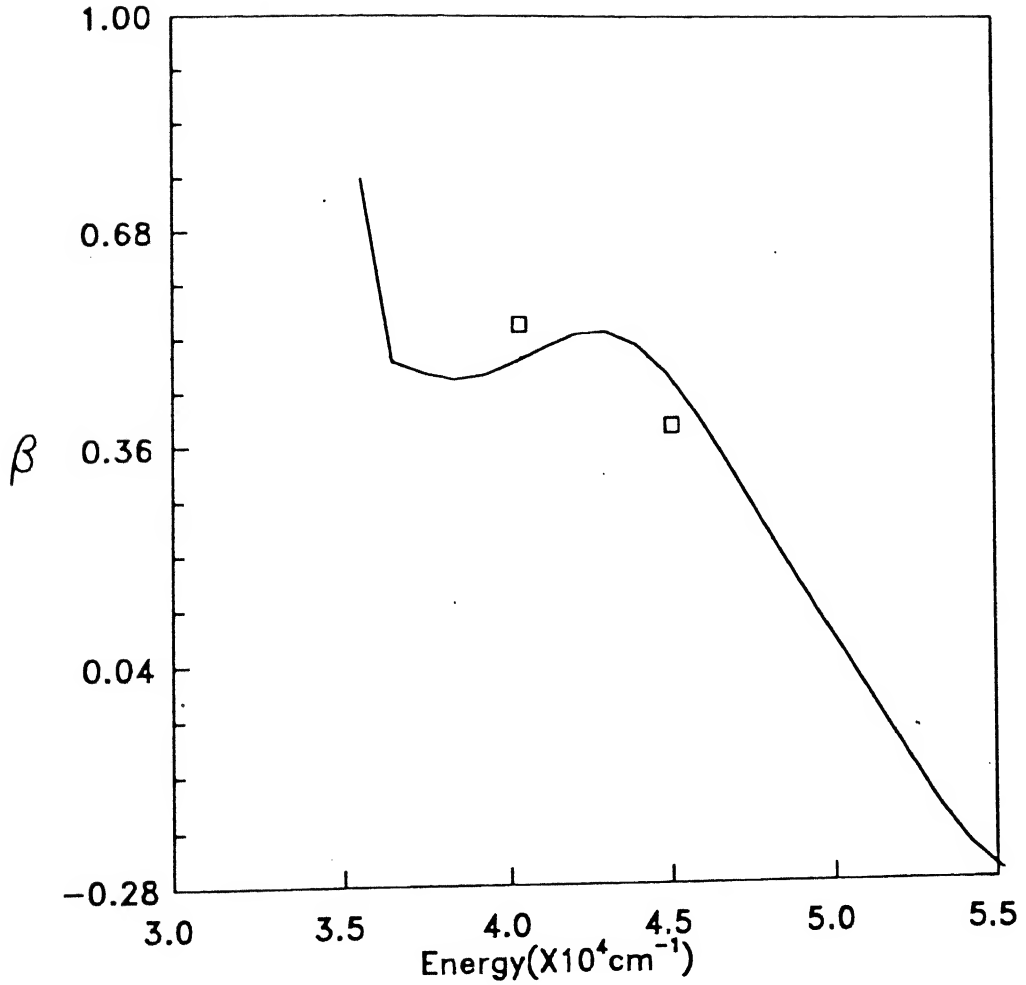

Figure 4.4. Anisotropy parameter (β) corresponding to H + I* channel as a function of excitation energy.

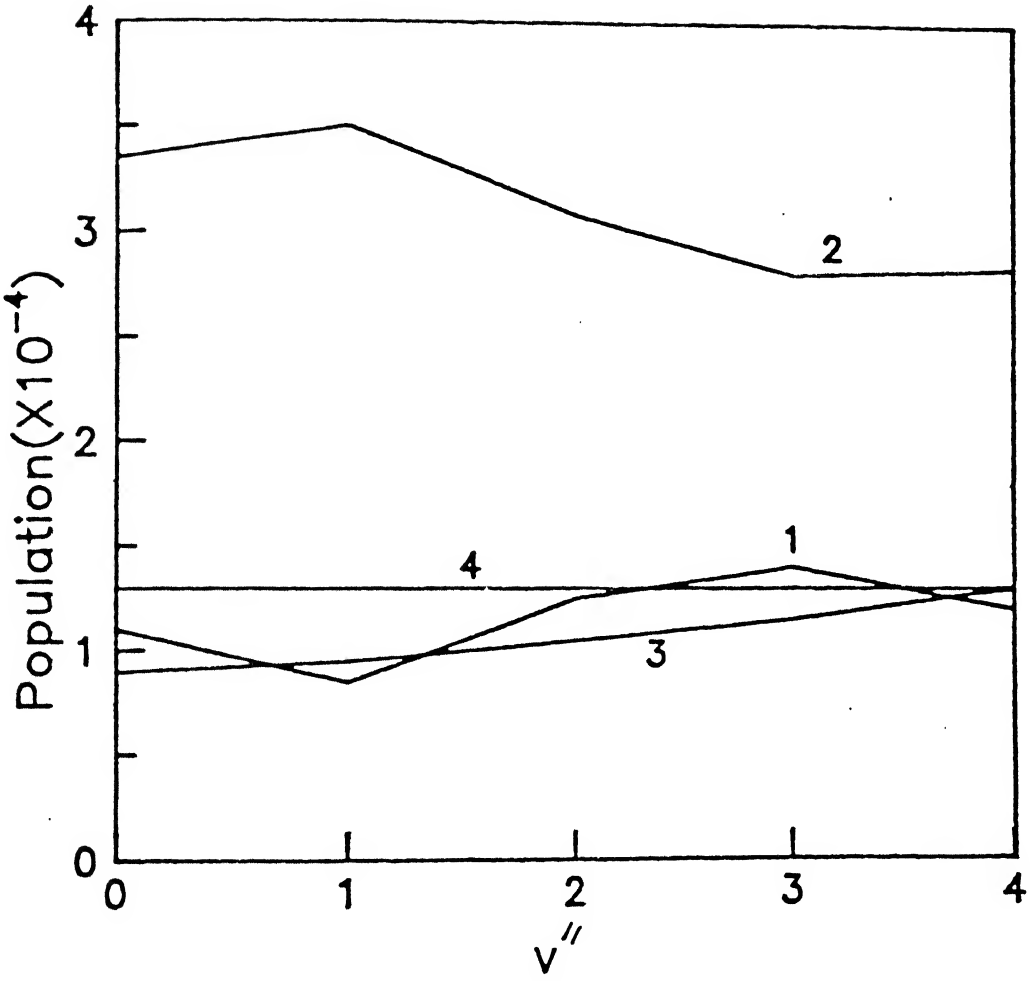

Figure 4.5. Steady state populations in the different electronic states for different v".

shows an oscillatory behaviour as a function of v". These results in turn can be understood by considering the nature of the initial vibrational wavefunctions prepared on the excited state $^3\Sigma_1$, for example, for different v" as illustrated in figure 4.6. Particularly from the wavefunction depicted for v"=4 in figure 4.6e, it is clear that a significant portion of it is present beyond the crossing point. Since the $^3\Sigma_1$ and $^1\Pi_1$ states cross (diabatically) at R = 3.8 au, vibrational excitation of HI prior to photodissociation assists the wavefunction in *escaping* from the non-adiabatic coupling region. Therefore it is understandable that Γ(E) is strongly dependent on v".

4.3 Conclusion

The time-dependent quantum mechanical calculation carried out for HI photodissociation from the ground vibrational (v"=0) state of the ground electronic state shows a good agreement with time-independent quantum mechanical results. The results obtained for the photodissociation of vibrationally excited HI shows an overall increase in Γ with v" and that it is highly structured as a function of the photoexcitation energy. These results have profound implications in that the branching ratio for two competing channels in a photodissociation process can be controlled by vibrational excitation. Also, this study suggests a means of enhancing the production of H atoms with a particular recoil energy for use in dynamics experiments.

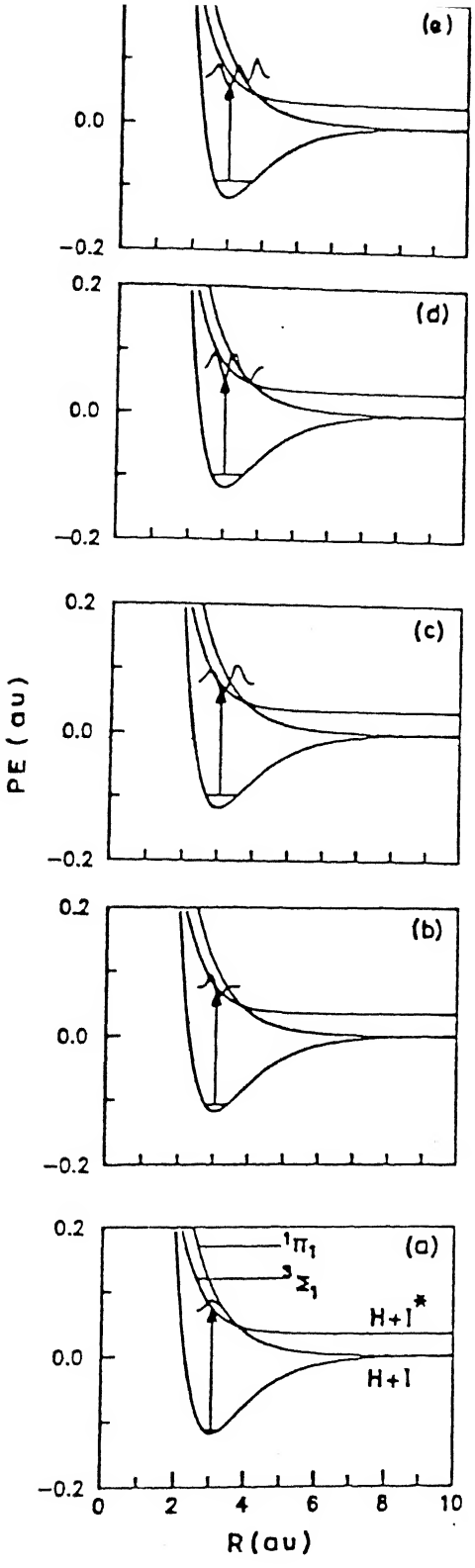

Figure 4.6. Illustartion of the initial vibrational wavefunctions transposed on the excited state $^3\Sigma_1$ vis-a-vis the non-adiabatic coupling region for different v". For the sake of clarity, we have included only the potential-energy curves for the ground electronic($^1\Sigma_0$) and $^1\Pi_1$ and $^3\Sigma_1$ states.

Chapter 5

Photodissociation and Predissociation Processes in Hydroxyl Radical

5.1 Introduction

Hydroxyl radical(OH) has been observed frequently in cometary gases and in interstellar clouds. It is one of the major constituents in the earth's atmosphere and in interstellar media. Also it is one of the important sources for O and H atoms in astrophysical environment[278, 279]. Therefore, understanding various dissociation pathways in OH becomes particularly important. Photodissociation and photon-induced predissociation are the major dissociative processes that occur in terrestrial atmosphere. Studies along this direction were initiated more than forty years ago[280]. However, precise information regarding the potential-energy(PE) curves for the system has become available only recently. The important PE curves involved in the photodissociation and predissociation processes in OH are shown in figure 5.1. *Ab initio* calculations carried out by Dalgarno and coworkers[282–284] showed that photoabsorption from the ground electronic state ($X^2\Pi$) to the excited states, $1^2\Sigma^-$, $1^2\Delta$, $B^2\Sigma^+$ and $2^2\Pi$, led to direct photodissociation. Photodissociation cross sections(σ) computed by them were later shown to be a factor of two smaller than the experimental results[284, 285].

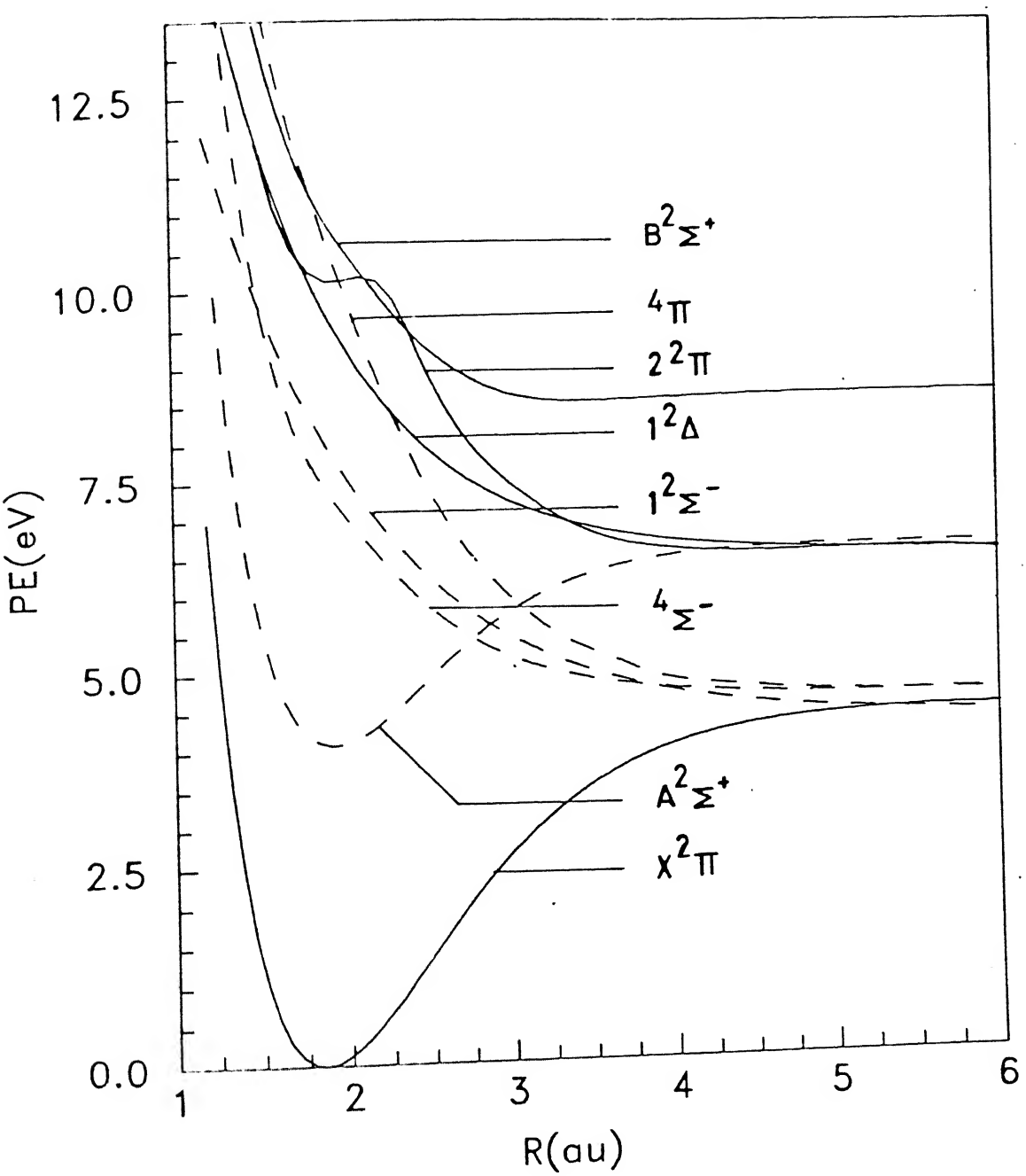

Figure 5.1. Potential-energy curves involved in photodissociation and predissociation processes in OH.

Predissociation in OH takes place[278] in the first absorption band ($A^2\Sigma^+$–$X^2\Pi$) due to spin-orbit coupling between the bound state $A^2\Sigma^+$ and the repulsive states $^4\Sigma^-$, $1^2\Sigma^-$ and $^4\Pi$, shown in figure 5.1 as dashed lines. The (A-X) band predissociation has been studied quite extensively by theory[287–289] as well as experiment[290–298]. For instance, Gaydon and Wolfhard[280] observed an anomalous decrease in spectral line intensities corresponding to all rotational levels of v' = 2 and higher rotational levels of v' = 1 while investigating the radiative lifetimes of the ($A^2\Sigma^+ - X^2\Pi$) transition and they attributed it to predissociation. Subsequent experimental and theoretical studies also confirmed the occurrence of a weak predissociation near $v' \leq 3$. In addition to this weak predissociation, Carlone and Dalby[289] and Czarny and coworkers[291] observed a strong predissociation near $v' \geq 5$. Czarny and coworkers suggested that the observed predissociation was due to spin-orbit interaction and they also made an estimate of the coupling between the $A^2\Sigma^+$ and the $^4\Pi$ state. They had also estimated the predissociation lifetimes to be of the order of 10^{-11} sec. Based on experimental observations[290–295] and *ab initio* calculations of Michels and Harris[286], it was proposed that the weak and the strong predissociations in OH were due to spin-orbit coupling between the bound state $A^2\Sigma^+$ and the repulsive states $^4\Sigma^-$ and $^4\Pi$ respectively.

Sink et al.[287] employed a multichannel scattering calculation to determine the dependence of predissociation linewidths (Γ) on the rotational-vibrational levels of $A^2\Sigma^+$. They included the *ab initio* values of the spin-orbit coupling between $A^2\Sigma^+$ and $^4\Sigma^-$, $^2\Sigma^-$ and $^4\Pi$. However, their spin-orbit coupling potentials were not explicitly dependent on the OH bond distance. Recently, Yarkony[298] has carried out an extensive configuration interaction (CI) calculation to determine the spin-orbit coupling matrix elements and their influence on the predissociation lifetimes. Unfortunately, the results reported

by him were restricted to the $^4\Sigma^-$ state and that too for the first four vibrational levels of the $A^2\Sigma^+$ state. Since (A - X) band laser-induced-fluorescence is used extensively to monitor OH produced in collision-free environments[299], there has been a lot of interest in understanding the details of the predissociation.

We decided to investigate both photodissociation and predissociation processes in OH using the TDQM approach to obtain an independent estimate of σ(E) and Γ and also to get a better understanding of the underlying mechanism. It is worthwhile to mention that the predissociation lifetimes(τ) are usually of the order of picoseconds and as a result there are only a few numerically exact TDQM studies available in the literature[167]. In our calculations we have employed the wave packet golden rule method[168] to determine Γ. This chapter is divided into three sections. In sections 2 and 3 we discuss the methodology and the results obtained for photodissociation and predissociation processes. The conclusions are given in the final section.

5.2 Photodissociation

As mentioned in the Introduction, photoabsorption from the ground electronic state ($X^2\Pi$) to $1^2\Sigma^-$, $1^2\Delta$, $B^2\Sigma^+$ and $2^2\Pi$ channels lead to direct photodissociation. Therefore, we have considered only these four states in our calculation. We have made use of the *ab initio* PE curves and the transition dipole moments reported earlier in the literature[282–284]. Potential energy values as a function of OH bond distance R, for the ground state, were fitted, using an extended Rydberg function[300]:

$$V(r) = -D_e(1.0 + a_1\rho + a_2\rho^2 + a_3\rho^3)exp(-\gamma\,\rho) + D_e \tag{5.1}$$

where $\rho = R$ - R_e with R_e the equilibrium bond distance and D_e the classical bond dissociation energy. The parameters a_1, a_2, a_3 and γ obtained from the fit are given in

Table 5.1: Extended Rydberg function parameters for the $X^2\Pi$ and $A^2\Sigma^+$ potential-energy curves of OH.

	$X^2\Pi$	$A^2\Sigma^+$
D_e(eV)	4.47	2.54
r_e(au)	1.8519	1.9294
$a_1(au^{-1})$	2.448 749 07	3.026 579 60
$a_2(au^{-2})$	1.609 992 94	2.693 375 05
$a_3(au^{-3})$	0.690 901 18	1.120 864 54
$\gamma(au^{-1})$	2.481 589 59	3.065 781 57

Table 5.2: $X^2\Pi$ state eigenvalues for v''=0–5.

v'	$E_{v'}(cm^{-1})$
0	1792.79
1	5263.87
2	8601.42
3	11751.86
4	14767.36
5	17597.10

table 5.1. The excited state PE curves and the transition dipole moments were interpolated smoothly using cubic splines.

Once the ground electronic state PE curve is known, the next step is the computation of the ground vibrational eigenfunction. In order to compute this we have made use of the spectral method[83, 84] which consists of two steps. In the first step, vibrational eigenvalues corresponding to the ground electronic state are computed and in the second step the vibrational eigenfunctions are computed. For the first step, we started with the initial wavefunction

$$\psi(R,0) \;=\; A\, e^{-B\,(R-R_d)^2} \tag{5.2}$$

where $A = 0.4454$, $B = 0.0309$ au^{-2} and $R_d = 3.5$ au and time-evolved using the split operator method on the ground electronic state PE curve. At each step of the propagation the autocorrelation function

$$c(t) \;=\; \langle \psi(R,0) | \psi(R,t) \rangle$$

was determined. We carried out the time evolution for 16,384 steps with each time step equal to 0.133 fs. After completing the time evolution, $c(t)$ was Fourier-transformed to obtain the power spectrum, $c(E)$ as shown in figure 5.2. For graphical resolution purpose we have actually plotted log $c(E)$ in figure 5.2 which shows several sharp maxima and each one of them corresponds to a particular eigenvalue of the bound state. In order to obtain a better energy resolution, the time-evolution had to be carried out for a long duration as determined by

$$\Delta E \;=\; \frac{\pi}{T} \tag{5.3}$$

where $T = NT \times DT$ with NT and DT the total number of time-steps and the time-increment respectively. In addition, to avoid the overlapping sidelobes of the energy spectrum, we

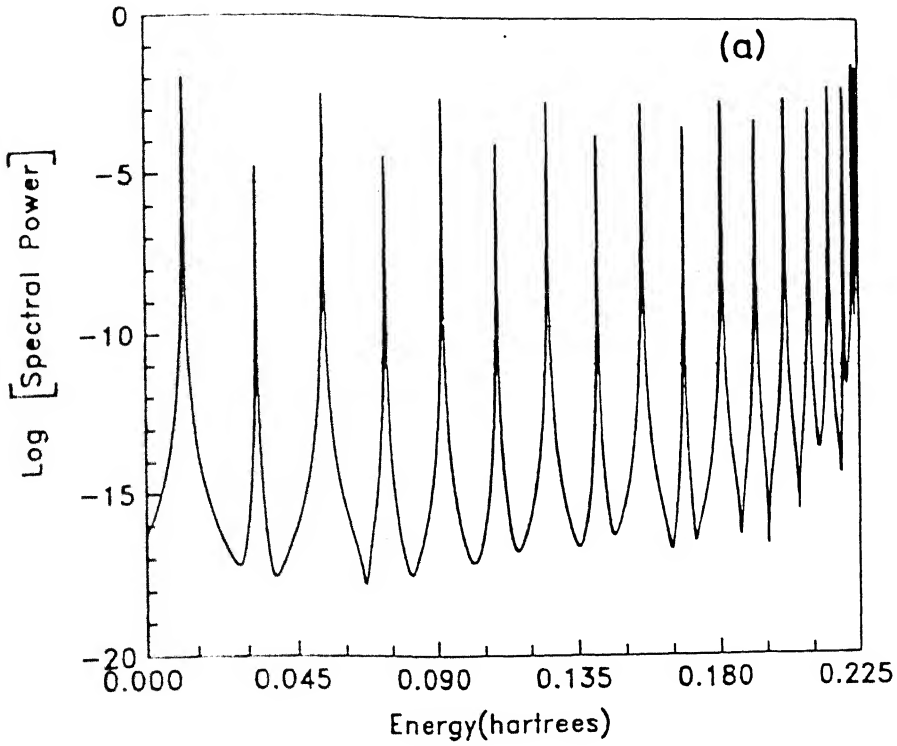

Figure 5.2. Log. of power spectrum as a function of energy for $X^2\Pi$ state.

multiplied the $c(t)$ by Hanning window function $w(t)/T$, before Fourier transformation, as suggested by Feit et al[83]. Also the accuracy of the eigenvalues could be improved further by using a single line fitting procedure[83]. The eigenvalues obtained for the first six vibrational levels are listed in table 5.2.

Once the eigenvalues were known, the vibrational eigenfunctions could be obtained from

$$\psi(R, E_i) = N \int_{-\infty}^{\infty} e^{iE_i t/\hbar} \frac{w(t)}{T} \psi(R, t)\, dt \tag{5.4}$$

where E_i is the eigenvalue of a particular vibrational level and N is the normalisation constant.

Photodissociation cross section(σ) was computed as a function of energy $E(= E_i + h\nu$, where ν is the frequency of the incident radiation and E_i the internal energy of the molecule) using the formula[179, 224]:

$$\sigma(E) = \frac{\pi\nu}{3\hbar c\epsilon_0} \int_{-\infty}^{\infty} e^{iEt/\hbar} \overbrace{< \phi(0)|\phi(t) >}^{C(t)} dt \tag{5.5}$$

where ϵ_0 is vacuum permittivity constant.

$$|\phi(t) >= e^{-iH_{ex}t/\hbar}|\phi(0) > \tag{5.6}$$

where

$$|\phi(0) >= \mu|\psi(0) > \tag{5.7}$$

Here H_{ex} is the Hamiltonian of the excited electronic state and $C(t)$ is the autocorrelation function defined as indicated in eq.(5.5).

The initial wavefunction for the ground vib-electronic state, ($\psi_{v''=0}$), obtained by the spectral method was transposed on each one of the excited electronic states after multiplying it with the corresponding transition dipole moment. Time-evolution of the transposed

wavefunction, $\phi(0)$, was accomplished by a second order differencing(SOD) scheme[85, 88] and the spatial derivative was obtained by the FFT method[85]. The spatial grid consisted of R = 1.5 (0.1) 14.2 au and we had to time evolve the wavefunction for states $1^2\Sigma^-$, $1^2\Delta$ and $B^2\Sigma^+$ for a total of 8192 steps with each time step being, Δt = 0.00241889 fs. This means that the photodissociation through these states is over in about 8 fs. This can also be seen from the readily decaying autocorrelation function ($|C(t)|$) for these states shown in figure 5.3a.

The photodissociation through the $2^2\Pi$ state took significantly longer time: about 25 fs. We had to time evolve the wavefunction for 16,384 steps with Δt = 0.001584 fs. It is clear from figure 5.3a that $|C(t)|$ for the $2^2\Pi$ state decays relatively slowly. An examination of the wavefunction reveals additional structures developing with time as illustrated in figure 5.4. As a matter of fact, the wavefunction spreads over the entire spatial grid and gets reflected from the edge. In order to avoid the reflections we used an absorbing potential[208]:

$$V_{abs} = \begin{cases} -iV_{i0}\frac{R-R_{abs}}{\Delta R_{abs}} & R_{abs} \leq R \leq R_{abs} + \Delta R_{abs} \\ 0 & R \leq R_{abs} \end{cases} \tag{5.8}$$

where V_{i0} is the height of the absorbing potential and ΔR_{abs} its width. We have used V_{i0} = 0.01 hartrees, R_{abs} = 10.5 au, ΔR_{abs} = 3.5 au. The difference in time-evolution on the $2^2\Pi$ state can be traced to the presence of a small *hump* in the PE curve which arises due to the strong interaction between $2^2\Pi$ and $3^2\Pi$ states (not shown). van Dishoeck et al[301] had suggested that this problem be handled using diabatic formulation but we have been able to solve it within the adiabatic representation.

Values of σ(E) computed from the autocorrelation functions for the different excited states are presented in figure 5.3b along with the earlier theoretical[282–284] and exper-

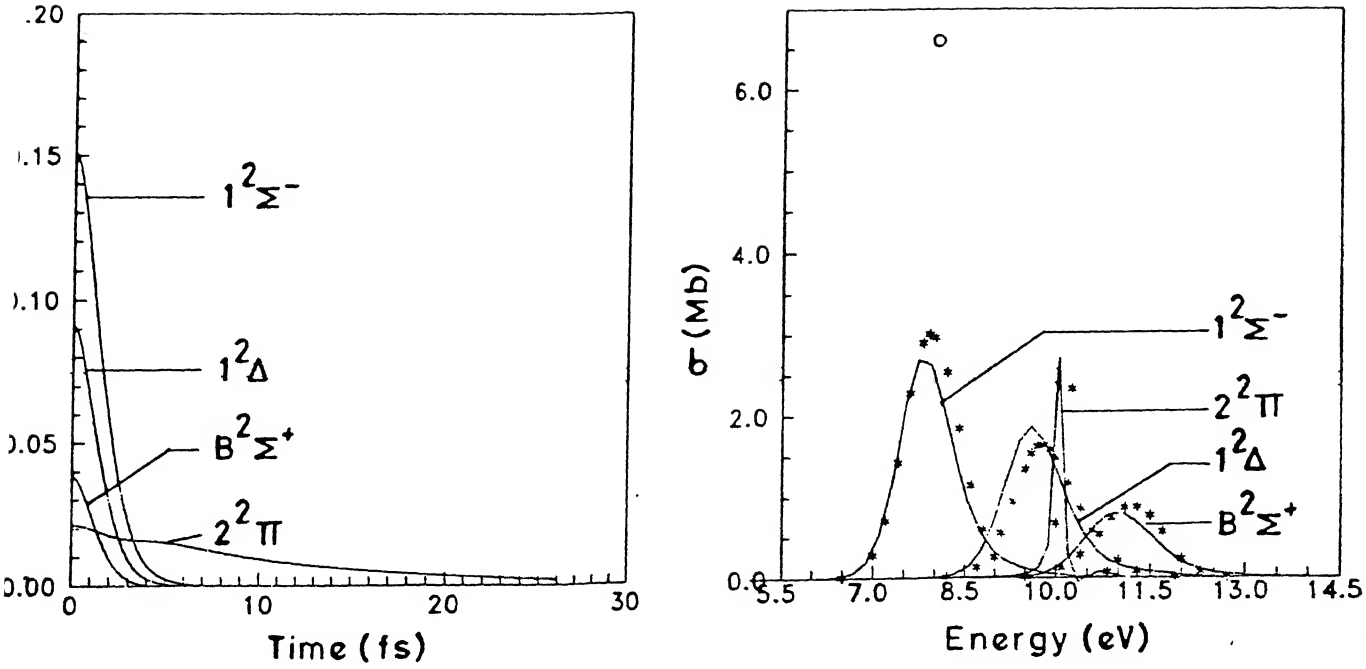

Figure 5.3. (a) Autocorrelation function ($|C(t)|$) and (b) the photodissociation cross section (σ(E)) corresponding to $1^2\Sigma^-$, $1^2\Delta$, $B^2\Sigma^+$ and $2^2\Pi$ states. 1 Mb = 1.0×10^{-18} cm^2

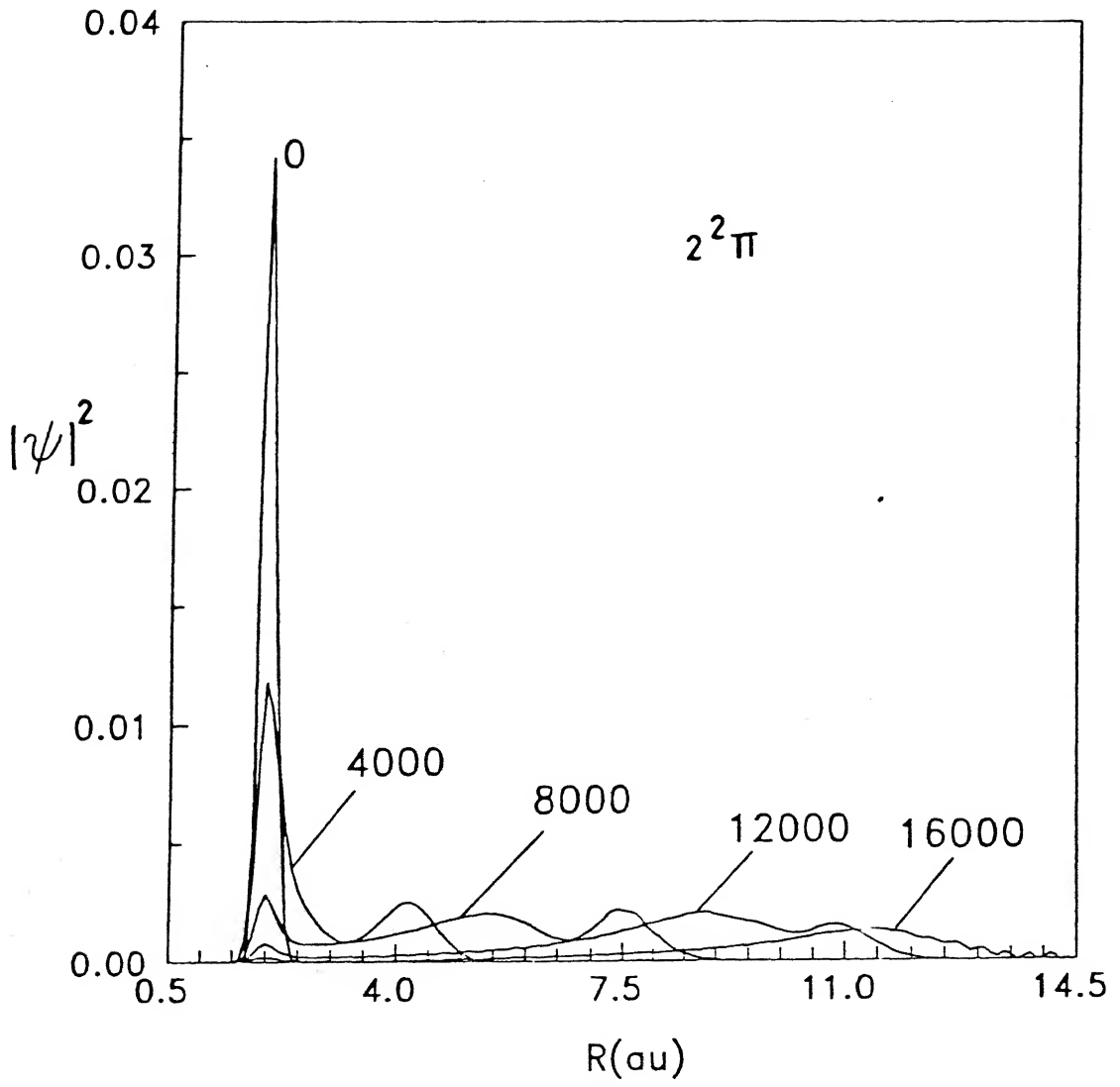

Figure 5.4. Plots of $|\psi|^2$ as a function of R at different time steps for photodissociation from $2^2\Pi$ state. Each time step = 0.001584 fs.

imental [284, 285] results. While the maxima in σ(E), including an additional hump for the $X^2\Pi$-$2^2\Pi$ excitation, are located at about the same place as in the time-independent quantal results, there is a noticeable discrepancy in the magnitude of the maximum σ values. A careful examination of the results reported by van Dishoeck and Dalgarno[283] reveals that their results are dependent on the choice of basis set and hence differences of the kind noticed in figure 5.3 are not surprising. In any case, the fact that the two different theoretical approaches yield nearly the same σ(E) implies that the observed discrepancy between theory and experiment is likely to be due to some error in the experimental results. One obvious source of error would be the uncertainty in the initial vib-rotational state of OH, in experiments.

5.3 Predissociation

It has been mentioned in the Introduction that the predissociation takes place in the first excited state, $A^2\Sigma^+$, due to spin-orbit coupling between $A^2\Sigma^+$ and $^4\Sigma^-$, $1^2\Sigma^-$ and $^4\Pi$ states (shown in figure 5.5). We have also mentioned that earlier investigations[287–298] on the OH predissociation suggested that the $^4\Sigma^-$ state is responsible for the observed weak predissociation near v' ≤ 2 and the $^4\Pi$ state is responsible for the strong predissociation near v' ≥ 5. Since the $^4\Sigma^-$ and $^4\Pi$ states cross the $A^2\Sigma^+$ state near v' $= 2$ and 5 respectively, the above proposed mechanism is quite self-explanatory. However, when we want to compute Γ and its dependence on various vibrational levels of $A^2\Sigma^+$ state, we have to consider not only the location of the crossing between the $A^2\Sigma^+$ and the repulsive states but also the role of the spin-orbit coupling between the states and its R dependence. Therefore, we have included the R-dependence of the spin-orbit coupling explicitly in our present calculation. Since Lee and Freed[288] have already shown that the asymptotic coupling

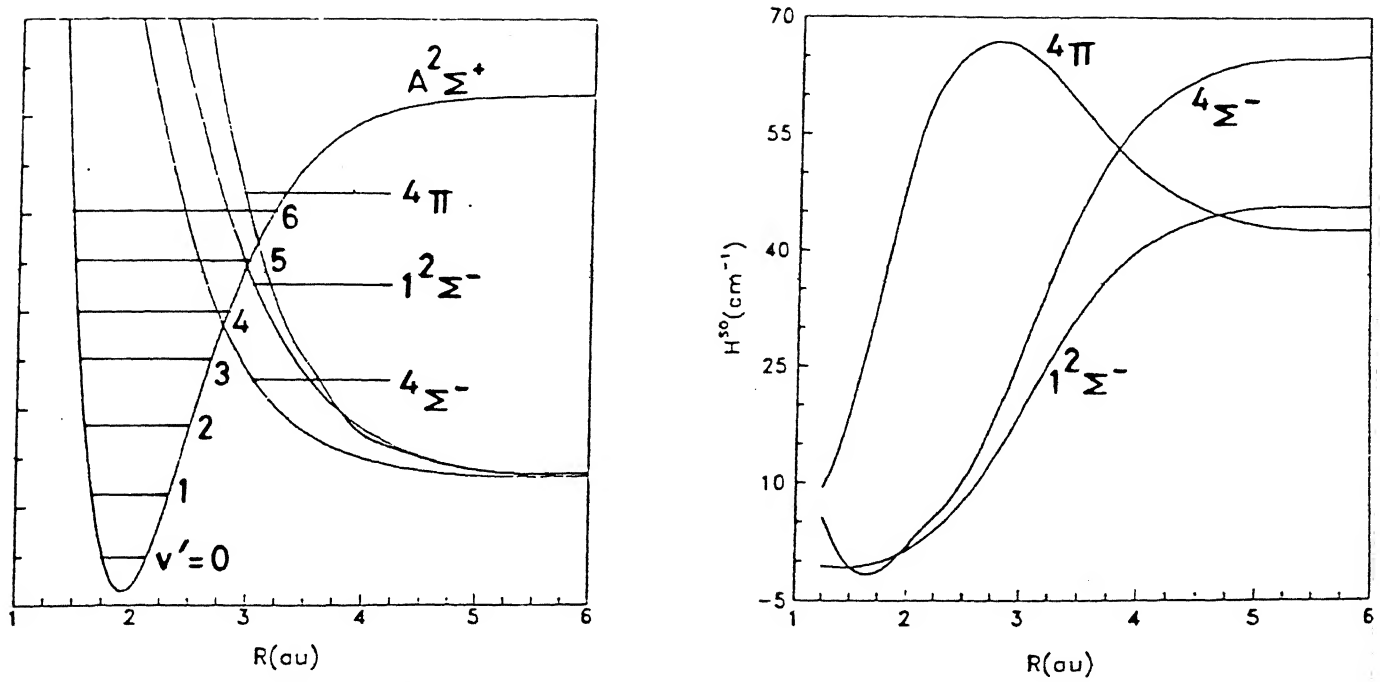

Figure 5.5. (a) Potential-energy curves that are responsible for the predissociation and (b) the spin-orbit coupling matrix elements as a function of R for the different repulsive states. For quick reference the energy levels of different v' states are superimposed in figure 5.5 (a).

between the repulsive states is not important while determining Γ, we have not considered the same in the present study.

The *ab initio* PE curves and the spin-orbit coupling matrix elements reported by Yarkony[298] were connected smoothly through cubic spline interpolation. Since isolated resonance approximation has been shown to be valid for the present system[287], we have computed the contribution due to continuum of each repulsive state α, independently and the total Γ is obtained by summation, i.e., $\Gamma^{tot} = \sum_\alpha \Gamma_\alpha$.

As has been pointed out by Villarreal et al.[168], an exact time-dependent treatment of predissociation would involve inordinately long time evolution(see section 2.3.7). Therefore we followed the wave packet golden rule treatment suggested by them[168] for computing Γ_α:

$$\Gamma_\alpha = \frac{1}{2\pi\hbar c}\int_{-\infty}^{\infty} e^{iE_i t/\hbar} < \phi_i(0)|\phi_i^\alpha(t) > dt \tag{5.9}$$

where $|\phi_i(0) > = H^{SO}\ |\psi_i(0) >$ and $|\phi_i^\alpha > = \mathrm{e}^{-iH_\alpha t/\hbar}\ |\phi_i(0) >$. $\psi_i(0)$ is the initial wavefunction corresponding to the $i^{th}(i = 1,2, \ldots, 7)$ vibrational level of the $A^2\Sigma^+$ state. H^{SO} represents the spin-orbit coupling matrix element and H_α is the Hamiltonian corresponding to α^{th} repulsive state. The time-evolution of the wavefunction on each repulsive state was accomplished by a second order differencing(SOD) scheme with the FFT routine[85] to obtain the spatial derivative of the wavefunction at any time t. The grid consisted of $R = 1.25\ (0.065)\ 9.505$ au and the time-evolution involved a total of 8192 steps with each time step being 0.00126 fs.

The *ab initio* PE values for the $A^2\Sigma^+$ state[298] were also fitted to an extended Rydberg function and the resulting parameters are included in table 5.1. The vibrational eigenvalues and eigenfunctions of the $A^2\Sigma^+$ state were obtained by the spectral method[82], using the computational scheme described in the earlier section for the $X^2\Pi$ state. The vibrational

eigenvalues were obtained from the power spectrum shown in figure 5.6a, and they are given in table 5.3 for v' = 0, 1, 2, ... 7. The corresponding eigenfunctions are shown in figure 5.6b. We have verified that the spacing between vibrational levels of $A^2\Sigma^+$ and $X^2\Pi$ states computed by us are comparable to the available experimental results[294].

The computed values of $\Gamma_\alpha(\alpha = {}^4\Sigma^-, 1^2\Sigma^-$ and $^4\Pi)$ are reported in table 5.4 and also plotted in figure 5.7 for different v' along with the available experimental and time-independent quantal results. Our results reproduce qualitatively the trend in Γ^{tot} with increasing v' reported earlier. That is, Γ^{tot} increases with increase in v' until it reaches a maximum at v'=6 and declines subsequently. Although it is not apparent from figure 5.7, it is clear from table 5.4 that our estimate of Γ^{tot} for v'=1 and 2 is substantially larger than that reported by others. The particularly low value of Γ obtained by Yarkony[298] can be explained readily as he considered only the predissociation into the $^4\Sigma^-$ state. Sink et al[287] had not included the variation of the spin-orbit coupling with R. The lower value of Γ obtained from experiments could be indicative of the reduced predissociation from the higher rotational states of OH.

For v'=3, Γ^{tot} computed by us is comparable to the value obtained from experiments and it falls exactly in between the two earlier theoretical estimates. For v'=4, our Γ^{tot} is close to the previous theoretical results, but is an underestimate when compared to experiment. For v'=5–7, there are no experimental results available and our results are in excellent accord with the results of Sink et al[287].

It is worth emphasising that the results in table 5.4 demonstrate clearly that the predissociation is dominated by the spin-orbit coupling with the $^4\Pi$ state[116]. The increase in Γ^{tot} with increase in v' through 6 can be easily understood from the location of the crossing points. As shown in figure 5.5, $^4\Sigma^-$, $1^2\Sigma^-$ and $^4\Pi$ states cross the $A^2\Sigma^+$ state

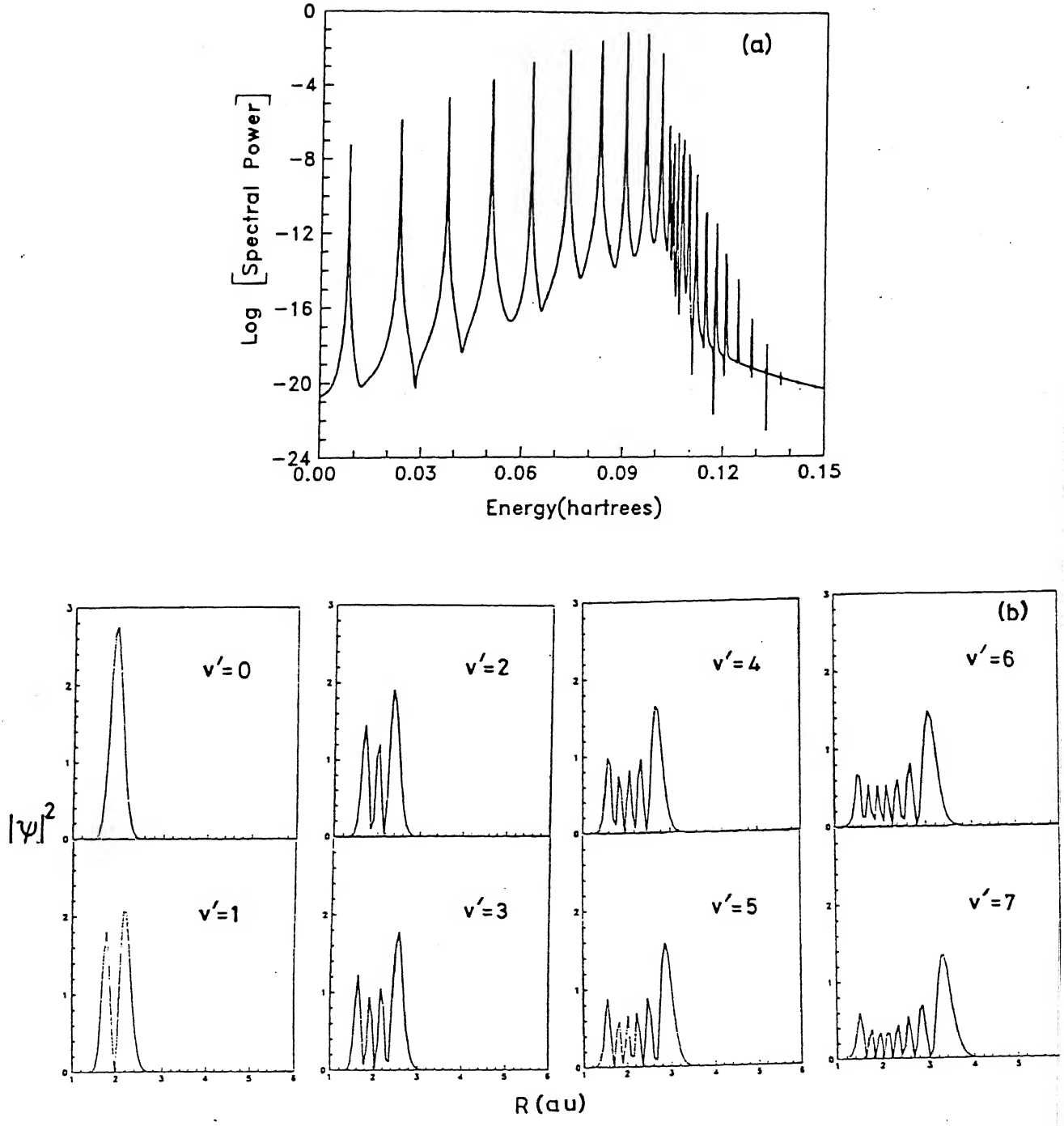

Figure 5.6. (a) Log. of power spectrum as a function of energy for $A^2\Sigma^+$ state and (b) $|\psi(R)|^2$ as a function of internuclear distance(R) for v' = 0, 1, 2, ... 7.

Table 5.3: $A^2\Sigma^+$ state eigenvalues for v'=0–7.

v'	$E_{v'}(cm^{-1})$
0	1440.07
1	4338.96
2	7125.64
3	9706.55
4	12120.33
5	14288.59
6	16271.85
7	17974.65

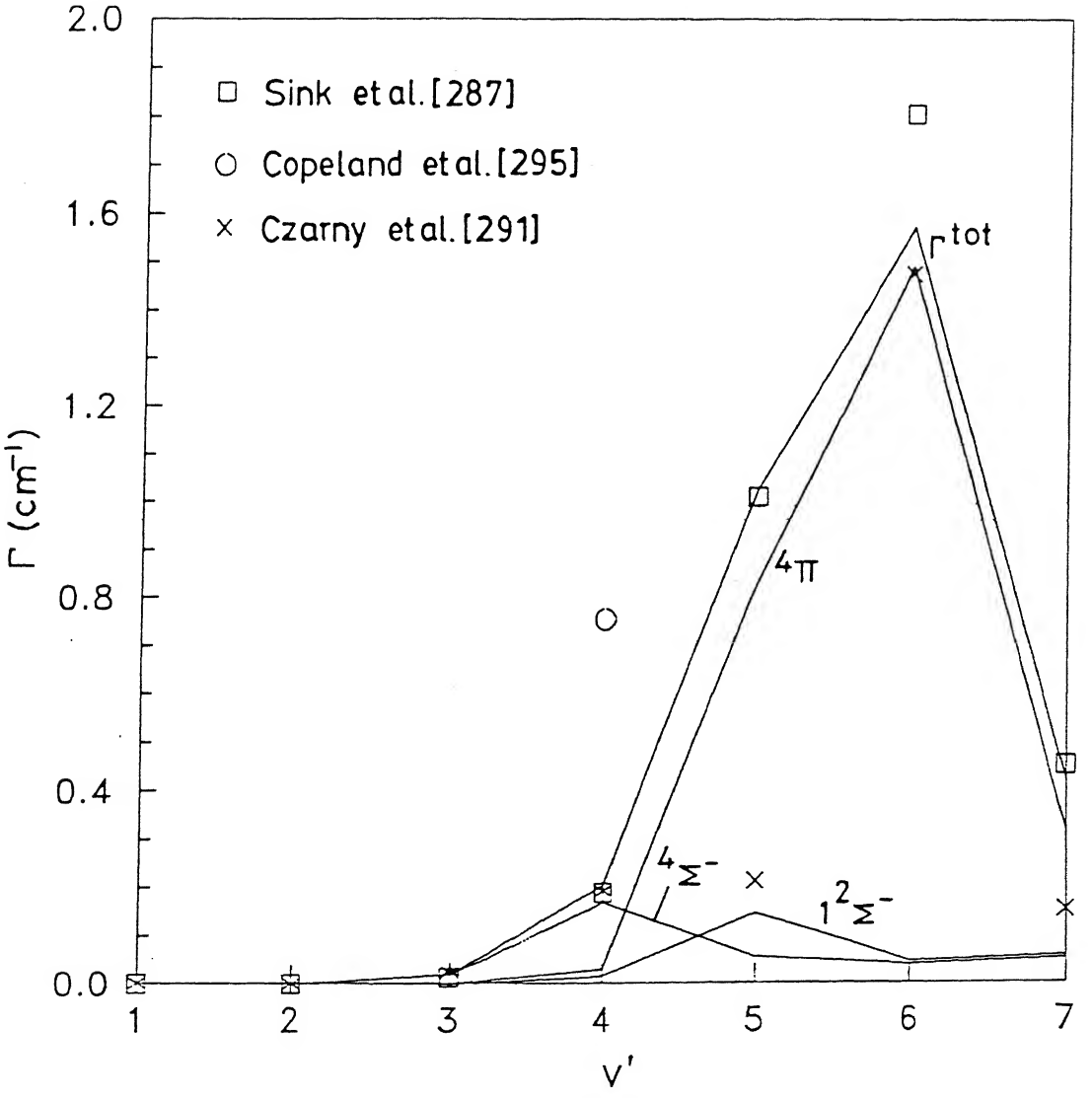

Figure 5.7. Predissociation linewidths (Γ_α) for each channel and the Γ^{tot} as a function of v'. Some of the earlier results are indistinguishable from the ones shown for v'=1–3 and therefore are not shown separately.

Table 5.4: Predissociation linewidths,Γ (in cm^{-1}) computed using the golden rule treatment.

The numbers in parentheses represent the powers of 10.

v'	$^4\Sigma^-$	$^2\Sigma^-$	$^4\Pi$	Γ^{tot}	Γ(others)	Ref.
1	8.2(-6)	3.6(-6)	7.6(-4)	7.7(-4)	9.0(-8)	[6a]
					6.6(-13)	[298]
					< 2.1(-7)	[7b]
2	2.9(-5)	7.7(-6)	8.4(-4)	8.7(-4)	2.3(-5)	[6a]
					3.3(-5)	[298]
					1.8(-5)	[7a]
					2.9(-5)	[7b]
3	1.9(-2)	4.1(-5)	9.6(-4)	2.0(-2)	1.2(-2)	[6a]
					2.4(-2)	[298]
					1.9(-2)	[7d]
					1.8(-2)	[7e]
4	1.7(-1)	1.5(-2)	2.9(-2)	2.1(-1)	1.9(-1)	[6a]
					1.9(-1)	[298]
					≈7.5(-1)	[7c]
5	5.4(-2)	1.4(-1)	8.3(-1)	1.0	1.0	[6a]
					2.1(-1)	[291]
6	3.9(-2)	4.4(-2)	1.5	1.6	1.8	[6a]
					1.5	[291]
7	4.9(-2)	5.6(-2)	3.1(-1)	4.2(-1)	4.5(-1)	[6a]
					1.5(-1)	[291]

near the vibrational levels v'=3–6 corresponding to R = 2–3 au for which H^{SO} increases with R. For $R > 3$ au, the H^{SO} for the dominant channel, $^4\Pi$, decreases with increase in R explaining the decline in Γ^{tot} beyond v'=6. For the $^4\Sigma^-$ and the $^2\Sigma^-$ channels H^{SO} continues to increase with increase in R thus explaining the continued increase in Γ in going from v'=6 to v'=7.

5.4 Conclusion

The TDQM approach has been applied to study both photodissociation and predissociation processes in OH. The photodissociation cross section values computed by us are comparable to the time-independent quantal results but a factor of two smaller than the experimental results.

The predissociation linewidths calculated using the Fermi golden rule treatment are in general accord with the earlier theoretical results. In general, it has been shown that Γ^{tot} increases with increase in v' through 6 and then it declines subsequently and that this is explainable on the basis of the R-dependence of the H^{SO} for the dominant channel $^4\Pi$.

Chapter 6

Summary and Conclusion

Time-dependent quantum mechanical approach is increasingly being used in recent years to investigate various elementary chemical processes such as photodissociation, predissociation, reactive scattering, molecule-surface scattering etc., In the present thesis the TDQM approach has been employed to study (i) photo-predissociation of NaI, (ii) photodissociation of HI and (iii) photodissociation and predissociation in OH radical. Important conclusions derived from our studies are summarised below.

In chapter1 of the thesis, we have reviewed the necessary background material related to the TDQM approach to photodissociation and predissociation processes. We have also presented a short literature review emphasising mainly on the recent studies.

Theoretical and computational methodologies related to the TDQM approach to photodissociation and predissociation processes have been presented in chapter 2. This chapter has been divided into three sections. In section 1, we have described the existing computational methodologies for implementing the TDQM approach. Section 2 of this chapter is devoted mainly for the interaction of light with molecules. We have presented a semiclassical and a quantum mechanical description of the photoabsorption process. We have also described, how the photodissociation cross section is computed in the time-domain.

Also we have presented a critical analysis of the nature of the wavefunction prepared by a laser pulse on the excited electronic state. In section 3, we have described the computational methodologies for investigating multieletronic state problems. Also the golden rule treatment for computing the predissociation linewidth is included in this chapter.

In chapter 3 of the thesis we have presented the results of the TDQM study of the photo-predissociation of NaI using ultrashort laser pulse. We have investigated the nature of the wave packet prepared by a femtosecond laser pulse, whose excitation frequency is chosen *near*, *very near* and *far from* resonance excitation frequency. Since the excitation frequencies are different, the WPs prepared on the excited electronic state also have different characteristics. The norm of the WP on the excited state during the pulse preparation step has been analysed. After the pulse preparation step is over, the WP is time evolved for about 3 ps on the covalent excited electronic state which is coupled to the ground electronic state. Due to the diabatic coupling between the ionic ground state and the covalent excited state, the time evolving WP bifurcates near the crossing point and a small fraction of it (as determined by the Landau-Zener curve crossing probability) leaks through the crossing to form neutral products Na and I and the remaining part of the WP oscillates between ionic and covalent turning points. Whenever the WP reaches near the crossing point a small fraction of it leaks through crossing. We have estimated the oscillation periods corresponding to photoexcitation wavelengths 300, 321 and 344 nm and our results are in good agreement with the experimental results of Zewail and coworkers. However, when the excitation wavelengths are *far from* resonance, i.e., $\lambda_{ex} = 360$ and 390 nm, the WP spreads immediately (in less than 0.5 ps) and shows several interference pattern. Therefore, oscillation periods estimated by us are not in agreement with experimental results. We have observed that the transient effect and the energy of the WP are

highly responsible for the unusual characteristics of the WP evolution.

In chapter 4 of the thesis, a detailed analysis of the photodissociation of HI in its first absorption band has been made. HI photodissociation takes place around 250nm resulting in H + I and H + I* formation. In this energy range, the following potential energy curves participate in the photodissociation: $^3\Pi_1$, $^1\Pi_1$, $^3\Sigma_1$ and $^3\Pi_0$. Among these, the former two correlate with the H + I channel and the later two correlate with the H + I* channel. Except for the $^3\Pi_0$ state, all other states are non-adiabatically coupled to each other. We have computed the photodissociation cross section(σ) corresponding to the photoexcitation from the ground vibrational level of the ground electronic state to all of the above mentioned excited states. We have made use of the PE curves, non-adiabatic coupling potentials and the coordinate dependent transition dipole moments reported earlier by Levy and Shapiro. Our computed σ and Γ values are in excellent agreement with the experimental and the time-independent quantum mechanical results. We have also computed the anisotropy parameter(β) for the H + I* channel and our β values as a function of excitation energy are in accord with the experimental and the time-independent quantal results. In addition, we show that the Γ value changes significantly with vibrational excitation of the parent molecule and point out vibrational excitation prior to photodissociation as a means of channel control. The results are interpreted in terms of the influence of the non-adiabatic coupling on the time-evolution of the wavefunction.

In chapter 5, we have described our results obtained for the photodissociation and predissociation processes in OH radical using the TDQM method. Since OH radical is one of the important constituents in the astrophysical environment, understanding various dissociation pathways in OH becomes particularly essential. Photodissociation in OH takes place due to electronic transition from the ground electronic state ($X^2\Pi$) to the

excited electronic states, $1^2\Sigma^-$, $1^2\Delta$, $B^2\Sigma^+$ and $2^2\Pi$. The PE curves and the coordinate dependent transition dipole moments are taken from the *ab initio* results of Dalgarno and coworkers. Our computed photodissociation cross sections are in good agreement with the time-independent quantal results and a factor of two less than the experimental results. Predissociation in OH takes place from its first absorption band ($X^2\Pi$–$A^2\Sigma^+$) due to spin-orbit coupling between the bound state $A^2\Sigma^+$ and the repulsive states $^4\Sigma^-$, $1^2\Sigma^-$ and $^4\Pi$. Using the recent *ab initio* results of PE curves and the spin-orbit matrix elements reported by Yarknoy we have obtained predissociation linewidths corresponding to predissociation from v'=1–7 of the $A^2\Sigma^+$ state. The results are analysed in terms of the crossings between the PE curves.

References

[1] Special issue of Chem. Phys. on "Photon-Induced Molecular Dynamics", **187** (1/2) 1–225 (1994).

[2] A. D. Bandrauk (Ed.), "Molecules in Laser Fields", Marcel Dekker, Inc. New York, 1993.

[3] R. Schinke, "Photodissociation Dynamics", Cambridge University Press, Cambridge, 1992.

[4] N. Sathyamurthy, "Recent Advances in Reaction Dynamics", Narosa, New Delhi; Springer-Verlag, Heidelberg, 1991.

[5] Special issue of Faraday Disscus. Chem. Soc. on, "Structure and Dynamics of Reactive Transition States", **91** (1991).

[6] R. P. Wayne, "Principles and Applications of Photochemistry", Oxford University Press, Oxford, 1988.

[7] P. R. Brooks and E. F. Hayes, "State-to-State Chemistry", ACS Symposium Series, Washington D. C., 1977.

[8] A. Ben-Shaul, Y. Haas, K. L. Kompa and R. D. Levine, "Lasers and Chemical Change", Springer-Verlag, Berlin, 1981.

[9] R. B. Bernstein, "Chemical Dynamics via Molecular Beam and Laser Techniques", Clarendon Press, Oxford, 1982.

[10] R. D. Levine and R. B. Bernstein, "Molecular Reaction Dynamics and Chemical Reactivity", Oxford University Press, Oxford, 1987.

[11] "Opportunities in Chemistry", National Academy Press, Washington D. C., 1985, p 68.

[12] D. L. Andrews, "Lasers in Chemistry", Springer-Verlag, Heidelberg, 1986.

[13] H. U. Keller, Space. Sci. Rev. **18**, 641 (1976).

[14] R. P. Wayne, "Chemistry of Atmospheres", Clarendon Press, Oxford, 1991.

[15] Special issue of on J. Chem. Soc. Faraday Trans."Chemistry in the Interstellar Medium", **89**(13), 2111-2320 (1993).

[16] G. Herzberg, "Spectra of Diatomic Molecules", Van Nostrand, Princeton, 1950.

[17] R. N. Zare and R. B. Bernstein, Physics Today **33**(11), November 1980, p 43.

[18] R. N. Zare and D. R. Herschbach, Proc. IEEE, **51**, 173 (1963).

[19] J. Solomon, C. Jonah, P. Chandra and R. Bersohn, J. Chem. Phys. **55**, 1908 (1971).

[20] Y. T. Lee and Y. R. Shen, Physics Today **33**(11), November 1980, p 52.

[21] A. E. de Vries, Comments At. Mol. Phys. **11**, 157 (1982).

[22] J. P. Simons, J. Phys. Chem. **88**, 1287 (1984).

[23] S. R. Leone, Science, **227**, 889 (1985).

[24] Special issue of Faraday Discuss. Chem. Soc. on "Dynamics of Molecular Photofragmentation", **82** (1986).

[25] M. N. R. Ashfold and J. E. Baggott, "Molecular Photodissociation Dynamics", Royal Society of Chemistry, London, 1987.

[26] J. W. Thoman, Jr., D. W. Chandler, D. H. Parker, M. H. M. Janssen, Laser Chem. **9**, 27 (1988).

[27] W. P. Hess, D. W. Chandler and J. W. Thoman, Jr., Chem. Phys. **163**, 277 (1992).

[28] M. Gruebele and A. H. Zewail, Phys. Today, May 1990, p 24.

[29] L. R. Khundkar and A. H. Zewail, Ann. Rev. Phys. Chem. **41**, 15 (1990).

[30] I. W. M. Smith, Nature, **343**, 691 (1990).

[31] J. C. Williamson and A. H. Zewail, Proc. Natl. Acad. Sci.(USA), **88**, 5021 (1991).

[32] M. Dantus and G. Roberts, Comments At. Mol. Phys. **26**, 131 (1991).

[33] A. H. Zewail (Ed.), "The Chemical Bond - Structure and Dynamics", Academic Press, New York, (1992).

[34] Special issue of J. Phys. Chem. on "Femtochemistry", **97**, 1993.

[35] G. G. Balint-Kurti and M. Shapiro, Chem. Phys. **61**, 137 (1981).

[36] M. Shapiro and R. Bershon, Ann. Rev. Phys. Chem. **33**, 409 (1982).

[37] P. Brumer and M. Shapiro, Adv. Chem. Phys. **60**, 371 (1985).

[38] G. G. Balint-Kurti and M. Shapiro, Adv. Chem. Phys. **60**, 403 (1985).

[39] D. C. Clary, J. Chem. Phys. **84**, 4288 (1986).

[40] R. Schinke, in "Collision Theory for Atoms and Molecules", F. A. Gianturco (Ed.), Plenum Press, New York, 1987.

[41] A. Banichevich, S. D. Peyerimhoff and J. A. Beswick, J. Chem. Phys. **96**, 6580 (1992).

[42] M. Shapiro, J. Phys. Chem. **97**, 7396 (1993).

[43] K. C. Kulander and E. J. Heller, J. Chem. Phys. **69**, 2439 (1978).

[44] N. E. Henricksen, Comments At. Mol. Phys. **21**, 153 (1988).

[45] B. R. Johnson and J. L. Kinsey, J. Chem. Phys. **87**, 1525 (1987); Phys. Rev. Lett. **62**, 1607 (1989); J. Chem. Phys. **91**, 7638 (1989).

[46] B. Hellsing and H. Metiu, Chem. Phys. Lett. **127**, 45 (1986).

[47] N. E. Henricksen, J. Zhang and E. J. Heller, J. Chem. Phys. **89**, 5607 (1988).

[48] D. Chasman, D. J. Tannor and D. G. Imre, J. Chem. Phys. **89**, 6667.

[49] J. Zhang, E. J. Heller, D. Huber, D. G. Imre and D. J. Tannor, J. Chem. Phys. **89**, 3602 (1988).

[50] J. Zhang and D. G. Imre, Chem. Phys. Letters, **149**, 233 (1988).

[51] B. Hartke, R. Kosloff and S. Ruhman, Chem. Phys. Lett. **158**, 238 (1989).

[52] J. Zhang, D. G. Imre and J. H. Frederick, J. Phys. Chem. **93**, 1840 (1989).

[53] H. Guo and G. C. Schatz, J. Chem. Phys. **93**, 393 (1990).

[54] G. G. Balint-Kurti, R. N. Dixon and C. C. Marston, J. Chem. Soc. Faraday Trans. **86**, 1741 (1990).

[55] F. LeQuéré and C. Leforestier, J. Chem. Phys. **94**, 247 (1990); J. Chem. Phys. **94**, 1118 (1991); Chem. Phys. Lett. **189**, 537 (1992).

[56] H. Guo, K. Q. Lao, G. C. Schatz and A. D. Hammerich, J. Chem. Phys. **94**, 6562 (1991).

[57] A. Untch, K. Weide and R. Schinke, J. Chem. Phys. **95**, 6496 (1991).

[58] J. L. Krause, K. C. Kulander, J. C. Light and A. E. Orel, J. Chem. Phys. **96**, 4283 (1992).

[59] H. Guo, J. Chem. Phys. **96**, 2731 (1992); J. Chem. Phys. **96**, 6629 (1992).

[60] J. Qian, C. J. Williams and D. J. Tannor, J. Chem. Phys. **97**, 6300 (1992).

[61] R. N. Dixon, Chem. Phys. Lett. **190**, 430 (1992).

[62] M. von Dirke and R. Schinke, Chem. Phys. Lett. **196**, 51 (1992).

[63] H. U. Suter, J. R. Huber, M. von Dirke and R. Schinke, J. Chem. Phys. **96**, 6727 (1992).

[64] G. G. Balint-Kurti, S. P. Mort and C. C. Marston, Comp. Phys. Commun. **74**, 289 (1993).

[65] R. N. Dixon, C. C. Marston and G. G. Balint-Kurti, J. Chem. Phys. **93**, 6520 (1990).

[66] D. G. Imre, J. L. Kinsey, A. Sinha and J. Krenos, J. Phys. Chem. **88**, 3950 (1984).

[67] E. J. Heller, J. Chem. Phys. **68**, 2066 (1978).

[68] E. J. Heller, J. Chem. Phys. **68**, 3891 (1978).

[69] S. -Y. Lee and E. J. Heller, J. Chem. Phys. **71**, 4777 (1979).

[70] S. -Y. Lee and E. J. Heller, J. Chem. Phys.**76**, 3035 (1982).

[71] D. J. Tannor and E. J. Heller, J. Chem. Phys. **77**, 202 (1982).

[72] R. L. Sundberg, E. J. Heller, Chem. Phys. Letters **93**, 586 (1982).

[73] E. J. Heller, R. L. Sundberg and D. J. Tannor, J. Phys. Chem. **86**, 1822 (1982).

[74] D. J. Tannor, M. Blanco and E. J. Heller, J. Phys. Chem. **88**, 6240 (1984).

[75] E. J. Heller, Acc. Chem. Res. **14**, 368 (1981).

[76] E. J. Heller in "Potential Energy Surfaces and Dynamics Calculations", D. G. Truhlar(Ed.), Plenum Press, New York, 1981.

[77] E. J. Heller, J. Chem. Phys. **62**, 1544 (1975).

[78] R. D. Coalson and J. L. Kinsey, J. Chem. Phys. **85**, 4322 (1986).

[79] R. D. Coalson, J. Chem. Phys. **86**, 6823 (1987).

[80] R. Heather and Metiu, Chem. Phys. Lett. **118**, 558 (1985).

[81] S. -I. Sawada, R. Heather, B. Jackson and H. Metiu, J. Chem. Phys. **83**, 3009 (1985).

[82] M. D. Feit and J. A. Fleck, Jr., Appl. Opt. **19**, 1154 (1980).

[83] M. D. Feit, J. A. Fleck, Jr. and A. Steiger, J. Comput. Phys. **47**, 412 (1982).

[84] M. D. Feit and J. A. Fleck, Jr. J. Chem. Phys. **78**, 301 (1983); *ibid.* **80**, 2578 (1984).

[85] R. Kosloff and D. Kosloff, J. Comput. Phys. **52**, 35 (1983).

[86] R. Kosloff and D. Kosloff, J. Chem. Phys. **79**, 1823 (1983).

[87] R. Kosloff, J. Phys. Chem. **92**, 2087 (1988).

[88] V. Mohan and N. Sathyamurthy, Comput. Phys. Rep. **7**, 213 (1988).

[89] C. C. Marston and G. G. Balint-Kurti, J. Chem. Phys. **91**, 3571 (1989).

[90] G. G. Balint-Kurti, R. N. Dixon and C. C. Marston, Int. Rev. Phys. Chem. **11**, 317 (1992).

[91] C. Leforestier, R. Bisseling, C. Cerjan, M. D. Feit, R. Friesner, A. Guldberg, A. Hammerich, G. Jolichard, W. Karrlein, H. -D. Meyer, N. Lipkin, O. Roncero and R. Kosloff, J. Comput. Phys. **94**, 59 (1991).

[92] T. N. Truong, J. J. Tanner, P. Bala, J. A. McCammon, D. J. Kouri, B. Lesyng and D. K. Hoffman, J. Chem. Phys. **96**, 2077 (1992).

[93] R. Kosloff, Ann. Rev. Phys. Chem. **45**, 145 (1994).

[94] N. Balakrishnan, C. Kalyanaraman and N. Sathyamurthy, Phys. Rep. (manuscript under prepartion).

[95] Thematic issue of Comput. Phys. Commun. on, "Time-Dependent Methods for Quantum Dynamics", K. C. Kulander(Ed.), **63**, 1–582 (1991).

[96] J. Broeckhove and L. Lathouwers, "Time-Dependent Quantum Molecular Dynamics", NATO ASI Ser. B 299, Plenum Press, New York, 1992.

[97] C. Cerjan (Ed.), "Numerical Grid Methods and Their Applications to Schrödinger's Equation", NATO ASI Ser. C 412, Academic Press, Kluver, 1993.

[98] H. Koppel, W. Domcke and L. S. Cederbaum, Adv. Chem. Phys. **57**, 59 (1984).

[99] M. Shapiro, J. Phys. Chem. **90**, 3644 (1986).

[100] Z. Xu, B. Koplitz and C. Wittig, J. Phys. Chem. **92**, 5518 (1988).

[101] J. F. Black, E. Hasselbrink, J. R. Waldeck and R. N. Zare, Mol. Phys. **71**, 1143 (1990); J. Chem. Phys. **92**, 3519 (1990).

[102] K. Weide, V. Staemmler and R. Schinke, J. Chem. Phys. **93**, 861 (1990).

[103] M. D. Person, P. W. Kash and L. J. Butler, J. Chem. Phys. **94**, 2557 (1991).

[104] Y. Matsumi, K. Tonokura and M. Kawasaki, J. Chem. Phys. **97**, 1065 (1992).

[105] S. -Y. Lee, J. Chem. Phys. **97**, 227 (1992).

[106] C. Reber and I. Zink, J. Chem. Phys. **96**, 2681 (1992).

[107] P. W. Kash and L. J. Butler, J. Chem. Phys. **96**, 892 (1992).

[108] J. Campos-Martinez, J. R. Waldeck and R. D. Coalson, J. Chem. Phys. **96**, 3613 (1992).

[109] U. Menthe and A. D. Hammerich, Chem. Phys. Lett. **211**, 7 (1993).

[110] C. -K. Ni and G. W. Flynn, Chem. Phys. Lett. **210**, 333 (1993).

[111] E. Jensen, J. S. Keller, G. C. G. Waschewsky, J. E. Stevens, R. L. Grahan, K. F. Freed and L. J. Butler, J. Chem. Phys. **98**, 2882 (1993).

[112] K. Tonokura, Y. Matsumi, M. Kawasaki, H. L. Kim, S. Yabushita, S. Fujimura and K. Saito, J. Chem. Phys. **99**, 3461 (1993).

[113] P. W. Kash, G. C. G. Waschewsky, R. E. Morss, L. J. Butler and M. M. Francl, J. Chem. Phys. **100**, 3463 (1994).

[114] Y. Wang and C. X. W. Qian, Chem. Phys. Lett. **219**, 389 (1994).

[115] E. E. Nikitin and Zülicke, "Selected Topics of the Theory of Chemical Elementary Processes", Lecture Notes in Chemistry, **8**, Springer-Verlag, Berlin, 1978.

[116] H. Lefebvre-Brion and R. W. Field, "Perturbations in the Spectra of Diatomic Molecules", Academic Press, Orlando, 1986.

[117] D. J. Tannor, R. Kosloff and S. A. Rice, J. Chem. Phys. **85**, 5805 (1986).

[118] P. Pernot, R. M. Grimes, W. A. Lester Jr. and Ch. Cerjan, Chem. Phys. Lett. **163**, 297 (1989).

[119] H. Guo, J. Chem. Phys. **99**, 1685 (1993).

[120] C. Kalyanaraman and N. Sathyamurthy, Chem. Phys. Lett. **209**, 52 (1993).

[121] R. D. Coalson, Chem. Phys. Lett. **147**, 208 (1988).

[122] R. D. Coalson, Adv. Chem. Phys. **73**, 605 (1989).

[123] J. Alvarellos and H. Metiu, J. Chem. Phys. **88**, 4957 (1988).

[124] X. -P. Jiang, R. Heather and H. Metiu, J. Chem. Phys. **90**, 2555 (1989).

[125] G. G. Balint-Kurti, C. L. Ward and C. C. Marston, Comput. Phys. Commun. **67**, 285 (1991).

[126] S. Das and D. J. Tannor, J. Chem. Phys. **91**, 2324 (1989).

[127] ; R. N. Zare, Mol. Photochem. **4**, 1 (1972).

[128] R. N. Zare, "Angular Momentum", Wiley-Interscience, New York, 1988.

[129] J. A. Beswick, M. Glass-Maujean and O. Roncero, J. Chem. Phys. **96**, 7514 (1992).

[130] L. D. A. Siebbeles and J. A. Beswick, J. Chem. Soc. Faraday Soc. **88**, 2565 (1992).

[131] S. O. Williams and D. G. Imre, J. Phys. Chem. **92**, 6636 (1988).

[132] S. O. Williams and D. G. Imre, J. Phys. Chem. **92**, 6648 (1988).

[133] H. Metiu and V. Engel, J. Opt. Soc. Am. **B7**, 1709 (1990).

[134] W. T. Pollard, S. -Y. Lee and R. A. Mathies, J. Chem. Phys. **92**, 4012 (1990).

[135] H. Metiu, Faraday Discuss. Chem. Soc., **91**, 1 (1991).

[136] V. Engel and H. Metiu, J. Chem. Phys. **95**, 3444 (1991).

[137] R. Bavli, V. Engel and H. Metiu, J. Chem. Phys. **96**, 2600 (1992).

[138] V. Engel, H. Metiu, R. Almeida, R. A. Marcus and A. H. Zewail, Chem. Phys. Lett. **152**, 1 (1988).

[139] V. Engel and H. Metiu, J. Chem. Phys. **90**, 6116 (1989).

[140] S. H. Lin and B. Fain, Chem. Phys. Lett. **155**, 216 (1989).

[141] V. Engel and H. Metiu, J. Chem. Phys. **91**, 1596 (1989); V. Engel, Comput. Phys. Commun. **63**, 228 (1991).

[142] H. Kono and Y. Fujimura, Chem. Phys. Lett. **184**, 497 (1991).

[143] H. Metiu and V. Engel, J. Chem. Phys. **93**, 5693 (1990).

[144] B. Hartke, Chem. Phys. Lett. **175**, 322 (1990).

[145] V. Engel and H. Metiu, J. Chem. Phys. **92**, 2317 (1990).

[146] Ch. Meier, V. Engel and J. S. Briggs, J. Chem. Phys. **95**, 7337 (1991).

[147] L. Valko, Phys. Rev. **A47**, 4123 (1993).

[148] K. L. Kompa and R. D. Levine, Acc. Chem. Res. **27**, 91 (1994).

[149] D. Neuhauser and H. Rabitz, Acc. Chem. Res. **26**, 496 (1993).

[150] N. E. Henricksen and B. Amstrup, Chem. Phys. Lett. **213**, 65 (1993).

[151] L. Shen, S. Shi and H. Rabitz, J. Phys. Chem. **97**, 8874 (1993).

[152] B. Amstrup, A. Lörincz and S. A. Rice, J. Phys. Chem. **97**, 6175 (1993).

[153] Y. Yan, R. E. Gillian, R. M. Whitnell, K. R. Wilson and S. Mukamel, J. Phys. Chem. **97**, 2320 (1993).

[154] C. Kalyanaraman and N. Sathyamurthy, Curr. Sci. **65**, 319 (1993).

[155] S. A. Rice, Science **258**, 412 (1992).

[156] P. Brumer and M. Shapiro, Acc. Chem. Res. **22**, 407 (1989); J. Chem. Phys. **97**, 6259 (1992); Annu. Rev. Phys. Chem. **43**, 257 (1992).

[157] J. Manz and G. K. Parmonov, J. Phys. Chem. **97**, 12625 (1993).

[158] P. Brumer and M. Shapiro, in,"Molecules in Laser Fields", A. D. Bandrauk (Ed.), Marcel Dekker, Inc. New York, 1993.

[159] D. J. Tannor, in,"Molecules in Laser Fields", A. D. Bandrauk (Ed.), Marcel Dekker, Inc. New York, 1993.

[160] S. Shi and H. Rabitz, Commput. Phys. Commun. **63**, 71 (1991); P. Gross, D. Neuhauser and H. Rabitz, J. Chem. Phys. **96**, 2834.

[161] E. D. Potter, J. L. Herek, S. Pedersen, Q. Liu and A. H. Zewail, Nature, **355**, 66 (1992).

[162] S. -P. Lu, S. M. Park, Y. Xie and R. J. Gordon, J. Chem. Phys. **96**, 6613 (1992).

[163] F. F. Crim in, "Molecular Photodissociation Dynamics", M. N. R. Ashfold and J. E. Baggott(Eds.), Royal Society of Chemistry, London, 1987.

[164] F. F. Crim, Science **249**, 1387 (1990).

[165] V. Engel, V. Staemmler, R. L. Vander Wal, F. F. Crim, R. J. Sension, B. Hudson, P. Andresen, S. Hennig, K. Weide and R. Schinke, J. Phys. Chem. **96**, 3201 (1992).

[166] F. F. Crim, Ann. Rev. Phys. Chem. **44**, 397 (1993).

[167] S. K. Gray and E. Wozny, J. Chem. Phys. **94**, 2817 (1991).

[168] P. Villarreal, S. Miret-Artés, O. Roncero, G. Delgado-Barrio, J. A. Beswick, N. Halberstadt and R. D. Coalson, J. Chem. Phys. **94**, 4230 (1991).

[169] O. Roncero, N. Halberstadt and J. A. Beswick, Chem. Phys. Lett. **226**, 82 (1994).

[170] C. Kalyanaraman and N. Sathyamurthy, Chem. Phys. **187**, 219 (1994).

[171] J. A. Beswick and J. Jortner, Adv. Chem. Phys. **47**, 363 (1981).

[172] J. A. Beswick and N. Halberstadt, "Dynamics of Weakly Bound Complexes", Kluwer, Dordrecht, 1993.

[173] M. H. M. Janssen, M. Dantus, H. Guo and A. H. Zewail, Chem. Phys. Lett. **214**, 281 (1993).

[174] A. Untch, R. Schinke, R. Cotting and J. R. Huber, J. Chem. Phys. **99**, 9553 (1993).

[175] V. J. Barclay, J. C. Polanyi, Y. Zeiri and R. Kosloff, J. Chem. Phys. **98**, 9185 (1993).

[176] R. N. Dixon, Chem. Phys. Lett. **190**, 430 (1993).

[177] Ch. Meier and V. Engel, Chem. Phys. Lett. **212**, 691 (1993).

[178] H. Guo, J. Phys. Chem. **97**, 2602 (1993).

[179] G. -J. Kroes, E. F. van Dishoeck, R. A. Beärda and M. C. van Hemert, J. Chem. Phys. **99**, 228 (1993).

[180] S. Chelkowski and A. D. Bandrauk, J. Chem. Phys. **99**, 4279 (1993).

[181] A. D. Bandrauk and H. Shen, J. Chem. Phys. **99**, 1185 (1993).

[182] J. -Y. Fang and H. Guo, J. Chem. Phys. **101**, 1231 (1994).

[183] A. D. Bandrauk, J. -M. Gauthier and J. F. McCann, J. Chem. Phys. **100**, 340 (1994).

[184] T. Schröder, R. Schinke, M. Mandziuk and Z. Bačić, J. Chem. Phys. **100**, 7239 (1994).

[185] N. Balakrishnan and G. D. Billing, J. Chem. Phys. **101**, 2968 (1994).

[186] N. Balakrishnan, Ph. D. Thesis, Indian Institute of Technology, Kanpur, 1992.

[187] W. H. Press, B. P. Flannery, S. A. Teukolsky and W. T. Vetterling, "Numerical Recipes", Cambridge University Press, 1986.

[188] A. Askar and A. S. Cakmak, J. Chem. Phys. bf 68, 2749 (1979).

[189] H. Tal-Ezer and R. Kosloff, J. Chem. Phys. **81**, 3967 (1984).

[190] C. J. Lanczos, J. Res. Natl. Bur. Stand. **45**, 225 (1950).

[191] C. Iung and C. Leforestier, Comput. Phys. Commun. **63**, 135 (1991).

[192] N. Marković and G. D. Billing, J. Chem. Phys. **97**, 8201 (1992).

[193] T. J. Park and J. C. Light, J. Chem. Phys. **85**, 5870 (1986).

[194] D. K. Hoffman, O. A. Sharafeddin, R. S. Judson and D. J. Kouri, J. Chem. Phys. **92**, 4167 (1990).

[195] O. A. Sharafeddin, D. J. Kouri, R. S. Judson and D. K. Hoffman, J. Chem. Phys. **93**, 5580 (1990).

[196] R. S. Judson, D. B. McGarrah, O. A. Sharafeddin, D. J. Kouri and D. K. Hoffman, J. Chem. Phys. **94**, 3577 (1991).

[197] D. J. Kouri and D. K. Hoffman, Chem. Phys. Letters, **186**, 91 (1991).

[198] A. D. Bandrauk and H. Shen, Chem. Phys. Letters, **176**, 428 (1991).

[199] A. D. Bandrauk and H. Shen, Can. J. Chem. **70**, 555 (1992).

[200] M. Sugawara, M. Kato and Y. Fujimura, Chem. Phys. Letters, **184**, 203 (1991).

[201] C. Leforestier and R. E. Wyatt, J. Chem. Phys. **78**, 2334 (1983).

[202] R. Kosloff and D. Kosloff, J. Comput. Phys. **63**, 363 (1986).

[203] D. Neuhauser and M. Baer, J. Phys. Chem. **93**, 2872 (1989).

[204] D. Neuhauser and M. Baer, J. Chem. Phys. **91**, 4651 (1989).

[205] D. Neuhauser, M. Baer, R. S. Judson and D. J. Kouri, J. Chem. Phys. **93**, 312 (1990).

[206] D. Neuhauser, M. Baer, R. S. Judson and D. J. Kouri, Chem. Phys. Letters, **169**, 372 (1990).

[207] M. S. Child, Mol. Phys. **72**, 89 (1991).

[208] D. Neuhauser, M. Baer, R. S. Judson and D. J. Kouri, Comput. Phys. Commun. **63**, 460 (1991).

[209] N. Balakrishnan and N. Sathyamurthy, Chem. Phys. Letters, **201**, 294 (1993).

[210] A. Vibók and G. G. Balint-Kurti, J. Chem. Phys. **96**, 7615 (1992).

[211] A. Vibók and G. G. Balint-Kurti, J. Phys. Chem. **96**, 8712 (1992).

[212] R. Heather and H. Metiu, J. Chem. Phys. **86**, 5009 (1987).

[213] R. Heather and H. Metiu, J. Chem. Phys. **88**, 5496 (1988).

[214] V. Engel and H. Metiu, J. Chem. Phys. **92**, 2317 (1990).

[215] D. H. Zhang and J. Z. H. Zhang, J. Chem. Phys. **95**, 6449 (1991).

[216] D. H. Zhang and J. Z. H. Zhang, J. Phys. Chem. **96**, 1575 (1992).

[217] D. H. Zhang, J. Z. H. Zhang and Z. Bačić, J. Chem. Phys. **97**, 927 (1992).

[218] D. H. Zhang, J. Z. H. Zhang and Z. Bačić, Chem. Phys. Letters, **194**, 313 (1992).

[219] J. Z. H. Zhang, Comput. Phys. Commun. **63**, 28 (1991).

[220] D. H. Zhang, O. A. Sharafeddin and J. Z. H. Zhang, Chem. Phys. **167**, 137 (1992).

[221] S. Das and D. J. Tannor, J. Chem. Phys. **92**, 3403 (1990).

[222] C. J. Williams, J. Quian and D. J. Tannor, J. Chem. Phys. 95, 1721 (1991).

[223] D. J. Tannor, A. Besprozvannaya and C. J. Willams, J. Chem. Phys. **96**, 2998 (1992).

[224] B. H. Bransden and C. J. Joachain, "Physics of Atoms and Molecules" , Longman, London, 1983.

[225] G. C. Schatz and M. A. Ratner, "Quantum Mechanics in Chemistry", Prentice Hall, New Jersey, 1993.

[226] W. Heitler, "Quantum Theory of Radiation", Clarendon Press, Oxford, 1954.

[227] R. Loudon, "The Quantum Theory of Light", Clarendon, Oxford, 1983.

[228] R. G. Gordon, Adv. Magn. Res. **3**, 1 (1968).

[229] L. I. Schiff, "Quantum Mechanics", McGraw-Hill Publishers, Singapore, 1985.

[230] D. P. Craig and T. Thirunamachandran, "Molecular Quantum Electrodynamics", Academic Press, London, 1984.

[231] E. Merzbacher, "Quantum Mechanics", John Wiely & Sons, New York, 1970.

[232] M. Jacon, O. Atabek and C. Leforestier, J. Chem. Phys. **91**, 1585 1989.

[233] D. J. Tannor and S. A. Rice, Adv. Chem. Phys. **70**, 441 (1988).

[234] M. V. Ramakrishna and R. D. Coalson, Chem. Phys. **120**, 327 (1988).

[235] S. O. Williams and D. G. Imre, J. Phys. Chem. **92**, 3363 (1988).

[236] B. Hartke, J. Raman Spectrosc. **32**, 131 (1991).

[237] M. V. Ramakrishna, J. Chem. Phys. **93**, 3258 (1990).

[238] J. Broeckhove, B. Feyen, L. Lathouwers, F. Arickx and P. Van Leuven, Chem. Phys. Lett. **174**, 504 (1990).

[239] R. D. Levine, "Quantum Theoy of Molecular Rate Processes", The Clarendon Press, Oxford, 1969.

[240] M. L. Sink and A. D. Bandrauk, J. Chem. Phys. **73**, 4451 (1980).

[241] A. H. Zewail, Science, **242**, 1645 (1988); A. H. Zewail and R. B. Bernstein, Chem. and Engg. News, Nov. 7, pp 24 (1988); M. J. Rosker, M. Dantus and A. H. Zewail, J. Chem. Phys. **89**, 6113 (1988);A. H. Zewail, J. Chem. Soc., Faraday Trans. **85**, 1221 (1989).

[242] A. H. Zewail, J. Phys. Chem. **97**, 12427 (1993).

[243] T. S. Rose, M. J. Rosker and A. H. Zewail, J. Chem. Phys. **88**, 6672 (1988); M. J. Rosker, T. S. Rose and A. H. Zewail, Chem. Phys. Lett. **146**, 175 (1989).

[244] R. S. Berry in "Alkali Halide Vapours", P. Davidovits and D. L. McFadden (Eds.), Academic Press, New York, 1979.

[245] T. S. Rose, M. J. Rosker and A. H. Zewail, J. Chem. Phys. **91**, 7415; A. Mokhtari, P. Cong, J. L. Herek and A. H. Zewail, Nature, **348**, 225.

[246] P. Cong, A. Mokhtari and A. H. Zewail, Chem. Phys. Lett. **172**, 109 (1990).

[247] S. -Y. Lee, W. T. Pollard and R. A. Mathies, J. Chem. Phys. **90**, 6146.

[248] S. E. Choi, J. C. Light, J. Chem. Phys. **90**, 2593 (1989).

[249] M. Shapiro, J. Phys. Chem. **97**, 7396 (1993).

[250] H. Guo, Chem. Phys. Lett. **193**, 527 (1992).

[251] J. Wang, A. J. Blake, D. G. McCoy and L. Torop, Chem. Phys. Lett. **175**, 225 (1990).

[252] J. C. Polanyi, Science **234**, 673 (1986).

[253] N. Sathyamurthy, Chem. Rev. **83**, 601 (1983); H. R. Mayne, Int. Rev. Phys. Chem. **10**, 107 (1991).

[254] P. R. Brooks, Chem. Rev. **88**, 407 (1988).

[255] N. Bloembergen and A. H. Zewail, J. Phys. Chem. **88**, 5459 (1984).

[256] R. Kosloff, S. A. Rice, P. Gaspard, S. Tersigni and D. J. Tannor, Chem. Phys. **139**, 201 (1989).

[257] J. W. Gadzuk, Chem. Phys. Letters, **136**, 402 (1987).

[258] B. Amstrup, R. J. Carlson, A. Matro and S. A. Rice, J. Phys. Chem. **95**, 8019 (1991).

[259] S. Chelkowski and A. D. Bandrauk, Chem. Phys. Letters, **186**, 264 (1991).

[260] A. P. Peirce, M. A. Dahleh and H. Rabitz, Phys. Rev. **A 37**, 4950 (1988); S. Shi and H. Rabitz, J. Chem. Phys. **97**, 276 (1992); R. S. Judson and H. Rabitz, Phys. Rev. Lett. **68** 1500 (1992).

[261] R. L. Vander Wal, J. L. Scott and F. F. Crim, J. Phys. Chem. **92**, 803 (1990); R. L. Vander Wal, J. L. Scott, F. F. Crim, K. Weide, and R. Schinke, J. Chem. Phys. **94**, 3548 (1991).

[262] H. Guo and G. C. Schatz, J. Chem. Phys. **92**, 1634 (1990).

[263] P. W. Kash and L. J. Butler, J. Chem. Phys. **96**, 8923 (1992).

[264] R. S. Mulliken, Phys. Rev. **51**, 310 (1937).

[265] R. S. Mulliken, J. Chem. Phys. **8**, 382 (1940).

[266] J. F. Ogilvie, Trans. Faraday Soc. **67**, 2205 (1971).

[267] I. Levy and M. Shapiro, J. Chem. Phys. **89**, 2900 (1988).

[268] H. Okabe, "Photochemistry of Small Molecules", Wiley-Interscience, New York, 1978.

[269] C. F. Goodev and A. W. C. Taylor, Proc. Roy. Soc. London, **152**, 221 (1935).

[270] R. D. Clear, S. J. Riley and K. R. Wilson, J. Chem. Phys. **63**, 1340 (1975).

[271] R. Schmiedl, H. Dugan, W. Meier and K. H. Welge, Z. Phys. **A 304**, 137 (1982).

[272] G. N. A. Van Veen, K. A. Monameel, T. Baller and A. E. de Vries, Chem. Phys. **80**, 113 (1983).

[273] M. A. Buntine, D. P. Baldwin, R. N. Zare and D. W. Chandler, J. Chem. Phys. **94**, 4672 (1991).

[274] D. Neuhauser, R. S. Judson, D. J. Kouri, A. D. Adelman, N. E. Shafer, D. A. V. Kliner and R. N. Zare, Science, **257**, 519 (1992).

[275] C. R. Quick Jr., R. E. Weston Jr., and G. W. Flynn, Chem. Phys. Letters, **83**, 15 (1981).

[276] C. A. Wight and S. R. Leone, J. Chem. Phys. **79**, 4823 (1983).

[277] R. Bersohn and S. H. Lin, Adv. Chem. Phys. **16**, 67 (1969).

[278] K. P. Kirby and E. F. van Dishoeck, Adv. At. Mol. Phys. **25**, 437 (1988).

[279] A. Dalgarno, J. Chem. Soc. Faraday Trans. **89**, 2111 (1993).

[280] A. G. Gaydon and H. G. Wolfhard, Proc. Roy. Soc. London, Ser. **A208**, 63 (1951).

[281] S. R. Langhoff, E. F. van Dishoeck, R. Wetmore and A. Dalgarno, J. Chem. Phys. **77**, 1379 (1982).

[282] E. F. van Dishoeck, S. R. Langhoff and A. Dalgarno, J. Chem. Phys. **78**, 4552 (1983).

[283] E. F. van Dishoeck and A. Dalgarno, J. Chem. Phys. **79**, 873 (1983).

[284] J. B. Nee and L. C. Lee, J. Chem. Phys. **81**, 31 (1984).

[285] R. J. Cody, C. Moralejo and J. E. Allen, Jr., J. Chem. Phys. **95**, 2491 (1991).

[286] H. H. Michels and F. E. Harris, Chem. Phys. Letters, **3**, 441 (1969).

[287] M. L. Sink, A. D. Bandrauk and R. Lefebvre, J. Chem. Phys. **73**, 4451 (1980).

[288] S. Lee and K. F. Freed, J. Chem. Phys. **87**, 5772 (1987).

[289] C. Carlone and F. W. Dalby, Can. J. Phys. **47**, 1945 (1969).

[290] D. W. Nageli and H. B. Palmer, J. Mol. Spectrosc. **23**, 44 (1967); H. B. Palmer and D. W. Nageli, J. Mol. Spectrosc. **28**, 417 (1968).

[291] J. Czarny, P. Felenbok and H. Lefebvre-Brion, J. Phys. **B4**, 124 (1971).

[292] K. R. German, J. Chem. Phys. **63**, 5252 (1975).

[293] J. Brzozowski, P. Erman and M. Lyyra, Phys. Scripta **17**, 507 (1978).

[294] J. A. Coxon, Can. J. Phys. **58**, 933 (1980).

[295] R. A. Copeland, J. B. Jeffries and D. R. Crosley, J. Mol. Spectrosc. **143**, 183 (1990).

[296] J. A. Gray and R. L. Farrow, J. Chem. Phys. **95**, 7054 (1991).

[297] D. E. Heard, D. R. Crosley, J. B. Jeffries, G. P. Smith and A. Hirano, J. Chem. Phys. **96**, 4366 (1992).

[298] D. R. Yarkony, J. Chem. Phys. **97**, 1838 (1992).

[299] P. Andresen, A. Bath, W. Gröger, H. W. Lülf, G. Meijer and J. J. ter Meulen, Appl. Opt. **27**, 365 (1988).

[300] J. N. Murrell and K. S. Sorbie, J. Chem. Soc. Faraday Trans.2, **68**, 1552 (1972).

[301] E. F. van Dishoeck, M. C.van Hemert, A. C. Allison and A. Dalgarno, J. Chem. Phys. **81**, 5709 (1984).